2.1.5.10 List of Acronyms and Abbreviations

CCP	CO_2 Capture Project
GEMBOCHS	Geologic and Engineering Materials: Bibliography Of Chemical Species (Thermodynamic/kinetic database and software library: Johnson and Lundeen, 1994a,b)
LDEC	Livermore Distinct Element Code (geomechanical modeling software: Morris et al., 2002, 2003)
NUFT	Non-isothermal Unsaturated Flow and Transport (reactive transport software: Nitao, 1998a,b, 2003)
SUPCRT92	SUPerCRiTical (geochemical modeling software and database: Johnson et al., 1992)

2.1.5.11 Report Appendices

2.1.5.11.1 Abstracts presented at technical conferences

2.1.5.11.1.1 American Association of Petroleum Geologists (AAPG) Annual Meeting
Salt Lake City, UT, May 11-14, 2003

TITLE:
CO_2 reservoirs: are they natural analogs to engineered geologic storage sites?
AUTHORS:
James W. Johnson, John J. Nitao, Stephen C. Blair, and Joseph P. Morris
Lawrence Livermore National Laboratory

ABSTRACT

Although CO_2 reservoirs are commonly referenced as natural analogs to engineered geologic storage sites, there are important distinctions between these settings that may preclude their direct correlation. Most importantly, natural CO_2 accumulations were established over geologic time frames, while CO_2 injection at potential sequestration sites represents a dramatically telescoped and therefore very different thermal, hydrological, geochemical, and geomechanical perturbation of the reservoir/cap rock system. This distinction raises two intriguing possibilities that warrant quantitative investigation. First, the currently secure cap rock of a given natural CO_2 accumulation may have evolved into such as a function of geochemical alteration that attended some degree of initial CO_2 migration through it. Second, whether or not such evolution took place, this same cap rock may be incapable of providing an effective hydrodynamic seal in the context of an engineered injection. There are two corresponding fundamental questions. First, what is the evolution of cap-rock integrity during formation of natural CO_2 reservoirs? Second, will such evolution be similar or appreciably different in engineered storage sites; i.e., what is its dependence on the rate, focality, and duration of CO_2 influx? These questions—upon which strict validity of the natural-analog concept hinges—can be addressed using the reactive transport modeling approach. In this study, we will conduct and compare reactive transport simulations of a well-characterized CO_2 reservoir under both natural and hypothetical anthropogenic "filling" modes. Our results will reveal the dependence of long-term cap-rock integrity on filling history, and thereby shed quantitative light on appropriateness of the natural-analog concept.

2.1.5.13.1.2 Second National Conference on Carbon Sequestration
Washington, DC, May 5-8, 2003

TITLE:
Reactive transport modeling of long-term cap rock integrity
during CO_2 injection for EOR or saline-aquifer storage

AUTHORS:
James W. Johnson, John J. Nitao, and Joseph P. Morris
Lawrence Livermore National Laboratory
ABSTRACT

CO_2 injection for EOR or saline-aquifer storage leads to concomitant geochemical alteration and geomechanical deformation of the cap rock, enhancing or degrading its seal integrity depending on the relative effectiveness of these interdependent processes. Injection-triggered mineral dissolution/precipitation reactions within typical shales continuously reduce microfracture apertures, while pressure and dependent effective-stress evolution first rapidly increase then slowly constrict them. Using our reactive transport simulator (NUFT), supporting geochemical databases and software (GEMBOCHS, SUPCRT92), and distinct-element geomechanical model (LDEC), we have evaluated the net effect of these initially opposing contributions to long-term cap-rock integrity—the single most important constraint on long-term isolation performance.

2.1.5.13.1.3 **Offshore Technology Conference (OTC)**
Houston, TX, May 5-8, 2003

TITLE:

Reactive transport modeling of geohazards associated with
offshore CO_2 injection for EOR and geologic sequestration

AUTHORS:

James W. Johnson, John J. Nitao, Stephen C. Blair, and Joseph P. Morris
Lawrence Livermore National Laboratory

ABSTRACT:

Offshore injection of CO_2 for EOR and geologic sequestration leads to geochemical alteration and geomechanical deformation of the cap rock, which—depending on the relative effectiveness of these interdependent processes—will enhance or degrade integrity of this hydrodynamic seal. For injection settings where geomechanical deformation dominates, cap-rock integrity may be significantly compromised, potentially triggering an environmental geohazard in the form of large-scale CO_2 release from the target reservoir and ultimately the seabed (worst-case scenario). The evolution of cap-rock permeability during and after CO_2 injection can be assessed through reactive transport modeling, an advanced computational method based on mathematical models of the coupled physical and chemical processes catalyzed by the injection event. Using our reactive transport simulator (NUFT) and supporting geochemical databases and software (GEMBOCHS, SUPCRT92), we have previously shown that within shale-capped sandstone reservoirs (e.g., at Statoil's North Sea Sleipner facility) CO_2(g)-shale interaction along water-wet fracture walls converts clay-rich assemblages to those dominated by carbonate minerals. A volume increase of 15-20% attends this kinetic process; hence, geochemical alteration reduces the aperture of microfractures, thereby reducing cap-rock permeability. In the present study, we address the concomitant geomechanical deformation by interfacing NUFT simulation results—primarily the evolving pressure anomaly along and above the reservoir-shale interface—with distinct-element geomechanical models (3DEC, LDEC), which yield the dependent stress-strain history: slip displacement, aperture widening, and increased cap-rock permeability. We then combine these geochemical and geomechanical contributions to provide a first-order estimate of their relative effectiveness and the extent to which cap-rock integrity is enhanced or degraded. When evaluating the long-term isolation performance of candidate geologic CO_2 injection sites, cap-rock integrity is the single most important risk-assessment concern. Reactive transport modeling provides a unique computational means of assessing the potential for cap-rock corruption and dependent geohazards associated with offshore CO_2 injection for EOR and geologic sequestration.

2.1.5.13.1.4 **American Chemical Society (ACS) National Meeting**
New York, Sep 7-11, 2003 (submitted May 10, 2003; accepted May 20, 2003)

TITLE:

Reactive transport modeling of cap rock integrity
during natural and engineered CO_2 sequestration

AUTHORS:

James W. Johnson, John J. Nitao, and Joseph P. Morris, Lawrence Livermore National Laboratory

ABSTRACT

Long-term cap rock integrity represents the single most important constraint on the long-term isolation performance of natural and engineered geologic CO_2 storage sites. CO_2 influx that forms natural accumulations and CO_2 injection for EOR or saline-aquifer disposal both lead to concomitant geochemical alteration and geomechanical deformation of the cap rock, enhancing or degrading its seal integrity depending on the relative effectiveness of these interdependent processes. Influx-triggered mineral dissolution/precipitation reactions within typical shales continuously reduce microfracture apertures, while pressure and effective-stress evolution first rapidly increase then slowly constrict them.

Using our reactive transport simulator (NUFT), supporting geochemical databases and software (SUPCRT92), and distinct-element geomechanical model (LDEC), we have evaluated the net effect of these initially opposing contributions to cap-rock integrity for both natural and engineered CO_2 influx. The extent of geochemical alteration is nearly independent of filling mode. In contrast, geomechanical deformation—which invariably results in net aperture opening for compartmentalized reservoirs—is significantly more pronounced during engineered influx. These results limit the extent to which natural and engineered storage sites are analogous, and suggest that in both settings shale cap rocks may evolve into effective seals.

2.1.6 Early Detection and Remediation of Leakage from CO_2 Storage Projects

Report Title

CO_2 Capture Project - An Integrated, Collaborative Technology Development Project for Next Generation CO_2 Separation, Capture and Geologic Sequestration

Early Detection and Remediation of Leakage from CO2 Storage Projects

Report Reference

2.1.6

Type of Report:	Semi-Annual Report
Reporting Period Start Date:	February 2003
Reporting Period End Date:	July 2003
Principal Author(s):	Sally Benson
Date Report was issued:	August 2003
DOE Award Number:	DE-FC26-01NT41145
Submitting Organization:	Lawrence Berkeley National Laboratory
Address:	1 Cyclotron Road MS 50A-4112 Berkeley, California 94720

2.1.6.1 Abstract

The need for methods of early detection and remediation of leakage from CO_2 storage projects is a recurrent theme in discussions with environmental NGO's about the acceptability of geologic storage of CO_2 as an approach to carbon management. To date, little, if any, research has been done that addresses this concern. The purpose of the proposed project is to prepare a scoping paper that identifies 1) monitoring approaches for early detection of leakage, 2) remediation options that could be used to eliminate or manage risks after leakage has been detected and 3) additional information and R&D that is needed to develop the remediation approaches identified. The overarching goal of the proposed study is to begin to develop approaches that can be used to manage human health and environmental risks to an acceptable level in the event that a storage project leaks.

2.1.6.2 Table of Contents

2.1.6.3 Introduction

The need for methods of early detection and remediation of leakage from CO_2 storage projects is a recurrent theme in discussions with environmental NGO's about the acceptability of geologic storage of CO_2 as an approach to carbon management. To date, little, if any, research has been done that addresses this concern. The purpose of the proposed project is to prepare a scoping paper that identifies 1) monitoring approaches for early detection of leakage, 2) remediation options that could be used to eliminate or manage risks after leakage has been detected and 3) additional information and R&D that is needed to develop the remediation approaches identified. The overarching goal of the proposed study is to begin to develop approaches that can be used to manage human health and environmental risks to an acceptable level in the event that a storage project leaks.

2.1.6.4 Experimental

The approach taken to this project is as follows:

1. Calculate a range of leakage rates from prototypical storage projects, including those performing effectively and those leaking at unacceptable rates.
2. Identify and develop the major leakage scenarios that are most likely to occur in geologic storage projects (e.g. leakage up abandoned wells, leakage up undetected faults or fractures in the reservoir seal, etc…).
3. Identify the consequences of leakage in each of these scenarios (e.g. degradation of groundwater quality, human exposure to elevated CO_2 concentrations, etc…)
4. Identify monitoring approaches that could be used for early detection of leakage in each of the scenarios (e.g. seismic imaging, satellite or air-borne imaging, surface IR detectors, etc…)
5. Survey and document remediation practices currently used in natural gas storage, oil and gas production, groundwater and vadose zone remediation, damn construction and maintenance and acid gas disposal.
6. Evaluate how and the extent to which existing remediation practices could be employed to remediate leakage in geologic storage projects.
7. Identify potential new approaches for remediation of geologic storage projects for scenarios where existing remediation approaches are not sufficient.
8. Identify additional knowledge or information needed to develop and build confidence in the effectiveness of new or improved remediation approaches.
9. Identify existing regulations that would be applicable to protecting human and ecosystem health at leaking geologic storage sites.

Work has begun on items number 1 through 5 listed above.

2.1.6.5 Results and Discussion

This project has just begun during the past two weeks. To date, we have developed a list of possible options for remediation of leaking storage projects. These options are listed I outline form below. For the final report, each of the methods will be described in detail, including a discussion of there applicability for remediation of geologic storage projects. In addition, we will perform numerical simulations of several hypothetical cases to evaluate their effectiveness.

a) *Ideas for vadose zone remediation*:
  i) passive methods
    (1) barometric pumping
    (2) baroballs
  ii) active methods
    (1) soil gas extraction
      (a) vertical wells
      (b) horizontal wells
      (c) drainage systems
      (d) trenches
    (2) covers
      (a) landfill cover – low permeability material
      (b) collection system below cover
    (3) sprinkling/irrigation to dissolve CO_2 and move it downward

b) *Ideas for groundwater remediation*:
  i) passive methods
    (1) natural attentuation by dissolution, migration, and mineralization
  ii) active methods
    (1) gas phase pumping
    (2) groundwater extraction to exsolve plume
    (3) single well dissolution system – inject CO2 then water (WAG)
  iii) methods to deal with other contamination due to dissolution of minerals by CO2 (e.g., As, Pb)
    (1) pump and treat with wells
      (a) vertical
      (b) horizontal
      (c) deep gravel trenches/drainage
    (2) containment by managing hydraulic heads
  iv) ideas for sealing faults in limited areas
    (1) foam injection
    (2) grout injection

c) *Ideas for managing surface fluxes*:
  i) fans to dissipate hazardous concentration of CO2 at night
  ii) trenches – gravel-filled with covers to collect CO2 from leaks such as faults or in the vadose zone

d) *Ideas for controlling leaks with in the storage reservoir*:
  i) lower reservoir pressure
    (1) inject at lower rate
    (2) stop injection
    (3) begin CO2 extraction
    (4) pump out groundwater peripherally to lower pressure

- ii) <u>extract CO2 before it reaches the leakage path</u>
  - (1) pump from reservoir before leakage point
- iii) <u>hydrofracture</u> to access new areas of the reservoir away from areas of leakage

e) *Ideas for remediating leakage from abandoned wells*:
- i) plug and abandon using techniques developed for oil and gas leaks

f) *Ideas for basement CO_2 remediation*
- i) Active or passive ventilation

g) *Ideas for remediation of CO_2 dissolved in deep lake*
- i) Controlled discharge of CO_2 through gas lift from depth (now used at Lake Nyos)

2.1.6.6 Conclusion

When completed, this project will have provided a list of remediation options for managing leaking geological storage projects. There are many options available, and this should provide greater assurance to regulators and the public that even in the event that a geological storage project leaks, actions can be taken to lessen or prevent risks to humans and the environment.

2.1.6.7 References

None.

2.1.7 Impact of CO2 Injection on Subsurface Microbes and Surface Ecosystems

Report Title

CO_2 Capture Project - An Integrated, Collaborative Technology Development Project for Next Generation CO_2 Separation, Capture and Geologic Sequestration

Impact of CO2 Injection on Subsurface Microbes and Surface Ecosystems

Report Reference

2.1.7

Type of Report:	Semi-Annual Report
Reporting Period Start Date:	February 2003
Reporting Period End Date:	July 2003
Principal Author(s):	T.C. Onstott, Dept. Geosciences, Princeton University
Date Report was issued:	August 2003
DOE Award Number:	DE-FC26-01NT41145
Submitting Organization:	Geolas
Address:	PO Box 663 New Hope, PA 18938

Impact of CO_2 Injections on Deep Subsurface Microbial Ecosystems and Potential Ramifications for the Surface Biosphere

T.C. Onstott, Dept. of Geosciences, Princeton University

Introduction

Liquid CO_2 injection into hydraulically tight, deep aquifers has been proposed as a means of carbon mitigation and is used to develop oil reservoirs. The extent to which subsurface microbial communities will play a role in the long-term fate of CO_2 is not known and it may depend upon numerous factors including the abundance, diversity and relative proportions of autotrophic to heterotrophic organisms in the community, the abundance of potential electron donors (e.g. H_2, acetate and fermenters), the formation of a separate gas phase in the aquifer, the ambient temperature and pressure.

Deep subsurface microbial communities are dominated by four physiological types, methanogens, sulfate or sulfur reducing bacteria, fermentative anaerobes and Fe(III) reducing bacteria. These encompass the majority of subsurface species encountered to date. Their presence or absence in the 16S rDNA clone libraries can be roughly correlated with the free energy of the redox reactions they utilize for energy maintenance and the availability of the reactants in these redox reactions. The combination of energy and availability, referred to in this report as the potential microbial power, is an important parameter for gauging microbial activity. To ascertain the probable impacts of CO_2 injection upon deep subsurface microbial communities we calculated the potential microbial power for a range of ground water chemistries and temperatures, in a carbonate and siliclastic aquifer subjected to high partial pressures of CO_2.

Background

Over the past 15 years scientists have discovered the existence of microbial communities surviving at depths up to 3.5 kilometers below the surface (kmbls.). The population density declines with depth from 1×10^8 cell g^{-1} just below the soil zone to 10^2-10^5 cell g^{-1} in solid rock at ~3 kmbls (Fig. 1). A majority of these microorganisms represent new species, new genera and perhaps in some cases new phyla on the microbial tree of life. Most of these deep-seated environments include autotrophic methanogens, acetogens and sulfate reducers that utilize CO_2 but struggle in an aqueous environment that is HCO_3^--poor, Ca-rich, alkaline and usually electron-acceptor limited. Ground water dating indicates that these communities can survive for ten's to hundred's of millions of years and indirect evidence suggests that they are self-sufficient in terms of nutrient and energy resources. In other words they do not rely upon downward transport of growth substrates from the surface photosphere, but are biologically and chemically isolated.

The biomass concentration and level of activity are controlled by temperature, water activity, porosity, permeability, substrate and trace metal concentrations, substrate availability and the free energy of the redox reactions utilized for metabolisms. Of the large number of redox reactions that are relevant to H, C, N, O, S and P cycling by microorganisms living at temperatures less than 120°C (Amend and Shock, 2001) , we have focused on 47 redox reactions, 42 of which are known to be associated with specific genera and 5 of which are abiotic (see Table 1).

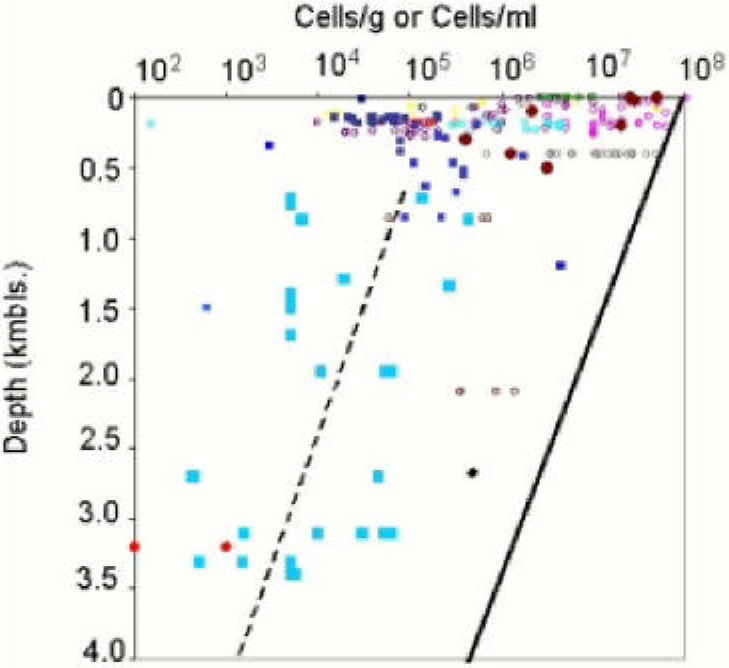

Fig. 1 Cellular density as a function of depth for sediments (filled and solid circles and ground water samples (filled squares). Solid turquoise squares and red dots represent our unpublished results from South Africa. The dashed line is the least squares best fit through our data. The solid line represents the extrapolation from ocean sediment data collected up to a depth of 800 meters.

The microbial diversity in deep subsurface environments has begun to be well established with application of 16S rDNA analyses (Gihring pers. comm., 2002). Some of the patterns that have begun to appear in this data include the following:

1. For many aquifers where ambient temperatures are <40°C and the depths are <500 meters, members of the Proteobacteria division are common. These include aerobic heterotrophs, methanotrophs, facultative anaerobes bacteria and chemolithotrophs (Fig. 2-4). Members of the Crenarchaeota and Euryarchaeota division of the Archaea are also common in this aquifer. The Proterobacteria also appear in drilling water and mine water and therefore appear to be the dominant type of microbial contaminants.

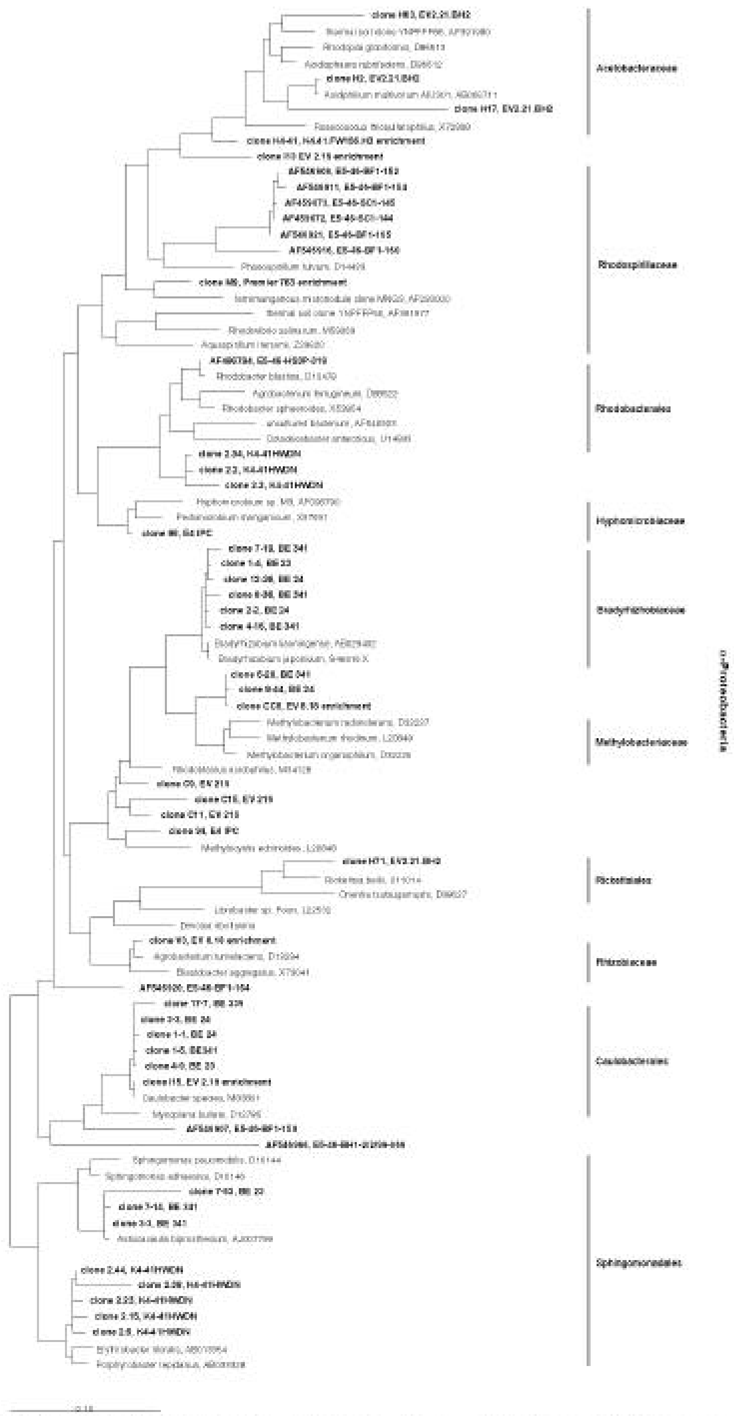

Fig. 2. Alpha Proteobacteria domain with subsurface and reference 16S sequences.

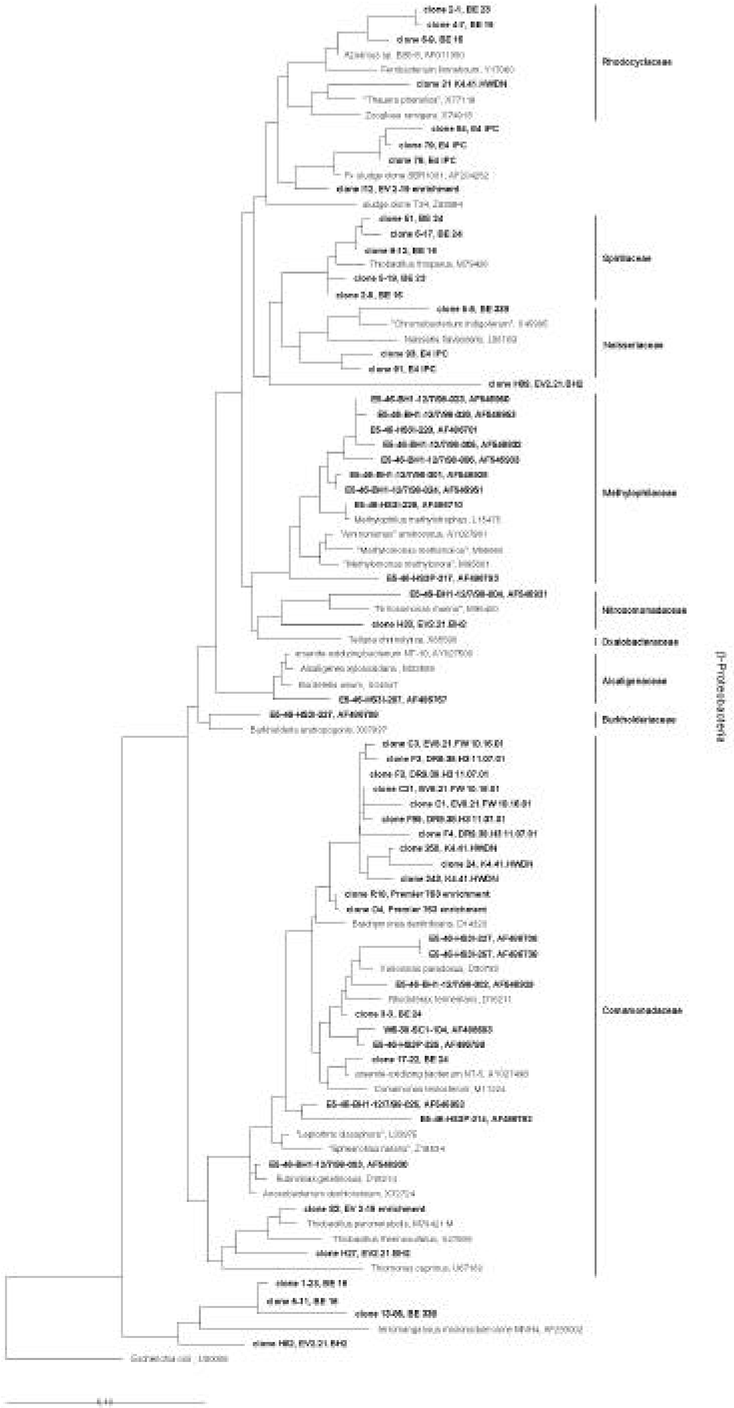

Fig. 3. Beta Proteobacteria domain with subsurface and reference 16S sequences.

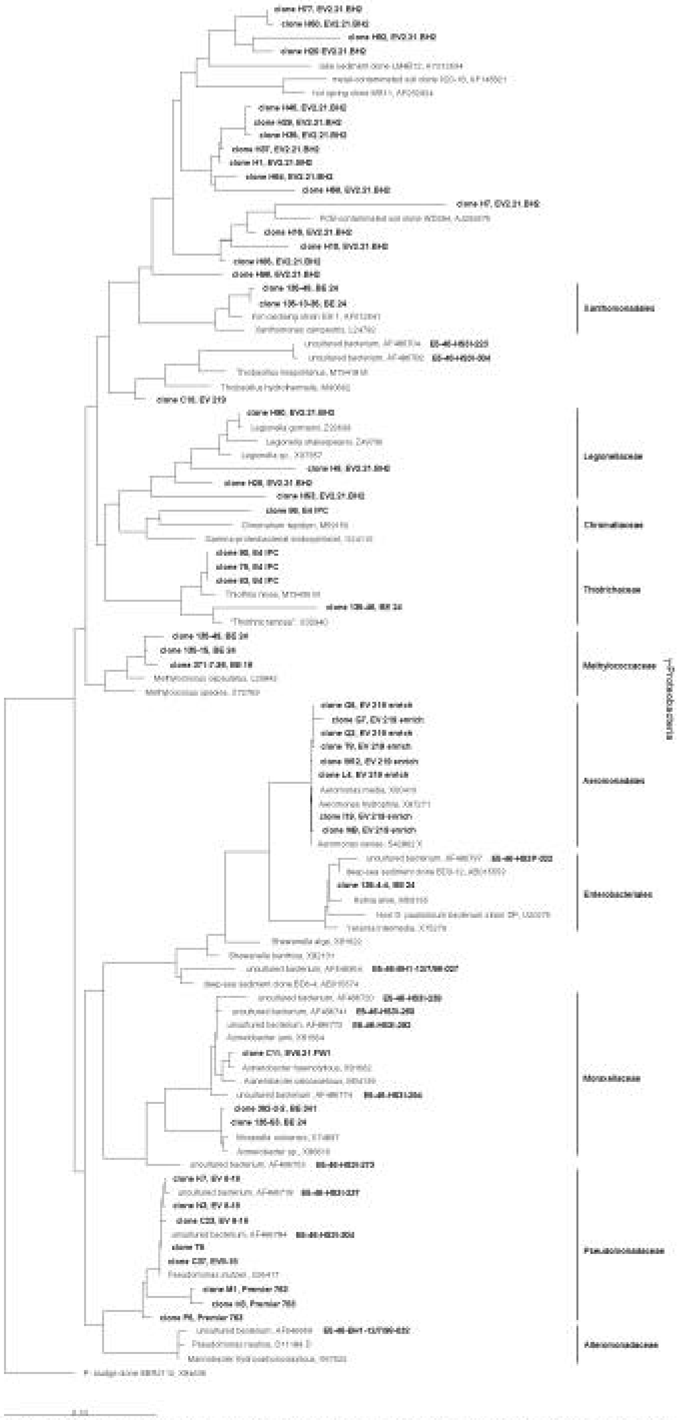

Fig. 4. Gamma Proteobacteria domain with subsurface and reference 16S sequences.

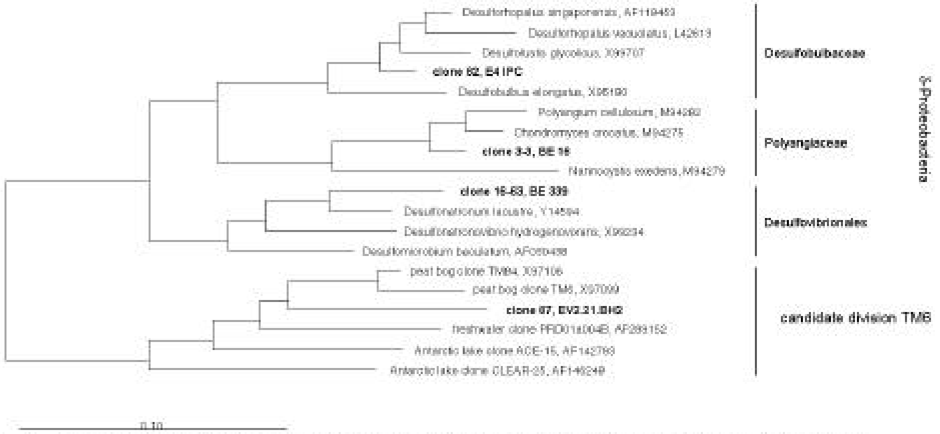

Fig. 5. Delta Proteobacteria domain with subsurface and reference 16S sequences.

2. The sulfate and S reducing bacteria of the δ *Proteobacteria* division, the Firmicutes (Fig. 6) and occasionally Archaea (Fig. 8) are common constituents of deep subsurface aquifers, particularly oil reservoirs where sulfate concentrations are > 100 μM. Fe(III) reducing members of Firmicutes and Thermus are found in those formations where sulfate concentrations are < 1 mM.
3. Thermophilic and hyperthermophilic members of Firmicutes, Thermus (Fig. 7) and Archaea (Fig. 8) are found in deep subsurface aquifers, though rarely, and phylogenetically are closely related to hyperthermophiles and thermophiles found in surface hot springs.
4. Approximately one third of the 16S rDNA clone sequences are not closely related to sequences in the ribosomal data base and may represent new species of unknown metabolic function.

These trends have also been seen in the 16S rDNA data of petroleum reservoirs (Hinton, pers. comm. 2003).

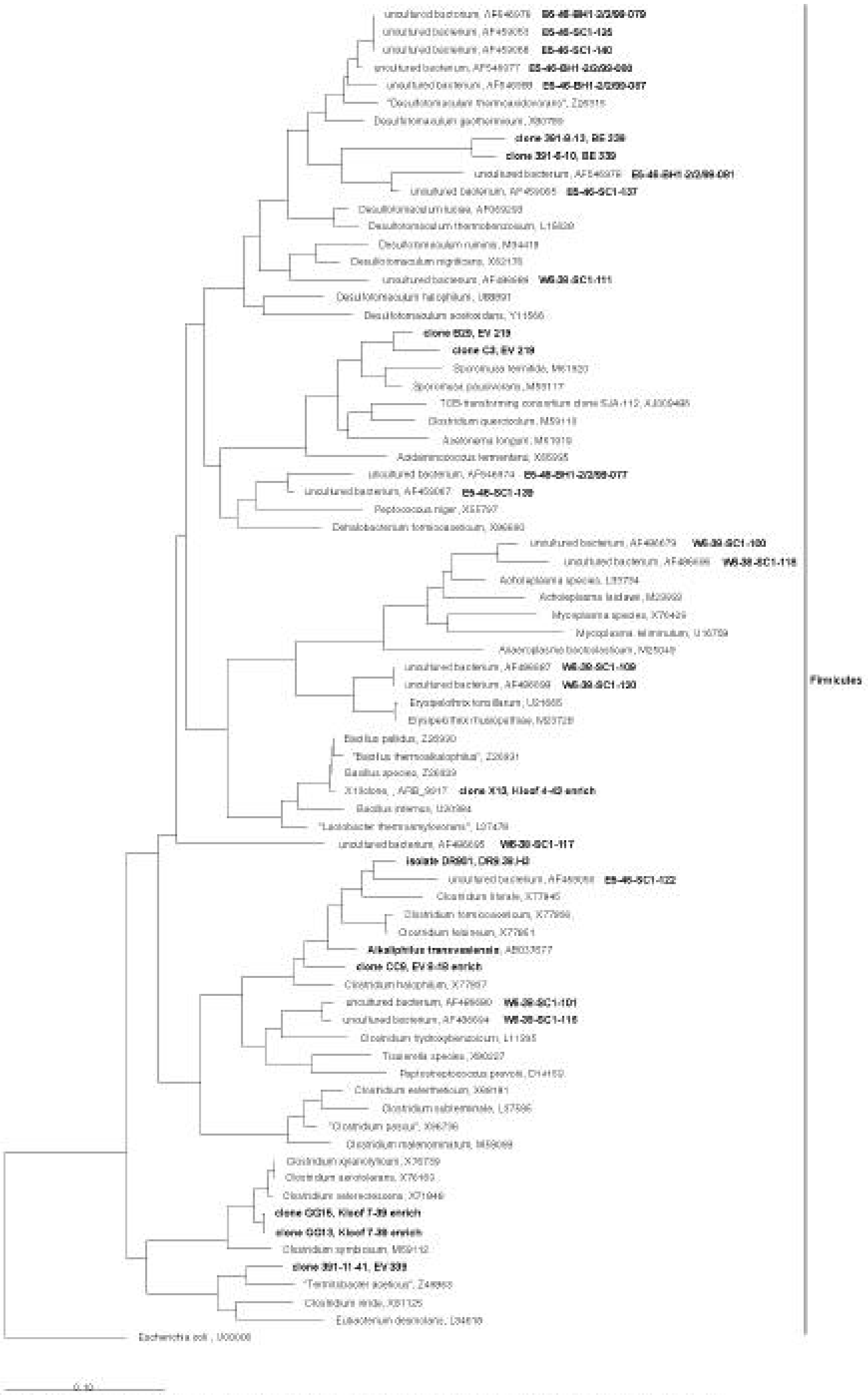

Fig. 6. Firmicutes domain with subsurface and reference 16S sequences.

Fig. 7. Thermus domain with subsurface and reference 16S sequences.

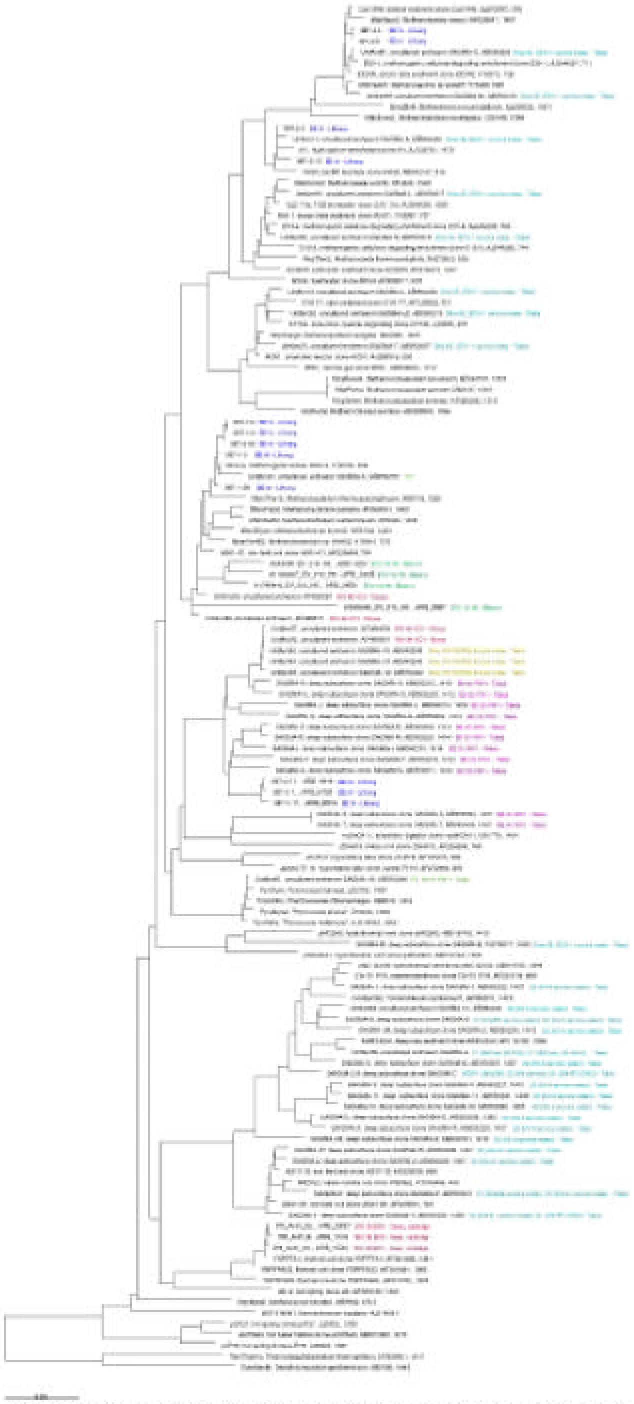

Fig. 9. Archaea domain with subsurface and reference 16S sequences.

Table 1. Microbially facilitated and abiogenic non-photosynthetic redox reactions

Reaction No.	Microbial Redox Reaction	Classification		Phylla
15	$CH_4 + 2O_2 -> HCO_3^- + H^+ + H_2O$	Aerobic	Methanotrophs	
11	Acetate + $2O_2 -> 2HCO_3^- + H^+$			
23	$2H_2 + O_2 -> 2H_2O$	Chemolithotrophs	Knall Gas Bacteria	β Proterobacteria, *Hydrogenophaga*
19	$2CO + O_2 + 2H_2O -> 2HCO_3^- + 2H^+$		Carbodoxybacteria	
44	$NH_3 + 1.5^* O_2 -> NO_2^- + H^+ + H_2O$		Nitrifiers	
46	$2NO_2^- + O_2 -> 2NO_3^-$		Nitrifiers	
17	$HS^- + 2O_2 -> SO_4^{2-} + H^+$		S-oxidizers	
16	$S_2O_3^{2-} + 2O_2 + H_2O -> 2SO_4^{2-} + 2H^+$			
21	$S + 1.5O_2 + H_2O -> SO_4^{2-} + 2H^+$			
18	$2HS^- + 2O_2 -> S_2O_3^{2-} + H_2O$			
25	$2HS^- + O_2 + 2H^+ -> 2S + 2H_2O$			
40	$4Fe^{2+} + O_2 + 10H_2O -> 4Fe(OH)_3 + 8H^+$		Fe-oxidizers	
47	$2Mn^{2+} + O_2 + 2H_2O -> 2MnO_2 + 4H^+$		Mn-oxidizers	
7	$4H_2 + NO_3^- + H^+ -> NH_3 + 3H_2O$	Nitrate Reducing		
1	$5H_2 + 2NO_3^- + 2H^+ -> N_2 + 6H_2O$			
8	Acetate + $NO_3^- + H_2O -> 2HCO_3^- + NH_3$			
2	Acetate + $1.6NO_3^- + 0.6H^+ -> 2HCO_3^- + 0.8H_2O + 0.8N_2$			*Firmicutes-Geobacillus*
4	$4CO + NO_3^- + 5H_2O -> 4HCO_3^- + NH_3 + 3H^+$			
6	$2.5CO + NO_3^- + 2H_2O -> 2.5HCO_3^- + 1.5H^+ + 0.5N_2$			
9	$S_2O_3^{2-} + NO_3^- + 2H_2O -> 2SO_4^{2-} + H^+ + NH_3$			
10	$HS^- + NO_3^- + H_2O -> SO_4^{2-} + NH_3$			
3	$2S + 1.5NO_3^- + 3.5H_2O -> 2SO_4^{2-} + 2.5H^+ + 1.5NH_3$			
45	$4Mn^{2+} + NO_3^- + 5H_2O -> 4MnO_2 + 7H^+ + NH_3$			
13	$5Fe^{2+} + NO_3^- + 12H_2O -> 5Fe(OH)_3 + 9H^+ + 0.5N_2$			
14	$NO_2^- + H^+ + NH_3 -> 2H_2O + N_2$		Anaamox	*Planctomycetales*

39	Acetate + 4Hematite + $15H^+ \rightarrow 8Fe^{2+} + 8H_2O + 2HCO_3^-$	Fe(III) Reducing		*Firmicutes*
33	CO + Hematite + $3H^+ \rightarrow 2Fe^{2+} + H_2O + HCO_3^-$			
41	H_2 + Hematite + $4H^+ \rightarrow 2Fe^{2+} + 3H_2O$			*Firmicutes*
5	Acetate + $4MnO_2 + 7H^+ \rightarrow 4Mn^{2+} + 4H_2O + 2HCO_3^-$	Mn(IV) Reducing		*Firmicutes*
28	$4H_2 + H^+ + SO_4^{2-} \rightarrow HS^- + 4H_2O$	Sulfate Reducing		
31	Acetate + $SO_4^{2-} \rightarrow 2HCO_3^- + HS^-$			*Firmicutes-Desulfotomaculum*
20	$4CO + SO_4^{2-} + 4H_2O \rightarrow 4HCO_3^- + HS^- + 3H^+$			
35	$CH_4 + SO_4^{2-} \rightarrow H_2O + HCO_3^- + HS^-$		Anaerobic Methane Oxidation	*δ Proterobacteria-Desulfosarcina* + *Euryarcheota-ANME-1&2*
37	$4H_2 + H^+ + 2HCO_3^- \rightarrow$ Acetate + $4H_2O$	CO_2 Reducing	Acetogen	
32	$4H_2 + H^+ + HCO_3^- \rightarrow CH_4 + 3H_2O$		Autotrophic Methanogen	*Euryarcheota*
30	4Formate + $H^+ + H_2O \rightarrow CH_4 + 3HCO_3^-$	Fermentation	Methanogen	*Euryarcheota*
36	Acetate + $H_2O \rightarrow CH_4 + HCO_3^-$		Aceticlastic Methanogen	*Euryarcheota*
38	$S_2O_3^{2-} + H_2O \rightarrow SO_4^{2-} + H^+ + HS^-$		S disproportionation	*δ Proterobacteria-Desulfocapsa* and *Firmicutes-Desulfotomaculum*
24	$S_2O_3^{2-} + 4H_2 \rightarrow 3H_2O + 2HS^-$			
42	Propanoate + $3H_2O \rightarrow$ Acetate + $HCO_3^- + H^+ + 3H_2$		Fermenters	
26	$H_2 + S \rightarrow HS^- + H^+$	S Reducer		*Thermotogales-Thermosipho* *Crenarcheota*
12	Acetate + $4S + 4H_2O \rightarrow 5H^+ + 2HCO_3^- + 4HS^-$			*Crenarcheota*
		Abiogenic Reactions		
43	HS^- + 4Hematite + $15H^+ \rightarrow SO_4^{2-} + 8Fe^{2+} + 8H_2O$			
22	$4CO + 5H_2O \rightarrow CH_4 + 3HCO_3^- + 3H^+$		Fisher-Troph	
27	$3H_2 + CO \rightarrow CH_4 + H_2O$			
34	$CO + 2H_2O \rightarrow HCO_3^- + H^+ + H_2$		Gas Shift Reaction	
29	$3H_2 + N_2 \rightarrow 2NH_3$		N_2 fixation	

Modeling Approach

The modeling involved the following four steps:

1. Geochemist workbench version 4 was utilized to calculate the free energy of the 47 reactions in table 1 for three reservoir temperatures, 20, 45 and 80°C, and for four ground water compositions (see Table 2). We have restricted the maximum temperature to the upper limit for thermophiles, because we have very little evidence to date for the existence of hyperthermophilicity in the deep subsurface with the exception of Stetter et al.'s (Stetter et al., 1993) discovery of hyperthermophilic Archaea associated with oil reservoirs. These four ground water types represent the average of 200 analyses of ground water collected at depths ranging up to 3.2 kmbls. in South Africa and is the only data set with sufficient detailed analyses to permit calculation of the free energy of the reactions in table 1. The coupling of geochemical analyses of ground water with partial equilibrium calculation of the free energy of redox reactions to determine the principal terminal electron acceptor process has been successfully applied to shallow contaminated aquifers (Jakobsen et al., 1998) . The four ground water types include dolomitic water, low salinity meteoric water, moderate salinity water and highly saline water. The dolomitic water is typical of carbonate dominated water and in terms of major cation and anion composition is comparable to that reported for the Madison limestone and Floridian aquifers (Plummer, 1977; Plummer et al., 1994) .
2. The pCO_2 was set 200 bars, equivalent to the hydrostatic pressure at 2 kmbls. and the four groundwater types were equilibrated with this high pCO_2. We assumed that CO_2 injection occurs as a separate phase. The change in pCO_2, pH and pe will impact the free energy for most of the 47 redox reactions in table 1. The formation of a separate phase in a H_2O saturated aquifer will result in a reduction of the dissolved gas concentrations and the amount of reduction will depend upon the volume ratio of gas to fluid. We did not attempt to model this effect, because the gas concentrations in Table 1 probably reflect the formation of a separate methane gas phase during depressurization. We also treated the CO_2 injection as a pulse injection so we could examine the processes that could mitigate the reduction in CO_2.
3. The final parameter variation involved dissolution of aquifer minerals by carbonic acid. For the dolomitic water dolomite and calcite was dissolved until both minerals obtained saturation and the pH and pe stabilized (Plummer, 1977) . In the case of the low salinity, moderate salinity and high salinity ground water, albite and calcite were chosen as the aquifer minerals. These two mineral phases not only appear to control major cation composition of the ground water types in South Africa and also that of saline water associated with petroleum reservoirs in the Gulf Coast (Helgeson et al., 1993) . The dissolution of these two minerals phases proceeded until they both attained saturation at which point pH and pe stabilized. Other minerals were allowed to precipitate during the dissolution reaction. These minerals included sulfide minerals that control trace metal concentrations, clay minerals that mitigate pH and Al concentrations, Chalcedony which controls Si concentrations, and Nahcolite that like Calcite is influenced by the pCO_2. Fe hydroxide surface protonation reactions

were not utilized in the simulations at 20°C, but their effect probably would have been to moderate the acid production of the high pCO_2.

4. To relate the free energy of the microbial redox reactions in Table 1 calculated in the first three steps to microbial activity or ATP production we made three assumptions. The first is that conservation of energy does occur during electron transport processes as first proposed by Thaur et al. (Thauer et al., 1977) for anaerobic reactions occurs for all of the metabolic pathways involved in the 42 microbial redox reactions listed in Table 1. Secondly, we assumed that conversion of this chemical energy to ATP takes place with a maximum efficiency, which is equivalent to saying that a minimum chemical free energy, ΔG, is required for ATP synthesis to occur. For normal bacteria, this minimum energy is 70 kJoules-mole^{-1} of reactant, but under certain conditions, ATP synthesis has been observed to proceed at 20 kJoules-mole^{-1} of reactant (Shink, 1997) and microbial activity has been recorded to occur in the lab at ~12-15 kJoules-mole^{-1} of organic reactant with syntrophic microbial consortia (Jackson and McInerney, 2002) . For the purpose of our calculations we have used a value of 20 kJoules-mole^{-1} as the minimum free energy required for ATP synthesis. Finally, we assumed that the maximum rate at which this energy could be accrued was given by the maximum rate of diffusion of the rate limiting reactant to the microorganism. This rate (moles s^{-1}) is approximately by $4\pi DrC$, where C is the concentration of the rate limiting reactant (moles kg^{-1}), D is the diffusivity of the reactant (cm^{2}-s^{-1}) and r is the radius of the microorganism. We assumed r was 0.5 µm for all simulations. The reactant diffusivity increases with temperature according to the Stokes-Einstein relationship and the values used are from Cussler (Cussler, 1984) . This assumption presumes that deep subsurface microorganisms are nonmotile, which is a safe presumption given their extraordinarily slow rates of growth (Phelps et al., 1994; Kieft and Phelps, 1997) . The potential microbial power (kJoules-s^{-1}) for a specific microbial redox reaction is equal to $4\pi DrC\Delta G$.

For example, 10^{-11} moles of ATP are required to produce one cell when acetate is the energy and carbon substrate. This means that $20x10^{-11}$ kJoules are required to produce one cell. If the potential microbial power for aceticlastic, sulfate reduction was ~10^{-12} joules s^{-1}, then sufficient energy would be accrued after ~200 seconds for a single cell. If the biomass concentration of the groundwater was $8x10^{9}$ cells kg^{-1} and all the cells in the groundwater were sharing in this one reaction, then the average doubling time for the cells would be 1.6 x 10^{11} seconds or ~10^{4} years cell^{-1}. This estimate is comparable to that of Phelps et al. (Phelps et al., 1994) , which was based upon geochemical reaction rates for the Middendorf aquifer calibrated by ^{14}C ages. The expression $4\pi DrC\Delta G$, therefore, offers a reasonable yardstick for assessing metabolic rates. This is considered a maximum potential for microbial power, however, as it ignores enzyme inhibition by competitive species or reactions. In the case of solid reactants, such as S and Fe(III) and Mn(IV) bearing oxides, we have assumed that the limiting reactant is the aqueous phase, not the solid phase, which clearly cannot be true all the time. We have also not corrected for the minimum concentration required for an enzyme to function or to be expressed. Nevertheless, we feel that the potential microbial power values for the different redox reactions can be used to assess the relative importance of one type of metabolism versus another.

Table 2. Geochemical composition of four deep groundwater types used in simulations.

ANIONS (PPM)

Ground Water Type	pH	pe	T°C	TOC (gfw=12)	DOC (gfw=12)	DIC (gfw = 44)	acetate	formate	propanoate	F	Cl
Dol	7.62	0.55	26	17.50	5.00	153.33	0.45	1.80	0.01	2.30	26
LowS	8.86	-3.03	41	1.00	1.50	29.99	0.65	0.09	0.05	3.63	102
ModS	8.78	-3.90	43	8.35	5.14	25.05	1.41	0.20	0.12	2.20	1,274
Brine	8.05	-3.89	44	8.83	13.95	8.52	2.98	1.11	0.67	0.93	13,680

	NO_2^-	SO_4^{2-}	HS^-	$S_2O_3^{2-}$	Br	NO_3^-	PO_4^{2-}	Total P as PO_4^{2-}	I
Dol	0.005	79.08	20.39	0.01	0.59	0.54	0.010	1.07	0.48
LowS	0.004	14.97	26.17	0.43	1.12	0.04	0.018	0.03	
ModS	0.060	34.42	15.53	0.87	6.50	0.16	0.011	2.08	0.87
Brine	0.069	120.93	20.72	0.68	76.02	0.14	0.024	6.16	3.22

CATIONS AND TRACE METALS(PPM)

	NH_3 (gfw=14)	Li	Na	Mg	K	Rb	Ca	Sr	Ba	Al	Si
Dol	0.02	0.01	16	29.62	1.41	0.003	57	0.169	0.131	0.468	7.38
LowS	0.18	0.07	78	0.07	2.11	0.181	11	0.156	0.017	0.061	15.45
ModS	0.42	0.49	555	2.93	6.67	0.071	197	4.202	0.649	0.267	9.28
Brine	0.45	2.85	3,876	134.41	46.99	0.826	3,619	96.828	15.172	0.261	8.12

	Mn	Fe	Mo	Cr	Co	Ni	Cu	Zn	As	W	U
Dol	0.042	0.309	0.020	0.037	0.007	0.020	0.008	0.030	0.0250	0.0296	0.0220
LowS	0.004	0.201	0.182	0.004	0.002	0.015	0.038	0.008	0.0115	0.0779	0.0239
ModS	0.746	0.328	0.050	0.019	0.002	0.011	0.007	0.068	0.0293	0.0726	0.0349
Brine	2.527	8.063		0.020	0.004	0.052	0.024	0.037	0.0574	0.0868	0.1027

DISSOLVED GASES (µMOLAR)

	H_2	He	Ar	N_2	CH_4	C_2H_6	C_3H_8	iso-C_4	n-C_4	CO
Dol	0.97	1.30	7.00	350.00	104.91	0.00	0.00	0.00	0.00	0.37
LowS	0.13	162.49	9.64	1,907.54	1,150.95	62.84	12.98	0.25	0.88	0.34
ModS	181.47	441.44	62.63	4,019.32	6,223.95	109.68	13.14	0.29	1.74	11.44
Brine	515.20	1,082.57	148.86	3,625.57	10,740.75	603.77	55.36	0.46	5.25	69.94

Results

Initial Conditions

The four groundwater types exhibit the following trends with increasing salinity and temperature (deeper ground water tends to be hotter and more saline):

1. The pe becomes more negative. As reliable dissolved O_2 measurements are difficult to make when concentrations are close to the detection limit of 0.3 mmolar, we have utilized the fO_2 predicted by the pe as our estimate of the dissolved O_2 for the model simulations.
2. With the exception of the dolomite water the pH decreases.
3. Sulfate concentrations increase while sulfide concentrations are relatively uniform.
4. The Fe and Mn concentrations increase.
5. Dissolved reduced gases and hydrocarbons increase.
6. Trace levels of nitrate and nitrite are present throughout with the highest nitrate concentration associated with the dolomite water.
7. The ammonia concentration increases.
8. The concentration of organic acids increases, whereas the concentration of inorganic carbon decreases.

These trends, particularly the increasing dissolved organic acids and reducing potential with depth or temperature is consistent with observations of pore water and ground water from basins where organic matter is far more abundant than our South African aquifers. With the dolomite, moderate salinity and highly saline groundwater, calcite is saturated and the concentration of the decreasing DIC is a direct reflection of the increasing Ca concentrations and elevated pH. If the pH were to remain constant during CO_2 injection, the Ca concentrations would remove a large fraction of the CO2 and precipitate it as calcite. The degree to which the microorganisms would facilitate such a process is a subject for the next stage of investigation (see Conclusions).

The first and most important question to be answered by the modeling is as follows. Do any of the microbial redox reactions that yield negative free energies for our subsurface groundwater types become positive under the conditions anticipated to occur with CO_2 injection? This would be considered a detrimental impact on those subsurface microorganisms relying upon those specific redox reactions.

The free energy and potential microbial power calculations for the four types of groundwater (Tables 3 and 4) provide a baseline against which to compare the community structure inferred from the 16S rDNA results and the simulated geochemical changes associated with CO_2 injection. The free energy calculations revealed the following.

1. The two microbial redox reactions that are the most obviously relevant to CO_2 injection are the CO_2 reducing methanogenesis and acetogenesis reactions (reactions 32 and 37 in Table 3 and Fig. 10). The free energy for both reactions decrease with increasing temperature and are marginally exothermic in the dolomitic and low salinity groundwater type where dissolved H_2 concentrations are <1 μM (Table 2),

but are exothermic in the moderate and high salinity water where H_2 concentrations are >100 µM.

2. Four all four groundwater types the ammonia oxidizing and the Mn oxidizing reactions were all positive regardless of temperature (reactions 44 to 47 in Table 3 and Fig. 10). The implication is that in order for these reactions to proceed the O_2 concentrations must be much higher than is typical even for microaerophilic ground water. This is also consistent with the absence of Nitrifying and Mn oxidizing organisms from the 16S rDNA results for aquifers. Nitrifying bacteria have been found associated with the more oxygenated drilling water. Anaerobic ammonia oxidation by reduction of nitrite, the anammox reaction (reaction 14 in Table 3 and Fig. 10) is energetically favorable in all four groundwater types, but the microorganisms associated with this reaction belong to the order of the *Planctomycetales* (Kuenen and Jetten, 2001) and the 16S rDNA signatures of this order have yet to be identified in the deep subsurface, although the anammox reaction has been detected in shallow marine sediments (Dalsgaard and Thamdrup, 2002; Thamdrup and Dalsgaard, 2002) .
3. Conversely Mn reduction (reaction 5 in Table 3 and Fig. 10) and nitrate reduction (reactions 1 to 4, 6 to 10 and 13) possessed highly negative free energies. Of the nitrate reducing reactions, those yielding N_2 as the product (reactions 1, 2, 6 and 13 in Table 3 and Fig. 10) were more exothermic than those yielding ammonia (reactions 3, 4 and 7 to 10 in Table 3 and Fig. 10).
4. Despite the extremely low concentrations of dissolved O_2 predicted by measured pe for the four groundwater types, aerobic reactions (reactions 11, 15 to 19, 21, 23 and 25 in Table 3 and Fig. 10) still retained highly negative free energies. These free energies increase with temperature as fO_2 increases. The most energetic reaction is acetate oxidation (reaction 11 in Table 3 and Fig. 10) followed by CH_4, thiosulfate, CO, HS^-, S, H_2 and the least exothermic aerobic reaction is oxidation of HS^- to S (reaction 25 in Table 3 and Fig. 10).
5. Reduction of S compounds to HS^- (reactions 12, 24, 26, 28, 31 and 35 in Table 3 and Fig. 10) are energetically favorable. The most exothermic reaction is the reduction of S to HS^- by acetate (reaction 12 in Table 3 and Fig. 10). The free energies of S reduction reactions with acetate increase with increasing temperature, whereas those with H_2 decrease with increasing temperature.
6. The anaerobic oxidation of CH_4 coupled to the reduction of SO_4^{2-} to HS^- is the least exothermic S reducing reaction. This reaction has been detected in shallow, anoxic marine sediments and methane clathrates where it appears to require the syntrophic activity of two microorganisms, one of which is a sulfate reducing bacteria. The free energy yields increase slightly with increasing CH_4 and SO_4^{2-} concentrations, but remain < -70 kJoules-mole^{-1}.

The free energy for reduction of hematite to Fe^{2+} is pH and temperature dependent with the reaction favored for low pH and low temperature (reactions 39 and 41 in Table 3 and Fig. 10). This holds true for the other Fe(III) oxides as well. In this report we have restricted the analysis to hematite under the presumption that amorphous $Fe(OH)_3$ and goethite would be the first phases to be reduced leaving hematite as the sole, remaining, Fe(III) oxide for deep, anaerobic environments. Microbial reduction of magnetite would

Table 3. Free energy (kJoules-mole^{-1}) for redox/microbial reactions in dolomitic, low salinity, moderate salinity and highly saline groundwater.

Microbial Redox Reactions*	1. Do 20	2. Do 45	3. Do 80	4. LS 20	5. LS 45	6. LS 80	7. MS 20	8. MS 45	9. MS 80	10. Br 20	11. Br 45	12.Br 80
1. $5H_2 + 2NO_3^- + 2H^+ -> N_2 + 6H_2O$	-983	-957	-920	-923	-892	-848	-1225	-993	-961	-1249	-1015	-984
2. Acetate + $1.6NO_3^- + 0.6H^+ -> 2HCO_3^- + 0.8H_2O + 0.8N_2$	-749	-744	-739	-736	-731	-725	-896	-740	-735	-907	-750	-747
3. $2S + 1.5NO_3^- + 3.5H_2O -> 2SO_4^{2-} + 2.5H^+ + 1.5NH_3$	-700	-700	-699	-697	-699	-702	-840	-698	-702	-833	-691	-690
4. $4CO + NO_3^- + 5H_2O -> 4HCO_3^- + NH_3 + 3H^+$	-655	-645	-627	-673	-665	-654	-855	-707	-703	-884	-732	-728
5. Acetate + $4MnO_2 + 7H^+ -> 4Mn^{2+} + 4H_2O + 2HCO_3^-$	-648	-631	-609	-627	-609	-584	-708	-567	-540	-790	-642	-626
6. $2.5CO + NO_3^- + 2H_2O -> 2.5HCO_3^- + 1.5H^+ + 0.5N_2$	-567	-559	-547	-576	-569	-559	-724	-597	-591	-740	-612	-608
7. $4H_2 + NO_3^- + H^+ -> NH_3 + 3H_2O$	-535	-516	-488	-490	-468	-439	-678	-547	-526	-700	-565	-543
8. Acetate + $NO_3^- + H_2O -> 2HCO_3^- + NH_3$	-497	-494	-490	-487	-485	-484	-594	-491	-492	-608	-503	-502
9. $S_2O_3^{2-} + NO_3^- + 2H_2O -> 2SO_4^{2-} + H^+ + NH_3$	-463	-458	-444	-468	-465	-462	-565	-466	-463	-560	-460	-455
10. $HS^- + NO_3^- + H_2O -> SO_4^{2-} + NH_3$	-448	-441	-432	-437	-430	-423	-525	-429	-422	-529	-432	-422
11. Acetate + $2O_2 -> 2HCO_3^- + H^+$	-264	-295	-336	-179	-203	-234	-166	-158	-186	-130	-126	-150
12. Acetate + $4S + 4H_2O -> 5H^+ + 2HCO_3^- + 4HS^-$	-264	-295	-336	-179	-203	-234	-166	-158	-186	-130	-126	-150
13. $5Fe^{2+} + NO_3^- + 12H_2O -> 5Fe(OH)_3 + 9H^+ + 0.5N_2$	-272	-294	-323	-324	-349	-385	-388	-347	-382	-372	-333	-365
14. $NO_2^- + H^+ + NH_3 -> 2H_2O + N_2$	-297	-293	-287	-291	-285	-275	-358	-292	-284	-358	-293	-287
15. $CH_4 + 2O_2 -> HCO_3^- + H^+ + H_2O$	-242	-271	-310	-158	-180	-209	-142	-136	-161	-102	-101	-122
16. $S_2O_3^{2-} + 2O_2 + H_2O -> 2SO_4^{2-} + 2H^+$	-230	-259	-290	-160	-182	-212	-137	-132	-156	-82	-83	-102
17. $HS^- + 2O_2 -> SO_4^{2-} + H^+$	-215	-242	-278	-128	-147	-172	-98	-96	-115	-52	-55	-70
18. $2HS^- + 2O_2 -> S_2O_3^{2-} + H_2O$	-200	-225	-266	-97	-112	-132	-58	-60	-74	-21	-26	-37
19. $2CO + O_2 + 2H_2O -> 2HCO_3^- + 2H^+$	-211	-223	-236	-182	-191	-202	-214	-187	-198	-203	-177	-188
20. $4CO + SO_4^{2-} + 4H_2O -> 4HCO_3^- + HS^- + 3H^+$	-207	-203	-194	-236	-236	-231	-330	-278	-281	-355	-300	-306
21. $S + 1.5O_2 + H_2O -> SO_4^{2-} + 2H^+$	-175	-200	-234	-118	-137	-163	-99	-99	-121	-58	-63	-81
22. $4CO + 5H_2O -> CH_4 + 3HCO_3^- + 3H^+$	-180	-174	-163	-206	-203	-195	-286	-237	-235	-304	-254	-254
23. $2H_2 + O_2 -> 2H_2O$	-151	-158	-167	-91	-93	-94	-125	-107	-110	-111	-94	-95

24. $S_2O_3^{2-} + 4H_2$ -> $3H_2O + 2HS^-$	-102	-91	-67	-85	-73	-56	-192	-154	-145	-201	-162	-154
25. $2HS^- + O_2 + 2H^+$ -> $2S + 2H_2O$	-80	-83	-89	-22	-20	-18	3	7	12	14	16	22
26. $H_2 + S$ -> $HS^- + H^+$	-76	-79	-83	-45	-46	-47	-63	-53	-55	-55	-47	-48
27. $3H_2 + CO$ -> $CH_4 + H_2O$	-90	-78	-58	-69	-55	-33	-153	-117	-102	-166	-129	-115
28. $4H_2 + H^+ + SO_4^{2} \rightarrow HS^- + 4H_2O$	-87	-74	-55	-53	-38	-16	-153	-117	-104	-170	-133	-121
29. $3H_2 + N_2$ -> $2NH_3$	-87	-74	-55	-57	-44	-29	-131	-100	-90	-150	-115	-102
30. 4Formate + $H^+ + H_2O$ -> $CH_4 + 3HCO_3^-$	-77	-69	-60	-47	-37	-24	-63	-44	-33	-91	-69	-61
31. Acetate + $SO_4^{2} \rightarrow 2HCO_3^- + HS^-$	-49	-53	-58	-51	-55	-62	-68	-62	-70	-79	-71	-80
32. $4H_2 + H^+ + HCO_3^-$ -> $CH_4 + 3H_2O$	-61	-45	-24	-24	-5	21	-108	-77	-58	-120	-87	-69
33. CO + Hematite + $3H^+$ -> $2Fe^{2+} + H_2O + HCO_3^-$	-54	-41	-20	-37	-23	-1	-58	-34	-15	-70	-46	-28
34. $CO + 2H_2O$ -> $HCO_3^- + H^+ + H_2$	-30	-32	-35	-46	-49	-54	-44	-40	-44	-46	-42	-46
35. $CH_4 + SO_4^{2} \rightarrow H_2O + HCO_3^- + HS^-$	-27	-29	-32	-30	-33	-37	-44	-41	-46	-51	-46	-52
36. Acetate + H_2O -> $CH_4 + HCO_3^-$	-22	-24	-26	-21	-23	-25	-24	-21	-24	-28	-25	-28
37. $4H_2 + H^+ + 2HCO_3^-$ -> Acetate + $4H_2O$	-38	-22	2	-3	17	46	-84	-55	-33	-92	-62	-41
38. $S_2O_3^{2-} + H_2O$ -> $SO_4^{2-} + H^+ + HS^-$	-15	-17	-12	-32	-35	-40	-39	-36	-41	-31	-29	-33
39. Acetate + 4Hematite + $15H^+$ -> $8Fe^{2+} + 8H_2O + 2HCO_3^-$	-59	-12	55	35	90	167	30	78	152	-5	46	114
40. $4Fe^{2+} + O_2 + 10H_2O$ -> $4Fe(OH)_3 + 8H^+$	24	-10	-57	19	-15	-63	55	13	-31	91	46	6
41. H_2 + Hematite + $4H^+$ -> $2Fe^{2+} + 3H_2O$	-24	-8	14	8	27	53	-13	6	30	-24	-4	18
42. Propanoate + $3H_2O$ -> Acetate + $HCO_3^- + H^+ + 3H_2$	23	10	-9	-6	-22	-44	56	35	17	63	41	24
43. HS^- + 4Hematite + $15H^+$ -> $SO_4^{2-} + 8Fe^{2+} + 8H_2O$	-10	41	112	86	145	229	99	140	222	74	117	195
44. $NH_3 + 1.5O_2$ -> $NO_2^- + H^+ + H_2O$	157	130	99	211	190	163	302	232	210	342	267	246
45. $4Mn^{2+} + NO_3^- + 5H_2O$ -> $4MnO_2 + 7H^+ + NH_3$	151	138	118	139	123	99	114	76	48	182	139	124
46. $2NO_2^- + O_2$ -> $2NO_3^-$	151	140	124	194	186	174	253	203	194	271	220	212
47. $2Mn^{2+} + O_2 + 2H_2O$ -> $2MnO_2 + 4H^+$	192	168	136	224	203	175	271	205	177	330	258	238

*The reactions are ordered from most negative to positive with respect to the free energy for the dolomite groundwater at 20°C. The microbial reaction numbers and column heading numbers refer to Fig. 10.

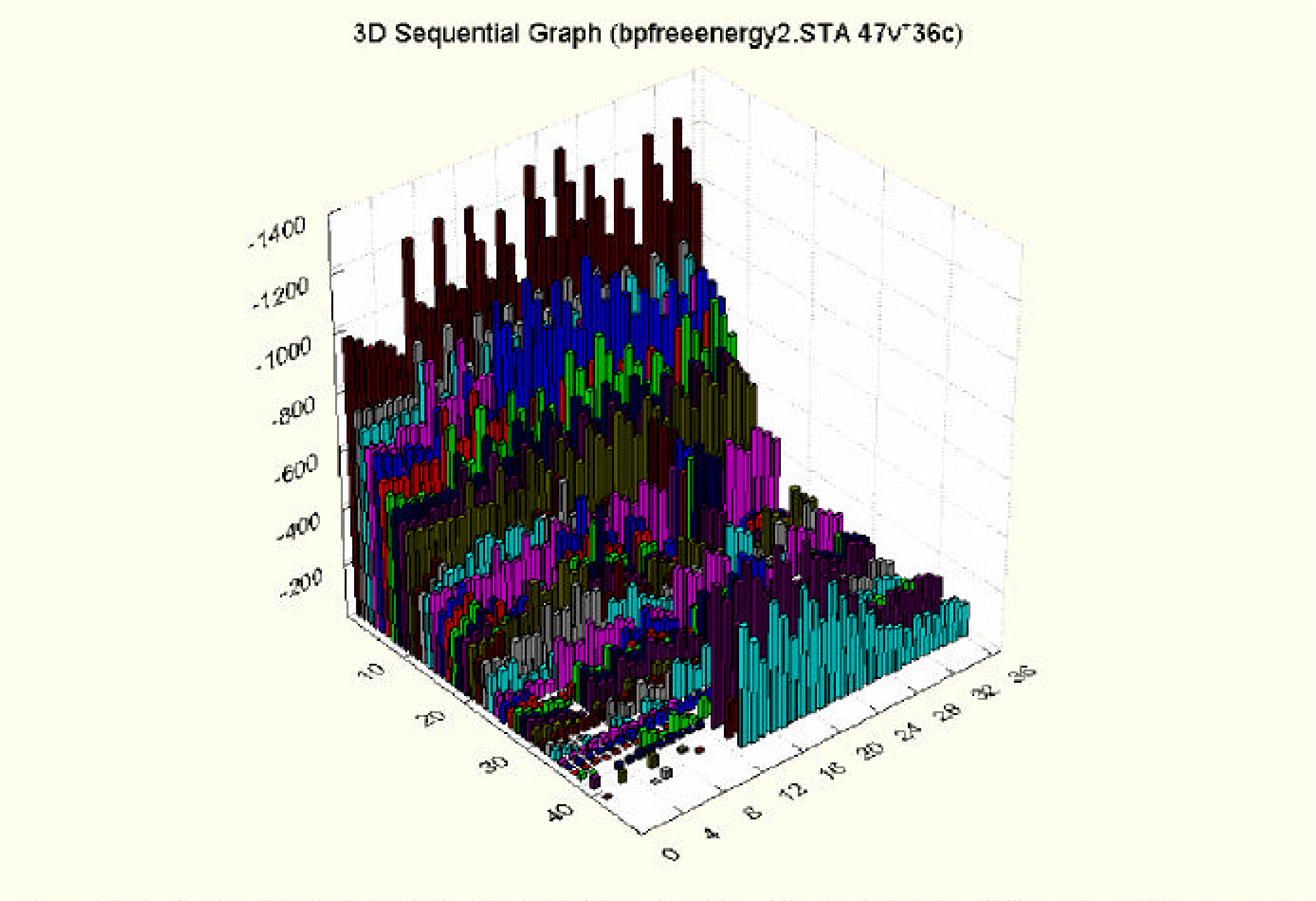

Fig. 10. Free energy in kJoules-mole^{-1} for microbial reactions and simulations defined in Tables 3, 5 and 7.

require even lower pH's than is typical of these environments. In the absence of a reaction that would regenerate Fe(OH)3 our model would suggest that microbial Fe(III) reduction would be restricted to mesophilic environments for groundwater with pH ~ 7.5. Because microbial Fe(III) reduction by either acetate or H_2 raises the pH of the environment this represents a severe restriction unless the aquifer is buffered to lower a lower pH or an acid producing reaction occurs at a comparable rate.

7. The free energy for oxidation of Fe^{2+} to $Fe(OH)_3$ is also pH and temperature dependent with the reaction favored for high temperatures and high pH (reactions 13 and 40 in Table 3 and Fig. 10). Fe^{2+} oxidation is weakly favored even for the minute amounts of dissolved O_2 present in our simulations. Fe^{2+} oxidation by nitrate, however, is strongly exothermic even for trace amounts of nitrate.
8. Of the organic fermentation reactions formate fermentation to CH_4 and CO_2 (reaction 30 in Table 3 and Fig. 10) was the most exothermic, followed acetate fermentation to CH_4 and CO_2 (reaction 36 in Table 3 and Fig. 10) and propionate fermentation to acetate, CO_2 and H_2 (reaction 42 in Table 3 and Fig. 10). The free energy for the formate reaction decreased with increasing temperature. The free energy for the acetate fermentation was remarkably constant at ~25 kJoules-mole^{-1} regardless of temperature or groundwater type. The free energy for propionate fermentation increased with decreasing temperature and was only microbially favored for the high temperature, low salinity water where the dissolved H_2 concentrations were <0.1 µM. Inorganic fermentation of thiosulfate, or thiosulfate disproportionation, is marginally favorable and sensitive to the pH of the groundwater with the free energy increasing as the pH increases. The free energy for formation of acetate from CO_2 and H_2 (reaction 37 in Table 3 and Fig. 10) was slightly greater than that of acetate fermentation to CH_4 and CO_2 with the exception of the low salinity water with H_2 concentrations ~0.1 µM. This suggests that if µM concentrations of H_2 are maintained that the conversion of CO_2 to CH_4 via acetogenesis and aceticlastic methanogenesis is viable. The production of H_2 by fermentation of propionate (or for that matter benzoate or butyrate) is not energetically favorable unless the H_2 concentrations ~0.1 µM. In other words, organic fermentative production of H_2 will not sustain the conversion of CO_2 to CH_4 for the conditions encountered in the deep subsurface and alternative abiotic reactions are required to do so.
9. Abiotic conversion of CO to H_2 and CO_2 or the Gas shift reaction (reaction 34 in Table 3 and Fig. 10) represents a possible source of H_2, is favorable even for the highly saline water with the highest dissolved H_2 concentrations and its free energy is greater than that of acetogenesis. A competing reaction for consumption of CO, however, is the abiotic conversion of CO to CH_4 and CO_2 or the Fischer-Tropsch reaction (reaction 22 in Table 3 and Fig. 10). This is energetically favorable for all groundwater types and has a greater free energy than the Gas shift reaction, but its free energy decreases with increasing temperature. This reaction is most favored for the highly saline groundwater probably because of the lower HCO_3^- and pH of this groundwater. This suggests that if the CO_2 produced by this reaction is converted to carbonate, then the Fischer-Tropsch reaction may compete with microbial conversion of CO_2 to methane. The abiotic conversion of H_2 to N_2 and NH_3 is favorable for all four groundwater types, becomes less favorable with increasing temperature, but is

strongly favored for environments where H_2 concentrations are high. The rates for the Gas shift, Fischer-Tropsch and ammonia generation reactions are unknown and at the temperatures modeled in this report depend upon the catalyst available (e.g. metal oxides or sulfides).

10. The normally rapid and abiotic reduction of hematite by oxidation of HS^- to SO_4^{2-} (reactions 43 in Table 3 and Fig. 10) is also not favored because of the high pH of these groundwater types. The reaction becomes slightly less positive if goethite or amorphous $Fe(OH)_3$ is considered, but this reaction is extremely sensitive to the pH regardless of the choice of Fe(III) oxides and for this pH range the free energy is close to zero or positive.

The potential microbial power calculations revealed that the most exothermic reactions were not the most powerful reactions. The microbial redox reactions were ordered in Table 4 and Figure 11 to reflect their importance and this revealed the following:

1. Many of the H_2 oxidizing reactions, such as the reduction of S and SO_4^{2-} to HS^- (reactions 1 and 3 in Table 4 and Fig. 11), the abiotic production of ammonia (reaction 2 in Table 4 and Fig. 11), methanogenesis and acetogenesis (reactions 7 and 12 in Table 4 and Fig. 11) were the most powerful reactions despite the low free energy yields for some of these reactions. This directly corresponded to the high H_2 concentration as the power varied by four orders of magnitude from the dolomite water, 10^{-13} kJoules-s^{-1}, to the highly saline water 10^{-9} kJoules-s^{-1}, and with diffusivity as the power increases by a factor of two from 20 to 80°C.
2. The anaerobic methane oxidation reaction (reactions 3 in Table 4 and Fig. 11) is the third most powerful reaction despite its low free energy yield for highly saline water and its power increases by two orders of magnitude from the dolomite water, 10^{-11} kJoules-s^{-1}, to the highly saline water, 10^{-19} kJoules-s^{-1}. This is a reflection of the high concentrations and diffusivities of its reactants.
3. Acetate oxidizing coupled with the reduction of MnO_2 to Mn^{2+}, and reduction of S and SO_4^{2-} to HS^- (reactions 5, 10 and 13 in Table 4 and Fig. 11) yield high potential power, 10^{-11} to 10^{-10} kJoules-s^{-1}, because of their high free energies and the amount and diffusivity of acetate.
4. CO consuming reactions (reactions 6, 8, 9 and 11 in Table 4 and Fig. 11), such as the Fischer-Tropsch reaction, are quite powerful reactions for the highly saline water. Their power values increase by three orders of magnitude from the dolomite water, 10^{-13} kJoules-s^{-1}, to the highly saline water, 10^{-10} kJoules-s^{-1}, and like the H_2 consuming reactions the value depends upon the CO concentration.

In the low salinity to highly saline groundwater all of the nitrate-reducing reactions (reactions 14-22 and 28 in Table 4 and Fig. 11) were nitrate limited and the annamox reaction nitrite limited (reaction 25 in Table 4 and Fig. 11). In the dolomite water, however, the electron donor was limiting. Because these reactions yielded the greatest free energy, however, the power of nitrate reducing reactions ranged from 10^{-12} to 10^{-10} kJoules-s^{-1}. These power values are comparable to those for the reduction of Fe(III) oxides (reactions 39 and 41 in Table 4 and Fig. 11). The potential microbial power for Fe^{2+} oxidation by nitrate (reaction 28 in Table 4 and Fig. 11) and reduction of hematite (reactions 30 and 31 in Table 4 and Fig. 11) are quite similar

Table 4. Potential microbial power in kJoules-s^{-1} for four types of groundwater.

Microbial Redox Reactions*	1. Do 20	2. Do 45	3. Do 80	4. LS 20	5. LS 45	6. LS 80	7. MS 20	8. MS 45	9. MS 80	10. Br 20	11. Br 45	12.Br 80
1. $H_2 + S$ -> $HS^- + H^+$	-1.8E-12	-3.2E-12	-5.8E-12	-1.5E-13	-2.5E-13	-4.4E-13	-2.8E-10	**-4.0E-10**	-6.9E-10	-6.9E-10	**-9.8E-10**	-1.7E-09
2. $3H_2 + N_2$-> $2NH_3$	-6.8E-13	-9.9E-13	-1.3E-12	-6.1E-14	-7.9E-14	-9.1E-14	-1.9E-10	-2.5E-10	-3.8E-10	-6.2E-10	-8.0E-10	-1.2E-09
3. $CH_4 + SO_4^{2-}$-> $H_2O + HCO_3^- + HS^-$	**-2.1E-11**	-4.0E-11	-7.3E-11	-4.2E-11	**-7.8E-11**	-1.5E-10	-1.3E-10	**-1.9E-10**	-3.7E-10	-3.9E-10	**-5.9E-10**	-1.1E-09
4. $4H_2 + H^+ + SO_4^{2-}$-> $HS^- + 4H_2O$	-5.1E-13	-7.5E-13	-9.7E-13	-4.3E-14	-5.1E-14		-1.7E-10	**-2.2E-10**	-3.3E-10	-5.3E-10	**-6.9E-10**	-1.1E-09
5. Acetate + $4MnO_2 + 7H^+$ -> $4Mn^{2+} + 4H_2O + 2HCO_3^-$	**-3.1E-11**	-5.3E-11	-8.7E-11	-4.6E-11	**-7.5E-11**	-1.2E-10	-9.4E-11	**-1.3E-10**	-2.0E-10	-2.1E-10	**-2.9E-10**	-4.7E-10
6. $3H_2 + CO$ -> $CH_4 + H_2O$	-7.1E-13	-1.0E-12	-1.4E-12	-7.4E-14	-9.9E-14	-1.0E-13	-1.7E-11	-2.2E-11	-3.2E-11	-1.3E-10	-1.7E-10	-2.5E-10
7. $4H_2 + H^+ + HCO_3^-$ -> $CH_4 + 3H_2O$	-3.6E-13	-4.6E-13	-4.1E-13	-1.9E-14			-1.2E-10	**-1.4E-10**	-1.8E-10	-1.3E-10	**-1.5E-10**	-2.1E-10
8. $4CO + SO_4^{2-} + 4H_2O$ -> $4HCO_3^-$ + HS- + $3H^+$	-2.2E-13	-3.7E-13	-6.1E-13	-2.2E-13	-3.8E-13	-6.4E-13	-9.2E-12	-1.3E-11	-2.2E-11	-6.9E-11	**-9.8E-11**	-1.7E-10
9. $4CO + 5H_2O$ -> $CH_4 + 3HCO_3^- + 3H^+$	-2.0E-13	-3.2E-13	-5.1E-13	-1.9E-13	-3.2E-13	-5.4E-13	-8.0E-12	-1.1E-11	-1.9E-11	-5.9E-11	-8.3E-11	-1.4E-10
10. Acetate + $4S + 4H_2O$ -> $5H^+ + 2HCO_3^- + 4HS^-$	**-1.3E-11**	-2.5E-11	-4.8E-11	-1.3E-11	**-2.5E-11**	-4.8E-11	-2.2E-11	**-3.5E-11**	-7.0E-11	-3.5E-11	**-5.6E-11**	-1.1E-10
11. CO + Hematite + $3H^+$ -> $2Fe^{2+} + H_2O + HCO_3^-$	-2.4E-13	-3.0E-13	-2.6E-13	-1.4E-13	-1.4E-13		-6.5E-12	-6.4E-12		-5.5E-11	**-6.0E-11**	-6.1E-11
12. $4H_2 + H^+ + 2HCO_3^-$ -> Acetate + $4H_2O$	-2.2E-13	-2.2E-13					-9.4E-11	**-1.0E-10**	-1.1E-10	-4.8E-11	**-5.5E-11**	-6.1E-11
13. Acetate + SO_4^{2-}-> $2HCO_3^- + HS^-$	-2.4E-12	-4.4E-12	-8.3E-12	-3.7E-12	**-6.8E-12**	-1.3E-11	-9.1E-12	-1.4E-11	-2.6E-11	-2.1E-11	**-3.2E-11**	-6.0E-11
14. $4CO + NO_3^- + 5H_2O$ -> $4HCO_3^- + NH_3 + 3H^+$	-7.1E-13	-1.2E-12	-2.0E-12	-6.2E-13	-1.1E-12	-1.8E-12	-2.4E-11	**-3.4E-11**	-5.7E-11	-2.5E-11	-3.5E-11	-5.9E-11
15. $2.5CO + NO_3^- + 2H_2O$ -> $2.5HCO_3^- + 1.5H^+ + 0.5N_2$	-9.9E-13	-1.6E-12	-2.8E-12	-8.5E-13	-1.5E-12	-2.5E-12	-2.1E-11	**-2.9E-11**	-4.8E-11	-2.1E-11	-2.9E-11	-4.9E-11
16. $S_2O_3^{2-} + NO_3^- + 2H_2O$ -> $2SO_4^{2-} + H^+ + NH_3$	-2.2E-13	-3.7E-13	-6.1E-13	-5.3E-12	**-8.9E-12**	-1.5E-11	-2.1E-11	**-2.9E-11**	-4.8E-11	-2.1E-11	-2.9E-11	-4.9E-11
17. $4H_2 + NO_3^- + H^+$ -> $NH_3 + 3H_2O$	**-3.1E-12**	-5.2E-12	-8.5E-12	-3.9E-13	-6.3E-13	-1.0E-12	-1.9E-11	-2.6E-11	-4.2E-11	-2.0E-11	-2.7E-11	-4.4E-11
18. Acetate + $NO_3^- + H_2O$ -> $2HCO_3^- + NH_3$	**-2.4E-11**	-4.1E-11	-7.0E-11	-4.5E-12	**-7.7E-12**	-1.3E-11	-1.4E-11	-2.3E-11	-3.9E-11	-1.7E-11	-2.4E-11	-4.0E-11
19. $5H_2 + 2NO_3^- + 2H^+$ -> $N_2 + 6H_2O$	**-4.6E-12**	-7.7E-12	-1.3E-11	-4.5E-12	**-7.5E-12**	-1.2E-11	-1.3E-11	-2.1E-11	-3.4E-11	-1.7E-11	-2.4E-11	-3.9E-11
20. $2S + 1.5NO_3^- + 3.5H_2O$ -> $2SO_4^{2-} + 2.5H^+ + 1.5NH_3$	**-5.7E-11**	-9.6E-11	-1.7E-10	-4.2E-12	**-7.3E-12**	-1.2E-11	-1.6E-11	-2.2E-11	-3.8E-11	-1.6E-11	-2.2E-11	-3.7E-11
21. Acetate + $1.6NO_3^- + 0.6H^+$ -> $2HCO_3^- + 0.8H_2O + 0.8N_2$	**-3.6E-11**	-6.2E-11	-1.1E-10	-4.3E-12	**-7.3E-12**	-1.2E-11	-1.3E-11	-2.2E-11	-3.7E-11	-1.6E-11	-2.2E-11	-3.7E-11
22. $HS^- + NO_3^- + H_2O$ -> $SO_4^{2-} + NH_3$	**-5.5E-11**	-9.1E-11	-1.6E-10	-4.0E-12	**-6.7E-12**	-1.1E-11	-1.5E-11	-2.1E-11	-3.4E-11	-1.5E-11	-2.1E-11	-3.4E-11
23. $CO + 2H_2O$ -> $HCO_3^- + H^+ + H_2$	-3.3E-14	-5.9E-14	-1.1E-13	-4.2E-14	-7.9E-14	-1.5E-13	-1.2E-12	-1.9E-12	-3.5E-12	-9.0E-12	-1.4E-11	-2.5E-11

24. Acetate + H_2O -> CH_4 + HCO_3^-	-1.1E-12	-2.0E-12	-3.7E-12	-1.6E-12	-2.8E-12	-5.2E-12	-3.2E-12	-4.8E-12	-9.1E-12	-7.4E-12	-1.1E-11	-2.1E-11
25. NO_2^- + H^+ + NH_3-> $2H_2O$ + N_2	-9.1E-13	-1.5E-12	-2.7E-12	-3.8E-13	-5.2E-13	-1.1E-12	-5.5E-12	-7.6E-12	-1.2E-11	-8.3E-12	-1.1E-11	-1.9E-11
26. $S_2O_3^{2-}$ + $4H_2$ -> $3H_2O$ + $2HS^-$	-4.9E-14	-7.4E-14	-9.2E-14	-6.8E-14	-9.9E-14	-1.3E-13	-8.4E-12	-1.1E-11	-1.8E-11	-6.6E-12	-9.0E-12	-1.4E-11
27. 4Formate + H^+ + H_2O -> CH_4 + $3HCO_3^-$	**-5.9E-12**	-9.1E-12	-1.4E-11	-1.8E-13	-2.5E-13	-2.8E-13	-5.2E-13	-6.0E-13	-7.8E-13	-3.7E-12	-4.8E-12	-7.1E-12
28. $5Fe^{2+}$ + NO_3^- + $12H_2O$ -> $5Fe(OH)_3$ + $9H^+$ + $0.5N_2$	**-3.2E-12**	-5.7E-12	-1.1E-11	-5.9E-13	-1.1E-12	-2.0E-12	-2.2E-12	-3.3E-12	-6.2E-12	-2.1E-12	-3.2E-12	-5.9E-12
29. $S_2O_3^{2-}$ + H_2O -> SO_4^{2-} + H^+ + HS^-				-6.6E-13	-1.2E-12	-2.5E-12	-1.7E-12	-2.7E-12	-5.1E-12	-1.0E-12	-1.6E-12	-3.0E-12
30. Acetate + 4Hematite + $15H^+$ -> $8Fe^{2+}$ + $8H_2O$ + $2HCO_3^-$	-2.9E-12											
31. H_2 + Hematite + $4H^+$ -> $2Fe^{2+}$+ $3H_2O$	-1.4E-12									-6.2E-11		
32. Propionate + $3H_2O$ -> Acetate + HCO_3^- + H^++ $3H_2$					-1.4E-13	-5.1E-13						
33. 2CO + O_2+ $2H_2O$ -> $2HCO_3^-$ + $2H^+$	-2.4E-61	-4.3E-54	-7.7E-46	-2.1E-70	-3.7E-64	-6.6E-56	-2.5E-74	-3.6E-67	-6.5E-59	-2.3E-77	-3.4E-70	-6.1E-62
34. $2H_2$ + O_2-> $2H_2O$	-1.7E-61	-3.1E-54	-5.4E-46	-1.0E-70	-1.8E-64	-3.1E-56	-1.4E-74	-2.1E-67	-3.6E-59	-1.3E-77	-1.8E-70	-3.1E-62
35. Acetate + $2O_2$-> $2HCO_3^-$ + H^+	-1.5E-61	-2.9E-54	-5.5E-46	-1.0E-70	-2.0E-64	-3.8E-56	-9.6E-75	-1.5E-67	-3.0E-59	-7.5E-78	-1.2E-70	-2.4E-62
36. CH_4+ $2O_2$-> HCO_3^- + H^+ + H_2O	-1.4E-61	-2.6E-54	-5.0E-46	-9.1E-71	-1.7E-64	-3.4E-56	-8.2E-75	-1.3E-67	-2.6E-59	-5.9E-78	-9.8E-71	-2.0E-62
37. S + $1.5O_2$ + H_2O -> SO_4^{2-}+ $2H^+$	-1.3E-61	-2.6E-54	-5.1E-46	-9.0E-71	-1.8E-64	-3.5E-56	-7.6E-75	-1.3E-67	-2.6E-59	-4.5E-78	-8.1E-71	-1.8E-62
38. $S_2O_3^{2-}$ + $2O_2$+ H_2O -> $2SO_4^{2-}$+ $2H^+$	-1.3E-61	-2.5E-54	-4.7E-46	-9.2E-71	-1.8E-64	-3.5E-56	-7.9E-75	-1.3E-67	-2.5E-59	-4.7E-78	-8.1E-71	-1.7E-62
39. HS^-+ $2O_2$-> SO_4^{2-}+ H^+	-1.2E-61	-2.3E-54	-4.5E-46	-7.4E-71	-1.4E-64	-2.8E-56	-5.6E-75	-9.3E-68	-1.9E-59	-3.0E-78	-5.3E-71	-1.1E-62
40. $2HS^-$ + $2O_2$ -> $S_2O_3^{2-}$ + H_2O	-1.2E-61	-2.2E-54	-4.3E-46	-5.6E-71	-1.1E-64	-2.2E-56	-3.4E-75	-5.8E-68	-1.2E-59	-1.2E-78	-2.5E-71	-6.0E-63
41. $2HS^-$ + O_2+ $2H^+$ -> 2S + $2H_2O$	-9.2E-62	-1.6E-54	-2.9E-46	-2.5E-71	-3.8E-65							
42. HS^-+ 4Hematite + $15H^+$ -> SO_4^{2-}+ $8Fe^{2+}$ + $8H_2O$												
43. $4Fe^{2+}$ + O_2 + $10H_2O$ -> $4Fe(OH)_3$ + $8H^+$			-3.7E-42			-4.1E-52			-2.0E-50			

* Microbial redox reactions have been ordered according to their power with the most powerful reactions for the 80°C brine appearing first. The microbial reaction numbers and column heading numbers refer to Fig. 11. The power is not reported for reactions for which the free energy was less negative than -20 kJoule-mole^{-1}.

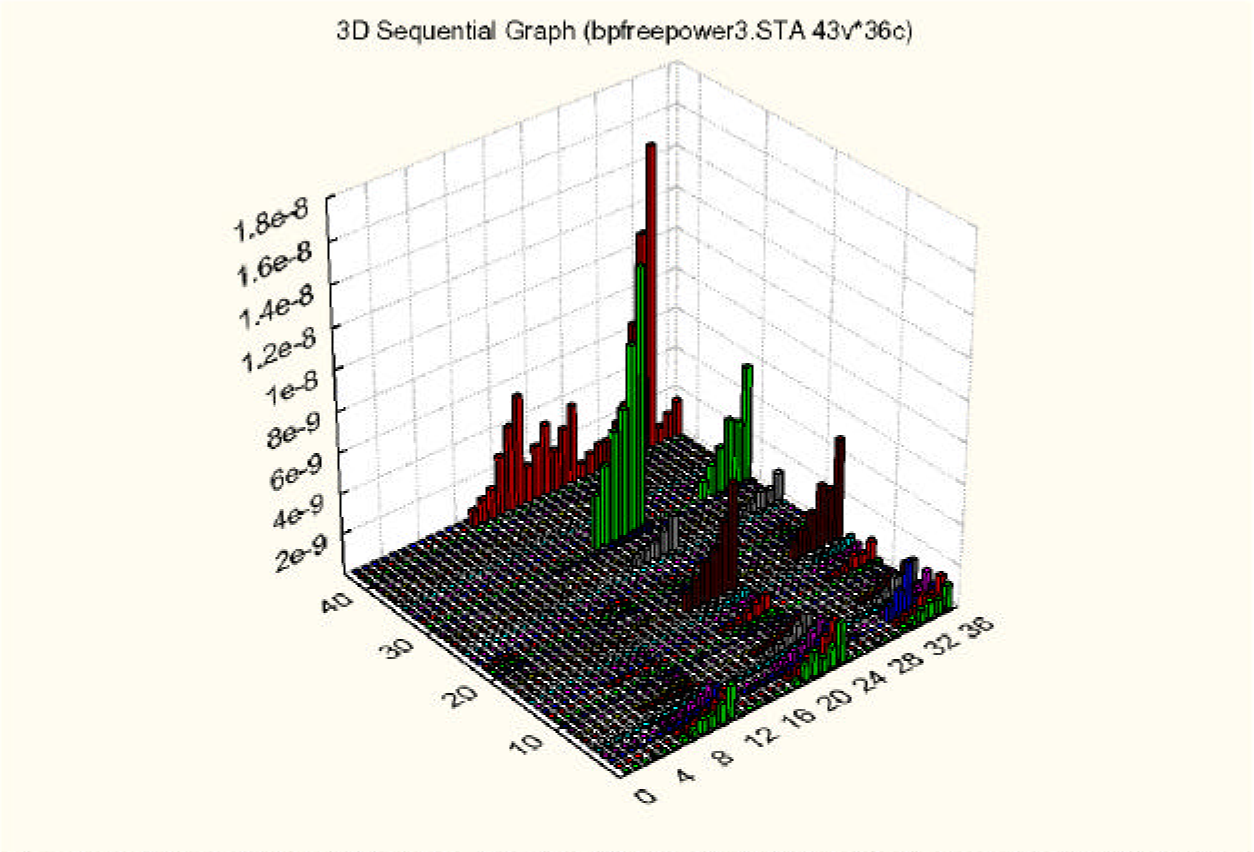

Fig. 11. Free energy flux or "potential microbial power" in kJoules-s^{-1} for simulated CO_2 injection into four different types of groundwater and aquifers.

suggesting that low levels of nitrate could contribute to sustaining microbial Fe(III) reduction at higher temperatures. and it is noteworthy that two Fe(III) reducing bacteria from the deep subsurface, ***Bacillus Infernus*** (Boone et al., 1995) and *Thermus Multireducens* (Kieft et al., 1999) were both capable of nitrate reduction as well.

5. The fermentative methanogenic reactions (reactions 24 and 27 in Table 4 and Fig. 11), propionate reaction (reaction 32 in Table 4 and Fig. 11) and thiosulfate disproportion (reaction 26 in Table 4 and Fig. 11) yielded power levels ranging from 10^{-13} to 10^{-11} kJoules-s^{-1}.
6. All of the aerobic reactions (reactions 33-41 and 43 in Table 4 and Fig. 11) were O_2 limited, which explains why their power levels are extremely low, $< 10^{-40}$ kJoules-s^{-1}, despite the high energy yield of aerobic reactions. In order for these reactions to be competitive with the above anaerobic reactions the O_2 concentrations need to be >0.1 μM.

If we select the 10 most powerful microbial redox reactions for each groundwater type we come to the following conclusions:

1. For the dolomite groundwater the total potential microbial power from the top ten reactions was $2x10^{-10}$ kJoules-s^{-1}. The most powerful reactions are the reduction of S and HS^- by nitrate. This appears consistent with the dominance of *Thiobacillus denitrificans* in the clone libraries from this aquifer. Other potential metabolic reactions are the reduction of S to HS^-, anaerobic methane oxidation, Mn reduction and other nitrate reduction reactions. This suggests that the community would contain a diverse populations of chemolithotrophs and heterotrophs and phylogenetically would probably be comprised of Proteobacteria. Because the oxidation of Fe by nitrate is among the top 10, the precipitation of $Fe(OH)_3$ is conceivable in which case microbial Fe reduction may also occur.
2. For the low salinity groundwater the total potential microbial power from the top ten reactions was $2x10^{-10}$ kJoules-s^{-1}. The type of reactions was quite similar to those of the dolomite with one exception. The microbial reduction of SO_4^{2-} to HS^- had become a more significant contributor to the total energy which means that the SO_4^{2-} generated by oxidation of S species to SO_4^{2-} by reduction of nitrate could potentially produce more reduced S species and a sulfur cycle could exist, fueled by nitrate and acetate.
3. For the moderate salinity groundwater the total potential microbial power from the top ten reactions was $1x10^{-9}$ kJoules-s^{-1}. The metabolic reactions are dominated by S and SO_4^{2-} reduction to HS^- and by reduction of CO_2 to methane and acetate. The change in microbial metabolic pathways is largely a reflection of the increasing H_2 concentrations. This appears consistent with the dominance of sulfate reducing members of the Firmicutes and the presence of methanogens in the clone libraries.
4. For the high salinity groundwater the total potential microbial power from the top ten reactions was $3x10^{-9}$ kJoules-s^{-1}. The metabolic reactions remain dominated by S and SO_4^{2-} reduction to HS^- and by reduction of CO_2 to methane and acetate. One difference between the high salinity and moderate salinity groundwater is that abiotic reactions appear competitive based upon their potential power. This appears to be

consistent with isotopic data reported from these groundwater types (Sherwood-Lollar et al., 1993) . Another difference is that CO oxidation by SO_4^{2-} reduction to HS^- and by reduction of hematite appears to be competitive, but microorganisms capable of coupling these electron donors and acceptors have not been isolated to our knowledge. Finally, the highly saline water was CO_2 limited for CO_2 reducing reactions, an observation that bears some significance in terms of the injection of CO_2.

5. The microbial power for the more saline groundwater types is greater than that of the dolomite and low salinity water and that power is concentrated into fewer reactions. The microbial power for the dolomite and low salinity water is more equally divided among the microbial redox reactions. This suggests that deeper, more saline groundwater microbial communities are less diverse than the shallower, less saline groundwater microbial communities, a trend which is borne out in the 16S rDNA data.

Injection of CO_2

The equilibration of the four groundwater types with 200 bars of CO_2 decreased the pH, 2.7 to 3.3, increased the pe, 1 to 7 and dramatically increased dissolved CO_2 and HCO_3^-concentrations, 2.5 to 8 and 0.002 to 0.004 moles/kg, respectively. Solubilization of trace mineral phases affected the concentrations of trace metals and phosphate which obviously have potential impact upon microbial processes. For the purposes of this study we have focused on the first three effects, which had the following significant impact upon the acid and CO_2 producing microbial redox reactions:

1. The fermentation reactions of acetate fermentation to CH_4 and CO_2 (reaction 36 in Table 5) and propionate fermentation to acetate, CO_2 and H_2 (reaction 42 in Table 5) were no longer favorable for any of the groundwater compositions. This would be a serious impediment to strictly aceticlastic methanogens, whereas the propionate reaction would be more dependent upon the pH_2.
2. The oxidation of reduced S compounds by O_2 (reactions 16-18, 21 and 25 in Table 5), which were marginally favorable in the highly saline groundwater became endothermic with injection of the CO_2. Given that aerobic S oxidizers are not found in this groundwater environment, this doesn't appear to be a significant perturbation.
3. Of the microbial reactions that were originally unfavorable prior to injection, the reduction of hematite to Fe^{2+} by oxidation of acetate (reaction 39 in Table 5) and H_2 (reaction 41 in Table 5) were far more exothermic due to the reduction in pH. The abiotic reduction of hematite by oxidation of HS^- (reaction 43 in Table 5) is also energetically favorable now.
4. The high CO_2 and HCO_3^-concentrations increased the free energy yield for CO_2 reducing methanogenic and acetogenic reaction (reactions 32 and 37 in Table 5). An increase in acetogenic activity may rescue the aceticlastic methanogens.
5. The aerobic oxidation of acetate (reaction 11 in Table 5) was less favorable because it is a proton and HCO_3^- producing reaction. Other acetate oxidation reactions, however, such as MnO_2 or nitrate reduction were more favorable.
6. The free energy of nitrate reduction reactions were greater with the N_2 producing reactions being more favored than before.

Table 5. Microbial redox reactions for groundwater equilibrated with 200 bars of CO_2.

Microbial Redox Reactions*	13. Do 20	14. Do 45	15. Do 80	16. LS 20	17. LS 45	18. LS 80	19. MS 20	20. MS 45	21. MS 80	22. Br 20	23. Br 45	24. Br 80
1. $5H_2 + 2NO_3^- + 2H^+ \rightarrow N_2 + 6H_2O$	-1246	-1122	-976	-1193	-1069	-924	-1305	-1182	-1036	-1321	-1197	-1053
2. Acetate + $1.6NO_3^- + 0.6H^+ \rightarrow 2HCO_3^- + 0.8H_2O + 0.8N_2$	-907	-832	-745	-890	-815	-728	-897	-822	-735	-899	-824	-738
3. $2S + 1.5NO_3^- + 3.5H_2O \rightarrow 2SO_4^{2-} + 2.5H^+ + 1.5NH_3$	-813	-747	-673	-799	-733	-655	-797	-733	-655	-797	-731	-653
4. $4CO + NO_3^- + 5H_2O \rightarrow 4HCO_3^- + NH_3 + 3H^+$	-724	-653	-569	-710	-640	-553	-754	-683	-597	-777	-706	-621
5. Acetate + $4MnO_2 + 7H^+ \rightarrow 4Mn^{2+} + 4H_2O + 2HCO_3^-$	-981	-895	-793	-1017	-932	-829	-966	-883	-781	-1012	-930	-837
6. $2.5CO + NO_3^- + 2H_2O \rightarrow 2.5HCO_3^- + 1.5H^+ + 0.5N_2$	-634	-574	-503	-622	-562	-491	-650	-591	-519	-664	-604	-534
7. $4H_2 + NO_3^- + H^+ \rightarrow NH_3 + 3H_2O$	-706	-631	-544	-670	-596	-507	-758	-683	-595	-772	-697	-610
8. Acetate + $NO_3^- + H_2O \rightarrow 2HCO_3^- + NH_3$	-616	-566	-508	-606	-555	-496	-610	-560	-501	-614	-564	-506
9. $S_2O_3^{2-} + NO_3^- + 2H_2O \rightarrow 2SO_4^{2-} + H^+ + NH_3$	-551	-501	-375	-564	-514	-456	-564	-515	-457	-560	-511	-453
10. $HS^- + NO_3^- + H_2O \rightarrow SO_4^{2-} + NH_3$	-544	-496	-441	-538	-490	-432	-537	-489	-432	-537	-489	-432
11. Acetate + $2O_2 \rightarrow 2HCO_3^- + H^+$	-344	-322	-438	-302	-282	-261	-101	-278	-261	-73	-71	-130
12. Acetate + $4S + 4H_2O \rightarrow 5H^+ + 2HCO_3^- + 4HS^-$	-344	-322	-438	-302	-282	-261	-73	-278	-261	-73	-71	-130
13. $5Fe^{2+} + NO_3^- + 12H_2O \rightarrow 5Fe(OH)_3 + 9H^+ + 0.5N_2$		-61	-73		-31	-44		-31	-42		-52	-58
14. $NO_2^- + H^+ + NH_3 \rightarrow 2H_2O + N_2$	-355	-324	-286	-348	-317	-282	-356	-324	-289	-355	-324	-288
15. $CH_4 + 2O_2 \rightarrow HCO_3^- + H^+ + H_2O$	-329	-306	-422	-293	-272	-250	-95	-271	-253	-66	-64	-121
16. $S_2O_3^{2-} + 2O_2 + H_2O \rightarrow 2SO_4^{2-} + 2H^+$	-278	-257	-305	-260	-241	-221	-55	-233	-217	-19	-18	-77
17. $HS^- + 2O_2 \rightarrow SO_4^{2-} + H^+$	-272	-252	-371	-234	-216	-197	-28	-207	-192	4	4	-56
18. $2HS^- + 2O_2 \rightarrow S_2O_3^{2-} + H_2O$	-266	-247	-437	-209	-191	-173	-1	-180	-166	27	26	-35
19. $2CO + O_2 + 2H_2O \rightarrow 2HCO_3^- + 2H^+$	-226	-204	-249	-203	-183	-159	-122	-200	-178	-118	-107	-123
20. $4CO + SO_4^{2-} + 4H_2O \rightarrow 4HCO_3^- + HS^- + 3H^+$	-180	-157	-128	-172	-150	-121	-216	-194	-165	-240	-217	-189
21. $S + 1.5O_2 + H_2O \rightarrow SO_4^{2-} + 2H^+$	-202	-191	-284	-172	-161	-151	7	-155	-148	7	4	-45

22. 4CO + 5H_2O -> CH_4 + 3HCO_3^- + 3H^+	-123	-103	-77	-114	-94	-68	-150	-130	-104	-170	-150	-124
23. 2H_2 + O_2-> 2H_2O	-217	-193	-237	-183	-161	-136	-124	-201	-177	-115	-102	-117
24. $S_2O_3^{2-}$ + 4H_2 -> 3H_2O + 2HS^-	-167	-140	-37	-158	-131	-99	-247	-221	-189	-257	-230	-199
25. 2HS^- + O_2+ 2H^+ -> 2S + 2H_2O	-140	-123	-175	-125	-109	-92	-21	-104	-88	-7	0	-23
26. H_2 + S -> HS^-+ H^+	-108	-97	-119	-92	-81	-68	-58	-100	-89	-58	-51	-58
27. 3H_2 + CO -> CH_4+ H_2O	-109	-86	-58	-84	-61	-33	-153	-130	-102	-166	-143	-115
28. 4H_2 + H^+ + SO_4^{2-}-> HS^- + 4H_2O	-161	-135	-103	-132	-106	-75	-220	-194	-163	-234	-208	-178
29. 3H_2 + N_2 -> 2NH_3	-166	-141	-113	-148	-122	-90	-210	-185	-153	-222	-197	-167
30. 4Formate + H^+ + H_2O -> CH_4 + 3HCO_3^-	-102	-88	-72	-60	-47	-31	-65	-51	-36	-81	-68	-53
31. Acetate + SO_4^{2-}-> 2HCO_3^- + HS^-	-72	-70	-67	-68	-66	-64	-73	-71	-69	-77	-75	-74
32. 4H_2 + H^+ + HCO_3^- -> CH_4 + 3H_2O	-104	-81	-52	-74	-50	-22	-154	-130	-102	-164	-141	-112
33. CO + Hematite + 3H^+ -> 2Fe^{2+} + H_2O + HCO_3^-	-156	-133	-103	-162	-139	-110	-173	-151	-122	-170	-148	-121
34. CO + 2H_2O -> HCO_3^- + H^+ + H_2	-5	-6	-6	-10	-11	-12	1	0	-1	-1	-2	-3
35. CH_4+ SO_4^{2-}-> H_2O + HCO_3^- + HS^-	-57	-54	-51	-59	-56	-53	-67	-64	-61	-70	-68	-65
36. Acetate + H_2O -> CH_4 + HCO_3^-	-15	-15	-16	-9	-9	-10	-6	-7	-8	-7	-7	-8
37. 4H_2 + H^++ 2HCO_3^- -> Acetate + 4H_2O	-89	-65	-36	-65	-40	-11	-147	-123	-94	-157	-133	-104
38. $S_2O_3^{2-}$ + H_2O -> SO_4^{2-} + H^+ + HS^-	-6	-5	66	-26	-25	-24	-27	-26	-26	-23	-22	-21
39. Acetate + 4Hematite + 15H^+ -> 8Fe^{2+} + 8H_2O + 2HCO_3^-	-515	-443	-352	-543	-473	-381	-549	-480	-392	-516	-449	-369
40. 4Fe^{2+} + O_2 + 10H_2O -> 4$Fe(OH)_3$ + 8H^+		206	95		241	198		247	204		335	258
41. H_2 + Hematite + 4H^+ -> 2Fe^{2+}+ 3H_2O	-151	-127	-97	-152	-128	-98	-174	-151	-121	-168	-146	-118
42. Propionate + 3H_2O -> Acetate + HCO_3^- + H^++ 3H_2	60	42	20	39	21	-1	102	84	62	109	91	68
43. HS^-+ 4Hematite + 15H^+ -> SO_4^{2-}+ 8Fe^{2+} + 8H_2O	-443	-373	-285	-475	-407	-317	-476	-409	-323	-439	-374	-296
44. NH_3+ 1.5* O_2-> NO_2^- + H^+ + H_2O	196	174	43	221	198	168	379	209	176	404	368	279
45. 4Mn^{2+}+ NO_3^- + 5H_2O -> 4MnO_2 + 7H^++ NH_3	364	330	284	411	377	333	398	322	280	398	367	331
46. 2NO_2^- + O_2-> 2NO_3^-	153	140	54	166	152	134	260	147	128	274	250	193
47. 2Mn^{2+}+ O_2+ 2H_2O -> 2MnO_2 + 4H^+	318	287	177	358	325	284	470	302	260	470	430	353

*The reactions are ordered from most negative to positive with respect to the free energy for the dolomite groundwater at 20°C. The microbial reaction numbers and column heading numbers refer to Fig. 10.

Table 6. Potential microbial power in kJoules-s^{-1} for four types of groundwater equilibrated with 200 bars of CO_2.

Microbial Redox Reactions*	13. Do 20	14. Do 45	15.Do 80	16. LS 20	17. LS 45	18.LS 80	19.MS 20	20.MS 45	21.MS 80	22. Br 20	23. Br 45	24.Br 80
1. $H_2 + S$ -> $HS^- + H^+$	-2.7E-12	-4.0E-12	-8.3E-12	-2.3E-13	-3.3E-13	-4.7E-13	-2.8E-10	**-8.3E-10**	-1.2E-09	-7.1E-10	**-1.1E-09**	-2.0E-09
2. $3H_2 + N_2$-> $2NH_3$	-1.4E-12	-1.9E-12	-2.6E-12	-1.2E-13	-1.7E-13	-2.1E-13	-3.5E-10	**-5.1E-10**	-7.1E-10	-9.1E-10	**-1.4E-09**	-1.9E-09
3. $CH_4 + SO_4^{2-}$-> $H_2O + HCO_3^- + HS^-$	**-4.7E-11**	-7.4E-11	-1.2E-10	-8.4E-11	**-1.3E-10**	-2.1E-10	-1.9E-10	**-3.1E-10**	-5.0E-10	-5.3E-10	**-8.7E-10**	-1.4E-09
4. $4H_2 + H^+ + SO_4^{2-}$-> $HS^- + 4H_2O$	-1.0E-12	-1.4E-12	-1.8E-12	-8.2E-14	-1.1E-13	-1.3E-13	-2.7E-10	**-4.0E-10**	-5.7E-10	-7.2E-10	**-1.1E-09**	-1.6E-09
5. Acetate + $4MnO_2 + 7H^+$ -> $4Mn^{2+} + 4H_2O + 2HCO_3^-$	**-5.2E-11**	-8.0E-11	-1.2E-10	-6.8E-11	**-1.0E-10**	-1.6E-10	-1.3E-10	**-2.0E-10**	-2.9E-10	-3.4E-10	**-5.2E-10**	-7.9E-10
6. $3H_2 + CO$ -> $CH_4 + H_2O$	-9.0E-13	-1.2E-12	-1.4E-12	-6.9E-14	-8.4E-14	-7.7E-14	-2.5E-10	**-3.6E-10**	-4.8E-10	-6.8E-10	**-9.9E-10**	-1.3E-09
7. $4H_2 + H^+ + HCO_3^-$ -> $CH_4 + 3H_2O$	-6.4E-13	-8.4E-13	-9.1E-13	-4.5E-14	-5.2E-14	-3.8E-14	-1.9E-10	**-2.7E-10**	-3.5E-10	-5.1E-10	**-7.3E-10**	-9.8E-10
8. $4CO + SO_4^{2-} + 4H_2O$ -> $4HCO_3^- +$ HS- + $3H^+$	-2.0E-13	-2.9E-13	-4.0E-13	-1.4E-13	-2.1E-13	-2.9E-13	-6.0E-12	-9.1E-12	-1.3E-11	-4.7E-11	-7.1E-11	-1.0E-10
9. $4CO + 5H_2O$ -> $CH_4 + 3HCO_3^- + 3H^+$	-1.4E-13	-1.9E-13	-2.4E-13	-9.5E-14	-1.3E-13	-1.6E-13	-4.2E-12	-6.1E-12	-8.2E-12	-3.3E-11	-4.9E-11	-6.8E-11
10. Acetate + $4S + 4H_2O$ -> $5H^+ + 2HCO_3^- + 4HS^-$	**-1.8E-11**	-2.9E-11	-6.6E-11	-2.0E-11	**-3.1E-11**	-4.9E-11	-9.7E-12	-6.2E-11	-9.8E-11	-2.4E-11	-4.0E-11	-1.2E-10
11. CO + Hematite + $3H^+$ -> $2Fe^{2+} + H_2O + HCO_3^-$	-6.9E-13	-9.9E-13	-1.3E-12	-5.4E-13	-7.8E-13	-1.0E-12	-1.9E-11	-2.8E-11	-3.8E-11	-1.3E-10	-1.9E-10	-2.7E-10
12. $4H_2 + H^+ + 2HCO_3^-$ -> Acetate + $4H_2O$	-5.5E-13	-6.8E-13	-6.3E-13	-4.0E-14	-4.2E-14		-1.8E-10	**-2.6E-10**	-3.3E-10	-4.9E-10	**-6.9E-10**	-9.1E-10
13. Acetate + SO_4^{2-}-> $2HCO_3^- + HS^-$	-3.8E-12	-6.2E-12	-1.0E-11	-4.5E-12	-7.3E-12	-1.2E-11	-9.7E-12	-1.6E-11	-2.6E-11	-2.6E-11	-4.2E-11	-6.9E-11
14. $4CO + NO_3^- + 5H_2O$ -> $4HCO_3^- + NH_3 + 3H^+$	-8.1E-13	-1.2E-12	-1.8E-12	-5.9E-13	-9.0E-13	-1.3E-12	-2.1E-11	-3.2E-11	-4.7E-11	-1.5E-10	-2.3E-10	-3.4E-10
15. $2.5CO + NO_3^- + 2H_2O$ -> $2.5HCO_3^- + 1.5H^+ + 0.5N_2$	-1.1E-12	-1.7E-12	-2.5E-12	-8.3E-13	-1.3E-12	-1.9E-12	-2.9E-11	-4.4E-11	-6.5E-11	-2.1E-10	-3.2E-10	-4.7E-10
16. $S_2O_3^{2-} + NO_3^- + 2H_2O$ -> $2SO_4^{2-} + H^+ + NH_3$	-2.4E-13	-3.7E-13	-4.7E-13	-5.3E-12	-8.1E-12	-1.2E-11	-2.8E-11	-4.3E-11	-6.3E-11	-1.9E-11	-2.9E-11	-4.3E-11
17. $4H_2 + NO_3^- + H^+$ -> $NH_3 + 3H_2O$	-4.4E-12	-6.6E-12	-9.5E-12	-4.1E-13	-6.2E-13	-8.8E-13	-9.4E-10	**-1.4E-09**	-2.1E-09	-2.4E-09	**-3.6E-09**	-5.3E-09
18. Acetate + $NO_3^- + H_2O$ -> $2HCO_3^- + NH_3$	**-3.3E-11**	-5.1E-11	-7.6E-11	-5.3E-12	-8.1E-12	-1.2E-11	-2.6E-11	-4.0E-11	-6.0E-11	-1.7E-11	-2.7E-11	-4.0E-11
19. $5H_2 + 2NO_3^- + 2H^+$ -> $N_2 + 6H_2O$	-6.2E-12	-9.3E-12	-1.4E-11	-5.3E-12	-8.1E-12	-1.2E-11	-2.6E-11	-3.8E-11	-5.6E-11	-1.9E-11	-2.8E-11	-4.2E-11
20. $2S + 1.5NO_3^- + 3.5H_2O$ -> $2SO_4^{2-} + 2.5H^+ + 1.5NH_3$	**-7.0E-11**	-1.1E-10	-1.6E-10	-4.6E-12	-7.0E-12	-1.1E-11	-2.3E-11	-3.5E-11	-5.3E-11	-1.5E-11	-2.3E-11	-3.5E-11
21. Acetate + $1.6NO_3^- + 0.6H^+$ -> $2HCO_3^- + 0.8H_2O + 0.8N_2$	**-4.8E-11**	-7.4E-11	-1.1E-10	-4.9E-12	-7.5E-12	-1.1E-11	-2.4E-11	-3.7E-11	-5.5E-11	-1.6E-11	-2.5E-11	-3.7E-11

22. HS^{-}+ NO_3^{-} + H_2O -> SO_4^{2-}+ NH_3	**-7.0E-11**	-1.1E-10	-1.6E-10	-4.6E-12	-7.0E-12	-1.0E-11	-2.3E-11	-3.5E-11	-5.2E-11	-1.5E-11	-2.3E-11	-3.5E-11
23. CO + $2H_2O$ -> HCO_3^{-} + H^+ + H_2												
24. Acetate + H_2O -> CH_4 + HCO_3^{-}												
25. NO_2^{-} + H^+ + NH_3-> $2H_2O$ + N_2	-5.5E-13	-8.4E-13	-1.2E-12	-3.2E-13	-4.9E-13	-7.3E-13	-2.2E-12	-3.4E-12	-5.0E-12	-5.5E-12	-8.4E-12	-1.3E-11
26. $S_2O_3^{2-}$ + $4H_2$ -> $3H_2O$ + $2HS^{-}$	-7.4E-14	-1.0E-13	-4.6E-14	-9.7E-14	-1.4E-13	-1.7E-13	-3.1E-10	**-4.6E-10**	-6.6E-10	-7.9E-10	**-1.2E-09**	-1.7E-09
27. 4Formate + H^+ + H_2O -> CH_4 + $3HCO_3^{-}$	-8.4E-12	-1.2E-11	-1.7E-11	-2.5E-13	-3.2E-13	-3.6E-13	-5.3E-13	-7.1E-13	-8.3E-13	-3.3E-12	-4.7E-12	-6.1E-12
28. $5Fe^{2+}$ + NO_3^{-} + $12H_2O$ -> $5Fe(OH)_3$ + $9H^+$ + $0.5N_2$		-1.1E-12	-2.3E-12		-4.6E-13	-1.1E-12		-6.9E-13	-1.6E-12		-3.5E-12	-3.8E-12
29. $S_2O_3^{2-}$ + H_2O -> SO_4^{2-} + H^+ + HS^{-}				-4.2E-15	-6.8E-15	-1.1E-14	-1.2E-12	-1.9E-12	-3.2E-12	-7.5E-13	-1.2E-12	-2.0E-12
30. Acetate + 4Hematite + $15H^+$ -> $8Fe^{2+}$ + $8H_2O$ + $2HCO_3^{-}$	**-2.7E-11**	-4.0E-11	-5.3E-11	-3.6E-11	**-5.3E-11**	-7.2E-11	-7.3E-11	-1.1E-10	-1.5E-10	-1.7E-10	-2.5E-10	-3.5E-10
31. H_2 + Hematite + $4H^+$ -> $2Fe^{2+}$+ $3H_2O$	**-1.3E-11**	-1.8E-11	-2.5E-11	-1.3E-12	-2.0E-12	-2.7E-12	-2.7E-09	**-4.0E-09**	-5.5E-09	-6.4E-09	**-9.3E-09**	-1.3E-08
32. Propionate + $3H_2O$ -> Acetate + HCO_3^{-} + H^++ $3H_2$												
33. 2CO + O_2+ $2H_2O$ -> $2HCO_3^{-}$ + $2H^+$	-2.6E-56	-4.0E-52	-8.1E-36	-2.3E-59	-1.1E-54	-5.2E-49	-1.4E-74	-3.9E-55	-5.8E-51	-1.4E-77	-2.1E-70	-4.0E-59
34. $2H_2$ + O_2-> $2H_2O$	-2.5E-56	-3.7E-52	-7.7E-36	-2.1E-59	-9.4E-55	-4.4E-49	-1.4E-74	-3.9E-55	-5.8E-51	-1.3E-77	-2.0E-70	-3.8E-59
35. Acetate + $2O_2$-> $2HCO_3^{-}$ + H^+	-2.0E-56	-3.1E-52	-7.1E-36	-1.7E-59	-8.2E-55	-4.2E-49	-5.8E-75	-2.7E-55	-4.3E-51	-4.2E-78	-6.9E-71	-2.1E-59
36. CH_4+ $2O_2$-> HCO_3^{-} + H^+ + H_2O	-1.9E-56	-3.0E-52	-6.9E-36	-1.7E-59	-7.9E-55	-4.1E-49	-5.5E-75	-2.6E-55	-4.1E-51	-3.8E-78	-6.2E-71	-2.0E-59
37. S + $1.5O_2$ + H_2O -> SO_4^{2-}+ $2H^+$	-1.6E-62			-1.3E-59	-6.3E-55	-3.3E-49		-2.0E-55	-3.2E-51			-3.4E-60
38. $S_2O_3^{2-}$ + $2O_2$+ H_2O -> $2SO_4^{2-}$+ $2H^+$	-1.6E-56	-2.5E-52	-5.0E-36	-1.5E-59	-7.0E-55	-3.6E-49	-3.2E-75	-2.3E-55	-3.5E-51	-1.1E-78	-1.7E-71	-1.3E-59
39. HS^{-}+ $2O_2$-> SO_4^{2-}+ H^+	-1.6E-56	-2.4E-52	-6.0E-36	-1.4E-59	-6.3E-55	-3.2E-49	-1.6E-75	-2.0E-55	-3.1E-51			-9.1E-60
40. $2HS^{-}$ + $2O_2$ -> $S_2O_3^{2-}$ + H_2O	-1.5E-56	-2.4E-52	-7.1E-36	-1.2E-59	-5.6E-55	-2.8E-49		-1.7E-55	-2.7E-51			-5.6E-60
41. $2HS^{-}$ + O_2+ $2H^+$ -> 2S + $2H_2O$	-1.6E-56	-2.4E-52	-5.7E-36	-1.4E-59	-6.4E-55	-3.0E-49	-2.4E-75	-2.0E-55	-2.9E-51			-7.4E-60
42. HS^{-}+ 4Hematite + $15H^+$ -> SO_4^{2-}+ $8Fe^{2+}$ + $8H_2O$	**-8.2E-10**	-1.2E-09	-1.5E-09	-2.9E-09	**-4.2E-09**	-5.6E-09	-1.8E-09	**-2.7E-09**	-3.5E-09	-2.0E-09	**-2.9E-09**	-3.9E-09
43. $4Fe^{2+}$ + O_2 + $10H_2O$ -> $4Fe(OH)_3$ + $8H^+$												

* Microbial redox reactions have been ordered according to their power with the most powerful reactions for the 80°C brine appearing first. The microbial reaction numbers and column heading numbers refer to Fig. 11. The power is not reported for reactions for which the free energy was less negative than -20 kJoule-mole^{-1}.

In terms of the potential microbial power values, the hematite reduction reaction by oxidation of HS^- (reaction 42 in Table 6) became the most powerful suggesting that this abiotic reaction will dominate in siliclastic aquifers where Fe(III) oxides and HS^- are present and will significantly ameliorate the low pH conditions. In the more saline aquifers where H_2 are high, the microbial reduction of Fe(III) oxides are equally important and will dominate if HS^- is limiting. These reactions will also raise the pH of the groundwater and promote precipitation of the CO_2 as carbonate.

In terms of the available microbial power for the top 10 reactions, the CO_2 injection has increased power levels by a factor of 10. This is primarily the result of the reduction in pH. For many of the microorganisms, this pH range falls below their optimal growth regime so that the increased power may not be immediately available until the pH increases. Initially after CO_2 injection, therefore, increase of the pH may be due to abiotic reactions such as redox reaction 42 in Table 6 or alteration of the aquifer minerals by the carbonic acid.

Dissolution of Aquifer Minerals

The low pH, CO_2 saturated, dolomitic groundwater was reacted with dolomite and calcite to simulate a carbonate aquifer. The low pH, CO_2 saturated, low, moderate and highly saline groundwater was reacted with albite and minor calcite to simulate a siliclastic aquifer (Helgeson et al., 1993) . The impacts on groundwater chemistry were as follows:

1. For the dolomite system, the pH increased from 3.1 to 4.6, the pe decreased from 9.5 to 7.5 and the dissolved CO_2 decreased slightly from 7.99 to 7.91 M. As dolomite and calcite dissolved, chalcedony, kaolinite, hydroxyapatite, fluorite and various metal sulfide minerals precipitated until dolomite and subsequently calcite attained saturation. The reaction led to a net increase in porosity of 0.3%. The only significant difference in simulations at higher aquifer temperatures is that more carbonate precipitation occurred with no significant change in the porosity.
2. For the low salinity groundwater, the pH increased from 2.9 to 7, the pe decreased from 5.7 to -2.8 and the dissolved CO_2 decreased from 7.99 to 0.2 M. In terms of pH and pe, these values are close to that of the initial groundwater (Table 2). As albite and calcite dissolved, chalcedony, kaolinite and nahcolite, the Na bicarbonate mineral, and minor sulfide mineral phases precipitated. The reaction led to a 20% reduction in porosity. For $80^\circ C$, the reaction increased the pH to 6, decreased the pe to -1.9 and reduced the dissolved CO_2 to 1.3 M with no significant change in the porosity primarily because nahcolite didn't precipitate.
3. For the moderate salinity groundwater, the pH increased from 2.9 to 7, the pe decreased from 2 to -3.4 and the dissolved CO_2 decreased slightly from 7.99 to 0.2 M. In terms of pH and pe, these values are close to that of the initial groundwater (Table 2). As albite and calcite dissolved, chalcedony, kaolinite, rhodochrosite and nahcolite, the Na bicarbonate mineral, and minor sulfide mineral phases precipitated. The reaction led to a 20% reduction in porosity. For $80^\circ C$, the reaction increased the pH to 6, decreased the pe to -1.8 and

reduced the dissolved CO_2 to 1.3 M with no significant change in the porosity primarily because nahcolite didn't precipitate.

4. For the moderate salinity groundwater, the pH increased from 2.7 to 6.9, the pe decreased from 2 to -3.3 and the dissolved CO_2 decreased slightly from 7.99 to 0.2 M. In terms of pH and pe, these values are close to that of the initial groundwater (Table 2). As albite and calcite dissolved, chalcedony, kaolinite, rhodochrosite, dolomite, witherite and nahcolite, the Na bicarbonate mineral, and minor sulfide mineral phases precipitated. The reaction led to a 20% reduction in porosity. For 80°C, the reaction increased the pH to 6, decreased the pe to -1.8 and reduced the dissolved CO_2 to 1.3 M with a 0.3% increase in the porosity primarily because nahcolite and the other carbonate minerals didn't precipitate, although minor siderite did.

With the dissolution reactions ameliorating some of the effects of CO_2 injection, the only significant change in the microbial redox reactions were the following:

1. The fermentation reactions of acetate fermentation to CH_4 and CO_2 (reaction 36 in Table 7) and propionate fermentation to acetate, CO_2 and H_2 (reaction 42 in Table 7) still remain unfavorable for any of the groundwater compositions. This would be a serious impediment to strictly aceticlastic methanogens, whereas the propionate reaction would be more dependent upon the pH_2.
2. The oxidation of reduced S compounds by O_2 (reactions 16-18, 21 and 25 in Table 7), which were marginally favorable in the highly saline groundwater remain endothermic after alteration of the siliclastic mineral assemblage. Given that aerobic S oxidizers are not found in this groundwater environment, this doesn't appear to be a significant perturbation. For the dolomite aquifer, the S oxidizing reactions remain exothermic despite the lower pH of the impacted system.
3. Of the microbial reactions that were originally unfavorable prior to injection, the reduction of hematite to Fe^{2+} by oxidation of acetate (reaction 39 in Table 7) and H_2 (reaction 41 in Table 7) are still exothermic due to the reduction in pH from 8 to 7. The abiotic reduction of hematite by oxidation of HS^- (reaction 43 in Table 7) is also energetically favorable.
4. The high CO_2 and HCO_3^- concentrations increased the free energy yield for CO_2 reducing methanogenic and acetogenic reaction (reactions 32 and 37 in Table 7) even after alteration of the aquifer mineral assemblage. An increase in acetogenic activity may rescue the aceticlastic methanogens. The extent to which these two reactions can be used to convert the CO_2 into methane and acetate depends upon whether an abiotically generated source of H_2 can be made available.

Discussion

The most readily identified impact in figure 11 on the potential microbial power is from reduction of hematite by HS^- oxidation. The power levels were generally larger than in the original groundwater systems and because of the reduction of 1 pH unit in the

Table 7. Microbial redox reactions after interaction of CO_2 saturated water with aquifer minerals.

Microbial Redox Reactions*	25. Do 20	26. Do 45	27.Do 80	28. LS 20	29. LS 45	30.LS 80	31.MS 20	32.MS 45	33.MS 80	34. Br 20	35. Br 45	36.Br 80
1. $5H_2 + 2NO_3^- + 2H^+$ -> $N_2 + 6H_2O$	-1224	-1103	-961	-1140	-1023	-885	-1252	-1135	-997	-1268	-1151	-1013
2. Acetate + $1.6NO_3^- + 0.6H^+$ -> $2HCO_3^- + 0.8H_2O + 0.8N_2$	-888	-816	-732	-849	-773	-690	-856	-781	-697	-860	-783	-700
3. $2S + 1.5NO_3^- + 3.5H_2O$ -> $2SO_4^{2-} + 2.5H^+ + 1.5NH_3$				-835	-765	-683	-833	-763	-680	-824	-754	-671
4. $4CO + NO_3^- + 5H_2O$ -> $4HCO_3^- + NH_3 + 3H^+$	-705	-636	-555	-702	-614	-525	-744	-657	-567	-766	-679	-589
5. Acetate + $4MnO_2 + 7H^+$ -> $4Mn^{2+} + 4H_2O + 2HCO_3^-$	-907	-831	-741	-812	-764	-691	-797	-739	-662	-799	-742	-671
6. $2.5CO + NO_3^- + 2H_2O$ -> $2.5HCO_3^- + 1.5H^+ + 0.5N_2$	-624	-565	-496	-622	-550	-476	-651	-579	-505	-664	-593	-518
7. $4H_2 + NO_3^- + H^+$ -> $NH_3 + 3H_2O$	-686	-614	-530	-618	-552	-471	-705	-639	-557	-718	-651	-570
8. Acetate + $NO_3^- + H_2O$ -> $2HCO_3^- + NH_3$	-595	-547	-493	-556	-507	-453	-560	-511	-457	-563	-513	-460
9. $S_2O_3^{2-} + NO_3^- + 2H_2O$ -> $2SO_4^{2-} + H^+ + NH_3$	-485	-446	-388	-567	-519	-460	-566	-518	-459	-558	-509	-451
10. $HS^- + NO_3^- + H_2O$ -> $SO_4^{2-} + NH_3$	-548	-499	-443	-540	-493	-436	-538	-491	-434	-534	-488	-430
11. Acetate + $2O_2$ -> $2HCO_3^- + H^+$	-483	-440	-415	-65	-64	-75	-36	-72	-83	-43	-39	-40
12. Acetate + $4S + 4H_2O$ -> $5H^+ + 2HCO_3^- + 4HS^-$				-65	-64	-75	-28	-72	-83	-37	-32	-31
13. $5Fe^{2+} + NO_3^- + 12H_2O$ -> $5Fe(OH)_3 + 9H^+ + 0.5N_2$	-132	-129	-127	-214	-186	-160	-168	-189	-163	-175	-188	-162
14. $NO_2^- + H^+ + NH_3$-> $2H_2O + N_2$	-356	-324	-286	-349	-316	-280	-358	-325	-288	-359	-326	-289
15. $CH_4 + 2O_2$-> $HCO_3^- + H^+ + H_2O$	-470	-426	-400	-62	-63	-73	-36	-74	-83	-43	-40	-40
16. $S_2O_3^{2-} + 2O_2 + H_2O$ -> $2SO_4^{2-} + 2H^+$	-373	-339	-310	-77	-76	-82	-43	-79	-85	-39	-35	-31
17. $HS^- + 2O_2$ -> $SO_4^{2-} + H^+$	-436	-392	-365	-49	-50	-58	-15	-52	-59	-15	-13	-11
18. $2HS^- + 2O_2$ -> $S_2O_3^{2-} + H_2O$	-499	-445	-420	-22	-25	-33	14	-26	-34	8	8	10
19. $2CO + O_2 + 2H_2O$ -> $2HCO_3^- + 2H^+$	-296	-264	-238	-105	-86	-73	-110	-109	-97	-123	-102	-85
20. $4CO + SO_4^{2-} + 4H_2O$ -> $4HCO_3^- + HS^- + 3H^+$	-156	-137	-112	-161	-121	-89	-206	-166	-134	-232	-191	-159
21. $S + 1.5O_2 + H_2O$ -> $SO_4^{2-} + 2H^+$							-18			-18	-16	-14

22. $4CO + 5H_2O \rightarrow CH_4 + 3HCO_3^- + 3H^+$	-123	-103	-77	-149	-108	-74	-184	-144	-110	-204	-164	-130
23. $2H_2 + O_2 \rightarrow 2H_2O$	-287	-253	-226	-64	-55	-46	-91	-100	-92	-99	-88	-75
24. $S_2O_3^{2-} + 4H_2 \rightarrow 3H_2O + 2HS^-$	-75	-61	-32	-105	-84	-60	-195	-174	-149	-207	-185	-160
25. $2HS^- + O_2 + 2H^+ \rightarrow 2S + 2H_2O$	-210	-183	-163	0	0	0	18	0	0	15	16	21
26. $H_2 + S \rightarrow HS^- + H^+$				-32	-27	-23	-43	-50	-46	-48	-42	-35
27. $3H_2 + CO \rightarrow CH_4 + H_2O$	-109	-86	-58	-86	-61	-33	-155	-130	-102	-168	-144	-115
28. $4H_2 + H^+ + SO_4^{2-} \rightarrow HS^- + 4H_2O$	-138	-114	-87	-78	-59	-35	-167	-148	-124	-183	-163	-140
29. $3H_2 + N_2 \rightarrow 2NH_3$	-148	-125	-100	-96	-81	-57	-158	-142	-118	-167	-151	-127
30. 4Formate + $H^+ + H_2O \rightarrow CH_4 + 3HCO_3^-$	-73	-63	-52	2	19	28	-2	14	24	-21	-4	6
31. Acetate + $SO_4^{2-} \rightarrow 2HCO_3^- + HS^-$	-46	-48	-50	-15	-14	-17	-22	-20	-24	-28	-26	-30
32. $4H_2 + H^+ + HCO_3^- \rightarrow CH_4 + 3H_2O$	-104	-81	-52	-65	-46	-20	-145	-126	-100	-156	-137	-111
33. CO + Hematite + $3H^+ \rightarrow 2Fe^{2+} + H_2O + HCO_3^-$	-120	-102	-78	-87	-73	-58	-94	-83	-68	-101	-89	-73
34. $CO + 2H_2O \rightarrow HCO_3^- + H^+ + H_2$	-5	-6	-6	-21	-16	-14	-10	-5	-2	-12	-7	-5
35. $CH_4 + SO_4^{2-} \rightarrow H_2O + HCO_3^- + HS^-$	-33	-34	-35	-13	-13	-15	-22	-22	-24	-27	-27	-29
36. Acetate + $H_2O \rightarrow CH_4 + HCO_3^-$	-13	-14	-15	-2	-1	-2	0	2	1	-1	1	0
37. $4H_2 + H^+ + 2HCO_3^- \rightarrow$ Acetate + $4H_2O$	-91	-67	-37	-62	-45	-18	-145	-128	-100	-155	-138	-110
38. $S_2O_3^{2-} + H_2O \rightarrow SO_4^{2-} + H^+ + HS^-$	63	53	55	-27	-26	-24	-28	-27	-26	-23	-21	-20
39. Acetate + 4Hematite + $15H^+ \rightarrow 8Fe^{2+} + 8H_2O + 2HCO_3^-$	-371	-318	-252	-202	-185	-158	-193	-187	-160	-199	-190	-164
40. $4Fe^{2+} + O_2 + 10H_2O \rightarrow 4Fe(OH)_3 + 8H^+$	97	85	56				280			271	225	205
41. H_2 + Hematite + $4H^+ \rightarrow 2Fe^{2+} + 3H_2O$	-116	-96	-72	-66	-57	-44	-84	-79	-65	-89	-82	-68
42. Propionate + $3H_2O \rightarrow$ Acetate + $HCO_3^- + H^+ + 3H_2$	60	42	20	30	16	-3	93	80	60	100	86	66
43. HS^- + 4Hematite + $15H^+ \rightarrow SO_4^{2-} + 8Fe^{2+} + 8H_2O$	-325	-270	-202	-186	-171	-141	-171	-167	-137	-171	-164	-134
44. $NH_3 + 1.5^* O_2 \rightarrow NO_2^- + H^+ + H_2O$	73	68	46	351	316	267	379	317	268	377	344	303
45. $4Mn^{2+} + NO_3^- + 5H_2O \rightarrow 4MnO_2 + 7H^+ + NH_3$	313	284	248	256	256	238	237	229	205	237	229	212
46. $2NO_2^- + O_2 \rightarrow 2NO_3^-$	78	77	64	281	255	222	288	244	212	284	260	233
47. $2Mn^{2+} + O_2 + 2H_2O \rightarrow 2MnO_2 + 4H^+$	212	196	163				384			381	355	320

*The reactions are ordered from most negative to positive with respect to the free energy for the dolomite groundwater at 20°C. The microbial reaction numbers and column heading numbers refer to Fig. 10.

Table 8. Potential microbial power (kJoules-s^{-1}) after interaction of CO_2 saturated water with aquifer minerals.

Microbial Redox Reactions*	25. Do 20	26. Do 45	27.Do 80	28. LS 20	29. LS 45	30.LS 80	31.MS 20	32.MS 45	33.MS 80	34. Br 20	35. Br 45	36.Br 80
1. $H_2 + S$ -> $HS^- + H^+$				-1.6E-13	-2.3E-13	-3.2E-13	-2.1E-10	**-4.1E-10**	-6.4E-10	-8.3E-10	**-7.0E-10**	-1.2E-09
2. $3H_2 + N_2$-> $2NH_3$	-1.2E-12	-1.7E-12	-2.3E-12	-1.6E-13	-2.2E-13	-2.6E-13	-2.6E-10	**-3.9E-10**	-5.5E-10	-9.6E-10	**-8.4E-10**	-1.5E-09
3. $CH_4 + SO_4^{2-}$-> $H_2O + HCO_3^- + HS^-$	**-2.7E-11**	-4.7E-11	-8.1E-11				-8.3E-10	**-1.4E-09**	-2.6E-09	-5.2E-10	**-4.3E-10**	-7.9E-10
4. $4H_2 + H^+ + SO_4^{2-}$-> $HS^- + 4H_2O$	-8.5E-13	-1.2E-12	-1.5E-12	-9.6E-14	-1.2E-13	-1.2E-13	-2.1E-10	**-3.1E-10**	-4.3E-10	-7.9E-10	**-6.8E-10**	-1.2E-09
5. Acetate + $4MnO_2 + 7H^+$ -> $4Mn^{2+} + 4H_2O + 2HCO_3^-$	**-3.0E-11**	-4.6E-11	-7.0E-11	-5.4E-11	**-8.5E-11**	-1.3E-10	-1.1E-10	**-1.7E-10**	-2.5E-10	-1.6E-10	-2.5E-10	-3.8E-10
6. $3H_2 + CO$ -> $CH_4 + H_2O$	-9.0E-13	-1.2E-12	-1.4E-12	-1.4E-13	-1.7E-13	-1.6E-13	-2.5E-10	**-3.6E-10**	-4.8E-10	-9.7E-10	**-8.0E-10**	-1.3E-09
7. $4H_2 + H^+ + HCO_3^-$ -> $CH_4 + 3H_2O$	-6.4E-13	-8.4E-13	-9.1E-13	-8.0E-14	-9.5E-14	-6.9E-14	-1.8E-10	**-2.6E-10**	-3.5E-10	-6.7E-10	**-5.7E-10**	-9.7E-10
8. $4CO + SO_4^{2-} + 4H_2O$ -> $4HCO_3^- +$ HS- + $3H^+$	-1.7E-13	-2.6E-13	-3.5E-13	-1.8E-13	-2.3E-13	-2.8E-13	-1.1E-11	-1.6E-11	-2.1E-11	-5.8E-11	-7.2E-11	-1.0E-10
9. $4CO + 5H_2O$ -> $CH_4 + 3HCO_3^- + 3H^+$	-1.4E-13	-1.9E-13	-2.4E-13	-1.7E-13	-2.0E-13	-2.3E-13	-1.0E-11	-1.3E-11	-1.7E-11	-5.1E-11	-6.1E-11	-8.2E-11
10. Acetate + $4S + 4H_2O$ -> $5H^+ + 2HCO_3^- + 4HS^-$				-4.3E-12	**-7.2E-12**	-1.4E-11	-3.7E-12	-1.6E-11	-3.1E-11	-7.3E-12	-1.1E-11	-1.8E-11
11. CO + Hematite + $3H^+$ -> $2Fe^{2+} + H_2O + HCO_3^-$	-5.4E-13	-7.6E-13	-9.9E-13	-3.9E-13	-5.5E-13	-7.2E-13	-2.1E-11	-3.1E-11	-4.3E-11	-1.0E-10	-1.3E-10	-1.8E-10
12. $4H_2 + H^+ + 2HCO_3^-$ -> Acetate + $4H_2O$	-5.6E-13	-6.9E-13	-6.5E-13	-7.7E-14	-9.3E-14		-1.8E-10	**-2.7E-10**	-3.5E-10	-6.7E-10	**-5.7E-10**	-9.6E-10
13. Acetate + SO_4^{2-}-> $2HCO_3^- + HS^-$	-1.5E-12	-2.7E-12	-4.7E-12	-1.0E-12	-1.5E-12	-3.3E-12	-2.9E-12	-4.4E-12	-8.8E-12	-5.6E-12	-8.6E-12	-1.7E-11
14. $4CO + NO_3^- + 5H_2O$ -> $4HCO_3^- + NH_3 + 3H^+$	-7.9E-13	-1.2E-12	-1.7E-12	-7.8E-13	-1.2E-12	-1.7E-12	-4.1E-11	-6.2E-11	-8.9E-11	-1.9E-10	-2.5E-10	-3.7E-10
15. $2.5CO + NO_3^- + 2H_2O$ -> $2.5HCO_3^- + 1.5H^+ + 0.5N_2$	-1.1E-12	-1.7E-12	-2.5E-12	-1.1E-12	-1.7E-12	-2.4E-12	-5.8E-11	-8.7E-11	-1.3E-10	-2.7E-10	-3.6E-10	-5.2E-10
16. $S_2O_3^{2-} + NO_3^- + 2H_2O$ -> $2SO_4^{2-} + H^+ + NH_3$	-2.7E-13	-4.1E-13	-6.0E-13	-7.1E-12	**-1.1E-11**	-1.5E-11	-2.8E-11	-4.2E-11	-6.1E-11	-1.9E-11	-2.8E-11	-4.2E-11
17. $4H_2 + NO_3^- + H^+$ -> $NH_3 + 3H_2O$	-4.2E-12	-6.4E-12	-9.3E-12	-7.6E-13	-1.1E-12	-1.6E-12	-8.7E-10	**-1.3E-09**	-1.9E-09	-3.1E-09	**-2.7E-09**	-5.0E-09
18. Acetate + $NO_3^- + H_2O$ -> $2HCO_3^- + NH_3$	**-2.0E-11**	-3.1E-11	-4.6E-11	-6.8E-12	**-1.0E-11**	-1.6E-11	-2.4E-11	-3.7E-11	-5.5E-11	-1.6E-11	-2.5E-11	-3.7E-11
19. $5H_2 + 2NO_3^- + 2H^+$ -> $N_2 + 6H_2O$	**-6.1E-12**	-9.2E-12	-1.3E-11	-7.0E-12	**-1.1E-11**	-1.6E-11	-2.4E-11	-3.7E-11	-5.4E-11	-1.8E-11	-2.7E-11	-4.0E-11
20. $2S + 1.5NO_3^- + 3.5H_2O$ -> $2SO_4^{2-} + 2.5H^+ + 1.5NH_3$				-6.4E-12	**-9.8E-12**	-1.5E-11	-2.4E-11	-3.7E-11	-5.5E-11	-1.6E-11	-2.4E-11	-3.6E-11

21. Acetate + 1.6NO_3^- + 0.6H^+ -> 2HCO_3^- + 0.8H_2O + 0.8N_2	**-3.0E-11**	-4.6E-11	-6.9E-11	-6.3E-12	**-9.8E-12**	-1.5E-11	-2.3E-11	-3.5E-11	-5.2E-11	-1.5E-11	-2.3E-11	-3.5E-11
22. HS^-+ NO_3^- + H_2O -> SO_4^{2-}+ NH_3	**-7.0E-11**	-1.1E-10	-1.6E-10	-6.2E-12	**-9.5E-12**	-1.4E-11	-2.3E-11	-3.5E-11	-5.2E-11	-1.5E-11	-2.3E-11	-3.5E-11
23. CO + 2H_2O -> HCO_3^- + H^+ + H_2			-1.9E-14									
24. Acetate + H_2O -> CH_4 + HCO_3^-												
25. NO_2^- + H^+ + NH_3-> 2H_2O + N_2	-1.1E-12	-1.7E-12	-2.5E-12	-5.4E-13	-8.2E-13	-1.2E-12	-5.5E-12	-8.4E-12	-1.3E-11	-1.1E-11	-1.7E-11	-2.5E-11
26. $S_2O_3^{2-}$ + 4H_2 -> 3H_2O + 2HS^-	-4.1E-14	-5.6E-14	-5.0E-14	-1.3E-13	-1.8E-13	-2.1E-13	-2.4E-10	-3.6E-10	-5.2E-10	-8.9E-10	**-7.7E-10**	-1.4E-09
27. 4Formate + H^+ + H_2O -> CH_4 + 3HCO_3^-	-4.5E-12	-6.5E-12	-9.0E-12							8.8E-14		
28. 5Fe^{2+} + NO_3^- + 12H_2O -> 5$Fe(OH)_3$ + 9H^+ + 0.5N_2		-2.9E-12	-4.7E-12		-1.4E-13	-2.0E-13		-3.5E-13	-5.1E-13		-7.0E-13	
29. $S_2O_3^{2-}$ + H_2O -> SO_4^{2-} + H^+ + HS^-				-7.5E-13	**-1.2E-12**	-1.9E-12	-1.6E-12	-2.5E-12	-4.0E-12	-9.0E-13	-1.4E-12	-2.2E-12
30. Acetate + 4Hematite + 15H^+ -> 8Fe^{2+} + 8H_2O + 2HCO_3^-	**-1.2E-11**	-1.8E-11	-2.4E-11	-1.3E-11	-2.1E-11	-3.0E-11	-2.6E-11	-4.2E-11	-6.0E-11	-4.0E-11	-6.4E-11	-9.2E-11
31. H_2 + Hematite + 4H^+ -> 2Fe^{2+}+ 3H_2O	**-9.2E-12**	-1.3E-11	-1.8E-11	-1.0E-12	**-1.5E-12**	-2.2E-12	-9.5E-10	-1.6E-09	-2.2E-09	-3.4E-09	**-3.2E-09**	-5.7E-09
32. Propanoate + 3H_2O -> Acetate + HCO_3^- + H^++ 3H_2												
33. 2CO + O_2+ 2H_2O -> 2HCO_3^- + 2H^+	-3.4E-45	-5.1E-43	-7.8E-37	-1.2E-77	-1.7E-70	-2.4E-62	-1.3E-79	-2.1E-70	-3.1E-62	-1.4E-79	-2.0E-72	-2.8E-65
34. 2H_2 + O_2-> 2H_2O	-3.3E-45	-4.9E-43	-7.4E-37	-7.3E-78	-1.1E-70	-1.5E-62	-1.0E-79	-1.9E-70	-3.0E-62	-1.1E-79	-1.7E-72	-2.5E-65
35. Acetate + 2O_2-> 2HCO_3^- + H^+	-2.8E-45	-4.3E-43	-6.8E-37	-3.7E-78	-6.2E-71	-1.2E-62	-2.1E-80	-7.0E-71	-1.3E-62	-2.5E-80	-3.8E-73	-6.6E-66
36. CH_4+ 2O_2-> HCO_3^- + H^+ + H_2O	-2.7E-45	-4.1E-43	-6.5E-37	-3.6E-78	-6.1E-71	-1.2E-62	-2.1E-80	-7.2E-71	-1.4E-62	-2.5E-80	-3.9E-73	-6.5E-66
37. S + 1.5O_2 + H_2O -> SO_4^{2-}+ 2H^+												
38. $S_2O_3^{2-}$ + 2O_2+ H_2O -> 2SO_4^{2-}+ 2H^+	-2.2E-45	-3.3E-43	-5.1E-37	-4.4E-78	-7.4E-71	-1.3E-62	-2.5E-80	-7.7E-71	-1.4E-62	-2.2E-80	-3.4E-73	-5.1E-66
39. HS^-+ 2O_2-> SO_4^{2-}+ H^+	-2.5E-45	-3.8E-43	-5.9E-37	-2.8E-78	-4.9E-71	-9.4E-63		-5.1E-71	-9.7E-63			
40. 2HS^- + 2O_2 -> $S_2O_3^{2-}$ + H_2O	-2.9E-45	-4.3E-43	-6.8E-37	-1.3E-78	-2.4E-71	-5.4E-63		-2.5E-71	-5.5E-63			
41. 2HS^- + O_2+ 2H^+ -> 2S + 2H_2O	-2.4E-45	-3.5E-43	-5.3E-37									
42. HS^-+ 4Hematite + 15H^+ -> SO_4^{2-}+ 8Fe^{2+} + 8H_2O	**-7.5E-10**	-1.1E-09	-1.3E-09	-1.3E-09	**-2.0E-09**	-2.8E-09	-6.6E-09	**-1.1E-08**	-1.5E-08	-7.9E-10	**-1.3E-09**	-1.8E-09
43. 4Fe^{2+} + O_2 + 10H_2O -> 4$Fe(OH)_3$ + 8H^+												

* Microbial redox reactions have been ordered according to their power with the most powerful reactions for the 80°C brine appearing first. The microbial reaction numbers and column heading numbers refer to Fig. 11. The power is not reported for reactions for which the free energy was less negative than -20 kJoule-mole^{-1}.

groundwater, microbial Fe(III) reduction reactions were more significant. If sufficient electron donors are available for both biotic and abiotic reactions and sufficient Fe(III) bearing oxides are present in the aquifer (as is usually the case) then these reactions will restore the aquifer's pH to its initial value.

The dolomite aquifer was more severely impacted by the simulated CO_2 injection beacuse the dissolution of the aquifer minerals failed to restore the pH to a range that is more commiserate with the pH ranges of some of the microorganisms. The most effective means of remediating this problem if it occurs in the real world is by the addition of H_2 to stimulate the CO_2 reducing methanogenesis and acetogenesis. If mafic igneous rocks are present that contain Fe bearing clinopyroxene, then the lower pH will automatically stimulate the release of H_2 by the oxidation of this ferrous iron to $Fe(OH)_3$ (Stevens and McKinley, 1995) .

Another factor associated with the lower pH produced by CO_2 injection is that it facilitates proton pumping reactions across the cell membrane. Microorganisms need to maintain an internal pH that is 1-2 units less than the external pH in order for the proton pumps to generate ATP. For pH's approaching 8.5 to 9, this becomes problematic because high internal pH's affect the aqueous species of phosphate making it more difficult to synthesis ATP. The microorganism is then required to expend energy in ion transport across the membrane to correct for this problem. A more neutral pH of 6 to 7 alleviates this energy drain. The greater availability of energy will also facilitate the fixation of N_2 which would help support growth of the microbial population. The lower pH's should also help solubilize phosphate for growth.

In aquifers where organic acids are naturally more abundant and the pH typically lower the impact of CO_2 injection should be less. For aquifers low in organic acids, CO_2 injection will lead to an increase in acetate if a sufficient source of H_2 is available. This in turn should lead to stimulation of overall microbial activity.

For long term sequestration of CO_2 the activity of Fe(III) reducing microorganisms will increase the pH and most likely lead to the precipitation of various carbonates. Microbial biomass may become concentrated at the gas/water boundary where electron donor/acceptor fluxes will be highest. As readily available Fe(III) is depleted it can be introduced. If this is not feasible and sulfate is not a major constituent in the groundwater, then methanogenic activity will begin to dominate and the proportion of CO_2 converted to CH_4 will depend upon the H_2 and acetate fluxes.

For rhizosphere and surface biosphere the most obvious impact would be due to a potential increase in crustal CH_4 flux and a decrease in H_2 flux. Since the fluxes of both gaseous species from fermentative communities in shallower, organic-rich aquitards are 10 to 100 times greater than the deep subsurface flux, this probably is not a showstopper.

Future research directions

The next phase of modeling will simulate microbial reactions by using the potential microbial power value to select the relative rates among the different microbial redox reactions. Additional observation on the dissolved gas concentrations in an aquifer where CO_2 injection is occurring and comparing those measurements to a similar aquifer where CO_2 injection is not taking place would provide constraints for a model to takes into account the changes in dissolved gas concentrations and its impact on the microbial redox reactions.

In siliclastic aquifers where Fe and Al oxyhydroxides are present, surface protonation reactions may moderate pH changes. This will be included in the next phase of modeling.

The above analysis predicts changes in the gas and aqueous geochemistry and in the composition of the microbial community in response to CO_2 injection. These predictions could be readily tested by collection and geochemical and 16S rDNA analyses of formation fluids at a CO_2 injection site and control site. This would represent the first critical step in validation of the model's predictions. If the microbial factor turns out to be important, then these observations could also provide the foundation upon which experiments could be performed, initially in the lab, on configuration of the injection stream to enhance optimal microbial activity. Geochemical and 16S rDNA analyses of formation fluids from a CO_2 rich gas reservoir would supply critical observations pertinent to long-term residence of CO_2 and would expand our understanding of the deep subsurface carbon cycle.

References

Amend, J.P., and Shock, E.L. (2001) Energetics of overall metabolic reactions of thermophilic and hyperthermophilic Archaea and Bacteria. *FEMS Microbiology Reviews* **25**: 175-243.

Boone, D.R., Liu, Y., Zhao, Z., Balkwill, D.L., Drake, G.R., Stevens, T.O., and Aldrich, H.C. (1995) Bacillus infernus sp. nov. an Fe(III) and Mn(IV)-reducing anaerobe from the deep terrestrial subsurface. *International Journal of Systematic Bacteriology* **45**: 441-448.

Cussler, E.L. (1984) *Diffusion Mass Transfer in Fluid Systems*. Cambridge: Cambridge University Press.

Dalsgaard, T., and Thamdrup, B. (2002) Factors Controlling Anaerobic Ammonium Oxidation with Nitrite in Marine Sediments. *Applied and Environmental Microbiology* **68**: 3802-3808.

Helgeson, H.C., Knox, A.M., Owens, C.E., and Shock, E.L. (1993) Petroleum, oil field waters and authigenic mineral assemblages: are they in metastable equilibrium in hydrocarbon reservoirs? *Geochimica et Cosmochimica Acta* **57**: 3295-3339.

Jackson, B.E., and McInerney, M.J. (2002) Anaerobic microbial metabolism can proceed close to thermodynamic limits. *Nature* **415**: 454-456.

Jakobsen, R., Albrechtsen, H.-J., Rasmussen, M., Bay, H., Bjerg, P.L., and Christensen, T.H. (1998) H_2 Concentrations in a Landfill Leachate Plume (Grindsted, Denmark): In Situ energetics of Terminal Electron Acceptor Processes. *Environ. Sci. Tech.* **32**: 2142-2148.

Kieft, T.L., and Phelps, T.J. (1997) Life in the slow lane: activities of microorganisms in the subsurface. In *The Microbiology of the Terrestrial Deep Subsurface*. P.S., A., and Haldeman, D.L. (eds). Boca Raton: CRC Lewis Publishers, pp. 137-164.

Kieft, T.L., Frredrickson, J.K., Onstott, T.C., Gorby, Y.A., Kostandarithes, H.M., Bailey, T.J. et al. (1999) Dissimilatory reduction of Fe(III) and other electron acceptors by a Thermus isolate. *Applied and Environmental Microbiology* **65**: 1214-1221.

Kuenen, J.G., and Jetten, M.S.M. (2001) Extraordinary Anaerobic Ammonium-Oxidizing Bacteria. *ASM News* **67**: 456-463.

Phelps, T.J., Murphy, E.M., Pfiffner, S.M., and White, D.C. (1994) Comparison between geochemical and biological estimates of subsurface microbial activities. *Microbial Ecology* **28**: 335-349.

Plummer, L.N. (1977) Defining reactions and mass transfer in part of the Floridian aquifer. *Water Resources Research* **13**: 801-812.

Plummer, N.L., Busby, J.F., Lee, R.W., and Hanshaw, B.B. (1994) Geochemical modeling of the Madison aquifer in parts of Montana, Wyoming and South Dakota. *Water Resources Research* **26**: 1981-2014.

Sherwood-Lollar, B., Frape, S.K., Weise, S.M., Fritz, P., Macko, S.A., and Welhan, J.A. (1993) Abiogenic methanogenesis in crystalline rocks. *Geochimica et Cosmochimica Acta* **57**: 5087-5097.

Shink, B. (1997) Energetics of Syntrophic Cooperation in Methanogenic Degradation. *Microbiology and Molecular Biology Reviews* **61**: 262-280.

Stetter, K.O., Hubert, R., Blochl, E., Kurr, M., Eden, R.D., Fielder, M. et al. (1993) Hyperthermophilic Archaea are thriving in deep North Sea and Alaskan oil reservoirs. *Nature* **365**: 743-745.

Stevens, T.O., and McKinley, J.P. (1995) Lithoautotrophic microbial ecosystems in deep basalt aquifers. *Science* **270**: 450-454.

Thamdrup, B., and Dalsgaard, T. (2002) Production of N_2 through Anaerobic Ammonium Oxidation Coupled to Nitrate Reduction in Marine Sediments. *Applied and Environmental Microbiology* **68**: 1312-1318.

Thauer, R.K., Jungermann, K., and Decker, K. (1977) Energy Conservation in Chemotrophic Anaerobic Bacteria. *Bacteriological Reviews* **41**: 100-180.

2.2 Optimization

2.2.1 Use of Depleted Gas and Gas-Condensate Reservoirs for CO2 Storage

Report Title

CO_2 Capture Project - An Integrated, Collaborative Technology Development Project for Next Generation CO_2 Separation, Capture and Geologic Sequestration

Use of Depleted Gas and Gas-Condensate Reservoirs for CO_2 Storage

Report Reference

2.2.1

Type of Report:	Semi-Annual Report
Reporting Period Start Date:	February 2003
Reporting Period End Date:	July 2003
Principal Author(s):	Akanni S. Lawal and Scott M. Frailey
Date Report was issued:	July 2003
DOE Award Number:	DE-FC26-01NT41145
Submitting Organization:	Center for Applied Petrophysical and Reservoir Studies (CAPRS) Texas Tech University
Address:	P. O. Box 43111 8th and Canton Lubbock, TX 79409-3111

2.2.1.1 Abstract

This research project is aimed at using laboratory measurement of the physical properties of carbon dioxide-hydrocarbon gas mixtures and reservoir simulation to investigate the phase behavior to be encountered by using depleted gas reservoirs for CO_2 storage. For the sole purpose of the measured Z-factor data, three temperatures of 100°F, 160°F and 220°F and pressures ranges from 14.7 psia to 5000 psia are selected for each of the specified gas types. The gas types are categorized by compositional analysis to three types, namely, dry gas, wet gas and retrograde gas. The analyses of results show that irrespective of the CO_2/hydrocarbon gas mixture's reservoir composition, dry and wet gas reservoirs remain as a vapor phase in the reservoir as well as at surface conditions, thereby showing no phase change in these reservoirs due to CO_2 storage. However, the same analysis is yet to be determined for the retrograde gas condensate reservoirs.

To quantify the volume of sequestered CO_2, enhanced gas recovery (EGR) and enhanced condensate recovery (ECR), a material balance model (MBE) has been developed to determine how much CO_2 that can be stored in the respective dry gas, wet gas and retrograde gas reservoirs. This material balance model is currently being analyzed to include fundamental fluid and petrophysical properties of gas reservoirs. The analysis of results shows that the model can provide estimates of CO_2 storage in the gas reservoirs. The knowledge gained from the MBE will be incorporated into the in-house commercial reservoir simulation model to determine EGR and ECR benefits of CO_2 storage in dry, wet and retrograde gas reservoirs.

2.2.1.2 Table of Contents

2.2.1.3 List(s) of Graphical Materials

2.2.1.4 Introduction

2.2.1.4.1 Background Information

Geologic formations, such as oil fields, coal beds and saline aquifers, are likely to provide the first large-scale opportunity for concentrated sequestration of carbon dioxide (CO_2). In fact, CO_2 sequestration is already taking place at West Sleipner off the coast of Norway, where approximately one million tonnes of CO_2 are sequestered annually as part of an off-shore natural gas production project. Developers of technologies for sequestration of CO_2 in geologic formations can draw from related experience gained over nearly a century of oil and gas production, groundwater resource management, and, more recently, natural gas storage and groundwater remediation. In some cases, sequestration may even be accompanied by economic benefits such as enhanced oil recovery (EOR), enhanced methane production from coal beds, enhanced production of natural gas from depleted fields, and improved natural gas storage efficiency through the use of CO_2 as a "cushion gas" to displace natural gas from the reservoir.

CO_2 can be sequestered in geologic formations by three principal mechanisms (Hitchon 1996; DOE 1993):

- First, CO_2 can be hydrostatically trapped as a gas or supercritical fluid under a low-permeability caprock, similar to the way that natural gas is trapped in gas reservoirs or stored in aquifers. Finding better methods to increase the fraction of pore space occupied by trapped gas will enable maximum use of the sequestration capacity of a geologic formation.

- Second, CO_2 can dissolve into the fluid phase. This mechanism of dissolving the gas in a liquid such as petroleum is called solubility trapping. In oil reservoirs, dissolved CO_2 causes the oil to swell slightly and lowers the viscosity of the residual oil so it flows more readily, providing the basis for one of the more common EOR techniques. The relative importance of solubility trapping depends on a large number of factors, such as the sweep efficiency (efficiency of displacement of oil or water) of CO_2 injection, the formation of fingers (preferred flow paths), and the effects of formation heterogeneity. Aqueous trapping involves the dissolution, and subsequent chemical dissociation, of the CO_2 into the formation fluid. Efficient aqueous and solubility trapping will reduce the likelihood that CO_2 gas will quickly return to the atmosphere.

- Thirdly, dissolved CO_2 can react either directly or indirectly with the minerals and organic matter in the geologic formations to become part of the solid mineral matrix. In most geologic formations, the formation of calcium, magnesium, and iron carbonates is expected to be the primary mineral-trapping processes. However, precipitation of these stable mineral phases is a relatively slow process with poorly understood kinetics. In coal formations, trapping is achieved by preferential adsorption of CO_2 to the solid matrix. Finding ways to optimize hydrodynamic trapping, while increasing the rate at which the other trapping mechanisms convert CO_2 to less mobile and stable forms, is one of the major challenges that must be addressed by an R&D program.

Maximizing the volume of sequestered CO_2 is an important aspect of reducing the overall cost of capture and sequestration, and this builds upon our understanding of geologic storage. Once the primary controls on geologic storage are understood, operating strategies can be developed to take advantage of those conditions that are favorable and to minimize the unfavorable. Characterizing and determining the sequestration capacity of a potential sink becomes a core technical capability for companies involved in the geologic sequestration of CO_2. The ability to accurately predict and subsequently maximize the volume of CO_2 sequestered in a sink will influence decisions and project economics. Getting this right is critical. The CCP seeks to develop new technologies that enable the low-cost capture of CO_2 from combustion sources. However, without an acceptable method of sequestering the CO_2, the benefits of these new capture technologies are limited. As already stated, geologic sequestration of CO_2 presents both technical challenges and perception issues. It is significant to recognize that geologic storage of CO_2 is a new paradigm, which not only includes new technologies, but new perceptions and attitudes as well. The ability to demonstrate the safe and environmentally benign nature of geologic sequestration will play a key role in commercializing new low-cost capture technologies.

2.2.1.4.2 Research Conceptual View

The maximum volume of any fluid injected into a geologic formation depends on the initial reservoir pressure (at the start of injection), pore volume, the type of fluids present in the pore spaces and the interaction of the injected fluid and the in-situ fluids. Consequently, an ideal geologic formation for storage would have a very low pressure (compared to discovery pressure), high solubility/miscibility between the injected fluid and the in-situ fluids, highly compressible in-situ fluids, and adsorption of the injected fluid onto the formation matrix. The case of geologic storage of CO_2 will be no different. Second only to a pure CO_2 reservoir, a hydrocarbon gas reservoir seems to be an ideal natural analog.

Injection into deep, briny water aquifers will be dependent on the solubility of CO_2 in water, which increases modestly with depth due to compensating effects of increasing temperature and pressure. It is unlikely that these aquifers will be depleted; as such the pressure of the aquifer will most likely be near its maximum geologic pressure. Furthermore, water compressibility is very low such that additional injection volume will increase reservoir pressure rapidly. Similarly, the geologic storage of CO_2 into CO_2 flooded oil reservoirs may be limited due to the pressure of the reservoir and the compressibility of oil and water in the reservoir. Because a mature CO_2 flood may experience relatively larger and larger volumes of injected water (over time) compared to CO_2 injected volumes until a final, large water slug follows the last CO_2 injected volume, the pressure of a mature CO_2 flood may be relatively high compared to the discovery pressure. Additionally, the compressibility of oil and water are relatively low such that CO_2 storage in the pore space may be limited to the solubility of CO_2 into the oil and water present at abandonment and the matrix of the reservoir.

Depleted or abandoned gas reservoirs may provide the single largest volume for geologic storage of CO_2 due to low reservoir pressure, highly compressible hydrocarbon gas, and the high solubility between CO_2 and hydrocarbon gas. CO_2 storage in a gas reservoir may enhance gas recovery. In the case of retrograde gas reservoirs, hydrocarbon liquid that condensed in the reservoir due to depletion may be vaporized and recovered by the CO_2 storage process. Some PVT reports suggest that at abandonment the retrograde condensate may saturate as much as 20% of the reservoir pore volume. A gas cycling system early in the life of the geologic storage of CO_2 may improve hydrocarbon gas production via miscible gas displacement and condensate production due to re-vaporization of the liquid condensate in the reservoir. The vaporization of condensate in the reservoir increases the available reservoir volume to sequester CO_2.

2.2.1.4.3 Project Objectives

The purpose of this project is to investigate the use of a depleted gas reservoir for the geologic storage of CO_2. Furthermore, a benefit may exist for the recovery of hydrocarbon gas and condensate that formed in the reservoir due to depletion below the dew point of the gas. Specifically, the scope of this work is to support the Sequestration, Monitoring and Verification Team (SMV) by studying depleted gas reservoirs to compliment, the EOR and saline aquifer studies of other researchers. The idea is to identify the geologic storage of CO_2 in terms of Mscf (or lbs) per acre-foot of reservoir formation as a function of initial pressure, reservoir temperature, hydrocarbon gas composition, water and oil saturation. To summarize, the three main objectives of the project are as follows:

- Study the feasibility of geologic storage of CO_2 in depleted or abandoned gas reservoirs.

- Determine EGR and EOR benefits of geologic CO_2 storage in dry gas, wet gas, and retrograde reservoirs.
- Develop guidelines for selecting optimal CO_2 storage reservoir candidates.

2.2.1.4.4 Process Flow Diagram

The Process Flow Diagram (Figure 4.1) describes the methodology used towards proving a reliable and resourceful means of validating the use of depleted gas reservoirs for CO_2 storage.

- Collect group of candidate gas reservoirs.

- Classify gases as dry, wet, or retrograde based on TTU gas identification chart.

- Estimate CO_2 storage using TTU charts developed as CO_2 storage (MMscf) vs. *CO_2 Sequestration Parameter* (CSP, yet-to-be-determined) for each of the three gas types. (*Reservoir-Variable* includes rock and fluid properties specific to a candidate gas reservoir.)

- Estimate gas and condensate recovery using TTU charts developed as gas and condensate recovery (MMscf and Mstb) vs. CO_2 storage (from TTU Chart) and *CSP*.

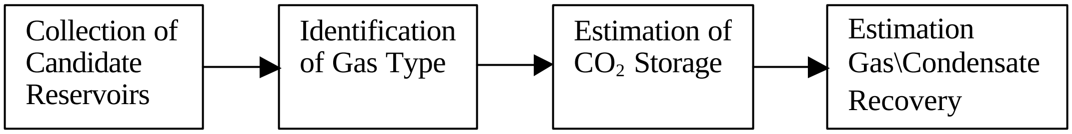

Figure 4.1 – Process Flow Diagram

2.2.1.4.5 Scope of Project Work

The major components of this work are as follows:

- Data Collection
- Compositional/Black Oil Reservoir Simulation
- Phase Behavior (Equation of State) Simulation
- Laboratory Work
- Engineering Analysis

The data collection requires identifying gas compositions in public and private sources that are classified by gas type. This allows development of a gas composition database.

Simple black oil reservoir models that are representative of the gas reservoir data collected will be used to estimate storage of CO_2 based on depleted pressure and initial pressure and simple Z-factor relationships to simulate the PVT effects on the hydrocarbon and CO_2 gases. Basically, this would identify the magnitude of the non-compositional effects of the geologic storage of CO_2. Phase behavior simulation would be required to confirm the use of Z-factors for the black oil simulation. (Commercially available reservoir simulation and equation of state computer programs have been donated to the TTU Petroleum Engineering Department for classroom and research use.)

After the successful completion of the phase behavior simulations, laboratory work is being conducted to obtain PVT relationships specific to gas reservoirs and CO_2 mixtures acquired in the data collection stage. Laboratory samples were mixed to reflect median depleted gas and condensate compositions so that fluids representative of current conditions could be studied in the presence of CO_2.

The results of the laboratory experiments will be incorporated into the phase behavior software to create PVT data for use in the compositional reservoir simulation. The compositional reservoir simulation includes the compositional benefits of CO_2 storage and also investigates the feasibility of a benefit of CO_2 storage that may enhance gas production and re-vaporize condensate deposited in the reservoir.

2.2.1.4.6 Project Plan and Timeline

There are two stages to this project, each one-year in duration (Table 4.1). To avoid delay, many of the components overlap so that integration of the results (via preliminary results) from each component could be tested prior to finalization of each component. For the laboratory work, some pure gas samples were purchased in order to create samples.

Table 4.1 – Project Timeline

Year	**2002**				**2003**			
Task	**Q1**	**Q2**	**Q3**	**Q4**	**Q1**	**Q2**	**Q3**	**Q4**
Data Collection	■	■						
Computer Simulation and Analysis			■	■		■	■	■
Laboratory Design			■	■	■			
Phase Behavior					■	■	■	
Reservoir Simulation			■	■		■	■	■
Black Oil			■			■		■
Compositional						■	■	■
Laboratory Work			■	■	■	■	■	
CO_2			■					
Dry Gas				■				
Wet Gas					■			
Retrograde						■		
Development of Results-Conclusions			■	■	■	■	■	■
Black Oil Approximations				■	■			
Reservoir Screening Criteria					■	■		
EOR/EGR Estimates					■	■		
CO_2 Storage Estimates						■	■	
Recommended Methodology							■	■
Documentation/Meetings	■			■				■

2.2.1.5 Executive Summary

This research project highlights and provides pertinent information on the relatively new CO_2 sequestration process for the storage of CO_2 in depleted gas reservoirs. Thus, comprehensive approaches that include extensive literature search, experimental studies, phase behavior and reservoir simulation modeling are used to convey the pertinent information. The objectives of this work are to investigate the feasibility of geologic formation for CO_2 Storage, to quantify the amount of CO_2 that can be sequestrated in gas reservoirs through PVT relationship with mixtures of CO_2-hydrocarbon gases, provide information about the benefits of Enhanced Gas Recovery (EGR) and Enhanced Condensate Recovery (ECR) by analysis of the condensate dropout due to CO_2 injection and develop guidelines for selecting optimal CO_2 reservoir candidates. This is the only R & D project that focuses on EGR/ECR in the US, however, one laboratory measurement of CO_2-hydrocarbon mixture in the same ranges of temperatures and pressures used in this project has been reported in Venezuela (Rojas-Requena, 1992) and a consortium was recently initiated in Canada (Alberta Research Council: March 2003) to examine the benefits of EGR/ECR using CO_2-methane mixtures. The highlights of the project are as follow:

Several sources of establishing compressibility factor (Z-factor) for mixtures of CO_2-hydrocarbon gases were considered to prove CO_2 sequestration concept in the laboratory. These sources include empirical correlations (Standing-Katz, Wichert-Aziz, and Dranchuk-Abou-Kassem), NIST database, corresponding state principles based on Kay's rule and pseudocritical properties concept reported by Stewart-Burkhardt-Voo and equations-of-state (EOS) modeling. The approach selected for the Z-factor of CO_2-hydrocarbon gas is laboratory measurement because currently available methods for predicting Z-factor for CO_2/HC mixture breakdown at high concentrations of acid gases: CO_2, N_2, H_2S and the remedies recommended in the literature are not useful if concentration of the respective acid gas is more than 5 mole %. The laboratory measurements are used to further evaluate the various Z-factor prediction methods. The framework of the Lawal-Lake-Silberberg (LLS) EOS was used to further improve the gas viscosity and Z-factor prediction capabilities of six equations of state (RK, SRK, PR, SW, PT and TB). Experimental data of Z-factors for pure CO_2 and mixtures of CO_2/dry gas/wet gas at three temperatures100°F, 160°F and 220°F for pressures ranges from 14.7 psia to 5000 psia were established with the TTU Ruska PVT cell. The EOS parameters are tuned to match the experimental data, thereby improving their capabilities to predict Z-factor at low and high pressures. Also, a universal scaling parameter has been established to match the Z-factors derived from Standing-Katz chart to measured Z-factor data of acid gases (CO_2, N_2, H_2S) and mixtures of hydrocarbon and sour reservoir gases. The tuned EOS and Z-factor chart provide the basis for PVT phase behavior modeling to be used for the proof of concept of CO_2-storage in depleted gas reservoirs.

On the basis of the conceptual view that a depleted gas reservoir can store more CO_2 than a depleted oil reservoir because gas is more compressible than oil and CO_2 occurs as supercritical fluid at reservoir temperatures and pressures, a commercial PVT simulator was charged with pure CO_2 and various designed mixture compositions of CO_2/dry gas/wet gas/retrograde gas to investigate whether CO_2 storage is feasible in depleted gas reservoirs. Prediction of pressure-temperature phase envelope and vapor phase Z-factor for CO_2/dry gas at pressures up to 5000 psia was established for specified temperatures. The same procedure was repeated for various designed mixture compositions of CO_2/wet gas/retrograde gas, in addition, liquid drop-out (due to dew point pressure of the mixture being higher than the dew point of the reservoir gas) for both CO_2 injection into wet gas and retrograde gas at various reservoir gas concentrations is predicted. Since mixing between the injected CO_2 and hydrocarbon gas is influenced by macroscopic dispersion in the pores of the porous medium at the displacement front in contrast to the megascopic dispersion that occurs in heterogeneous porous medium due to the fluid flow velocity in the different layers, the results from the PVT simulator are used to interpret the phase behavior of CO_2 storage in depleted reservoirs. The highlight of the phase behavior studies is that the CO_2 storage in dry gas or wet gas reservoirs remain gaseous at reservoir temperatures and pressures irrespective of the injected CO_2 concentrations. However, retrograde gases drop liquid into the reservoir during depletion, but are vaporized by higher concentrations of CO_2 injection. That is, CO_2 storage in retrograde reservoirs has the beneficial effect of EGR/ECR as demonstrated by the P-T envelope becoming "drier" instead or becoming "wetter." However, to evaluate the performance of CO_2 injection in a real displacement, a computational reservoir simulator has to be used to quantify the performance of retrograde reservoir with CO_2 injection. But, the traditionally used pressure/Z plot has been confirmed to be useful for analyzing CO_2 injection into dry gas or wet gas reservoirs.

Pressure/Z-factor (P/Z) plot can provide a phenomenological approach to establish a CO_2 sequestration parameter in a reservoir with no appreciable water influx. Therefore, the continued development of the CO_2 sequestration parameter (CSP) to be used to determine sequestered CO_2 volume (SCV), EGR and ECR is based on a novel combination of reservoir engineering fundamental equations, that is, P/Z plot, volumetrics, and diffusion-dispersion term for the porous media. Since mixing between the injected CO_2 and reservoir gas is influenced by macroscopic dispersion in the pores of the porous medium and dispersion is affected by permeability and viscosity, it is possible to draw the inference that permeability and viscosity have been acknowledged in the CSP. Therefore, CSP can be expressed in term of reservoir bulk volume, porosity, permeability, viscosity, gas formation volume factor, and diffusion-dispersion factor, that is, CSP can be symbolically represented as $CSP = f\ (B_g, V_B, k, \mu, \phi, K_d)$. The highlight of this analysis is that CSP can be used to group compositional reservoir simulation results into a family of curves that can subsequently be used to predict the volume of sequestered CO_2 in a depleted gas reservoir. This also demonstrates that the traditionally used P/Z versus G_p plot for analyzing gas reservoirs is useful for analysis volume of CO_2 sequestrated in depleted gas reservoirs. Thus, this research project highlights and provides pertinent information for CO_2 sequestration process and also, it is very useful for quantifying the volume of CO_2 storage in depleted gas reservoirs.

The results of the laboratory experiments will be incorporated into the phase behavior software to create PVT data for use in the compositional and black-oil reservoir simulation. In order to correlate the ultimate sequestered CO_2 volume (USCV) with the CSP, multiple data sets from controlled reservoir examples for each of the three gas types are required to develop a usable correlation. The only controlled reservoir examples are via reservoir simulation models. Consequently, data sets will be synthetically generated using the compositional reservoir models. Using a representative range of the CSP parameter as input into the compositional reservoir simulation models, estimates of the sequestered CO2 volume will be made. The final result will be CSV versus CSP for each gas type.

Likewise, to develop a correlation between SCV and the CSP to EGR and ECR, the same compositional model results used to the CSV vs. CSP graphs will be used to correlate EGR/ECR with CSP. The final result will be EGR and ECR vs CSP for a family of SCV curves. Methodically, the gas type, reservoir fluid and rock properties, and the initial sequestration pressure are used to calculate the CSP. CSV is graphically estimated based on CSP. EGR and ECR are estimated based on CSV and CSP for a specific gas type.

To attempt a simplification of the final correlations of CSV vs. CSP and EGR/ECR vs CSP for a family of SCV curves, black oil reservoir models will be used to simulate the compositional behavior identified with the compositional models. The compositional reservoir simulation provides the compositional benefits of CO_2 storage and also investigates the feasibility of a benefit of CO_2 storage that may enhance gas production and re-vaporize condensate deposited in the reservoir. The highlight of the simulation results is the development of guidelines for selecting optimal CO_2 reservoir candidates in terms of USCV, EGR and ECR. Therefore, the significance of this project is beyond reproach.

2.2.1.6 Experimental

2.2.1.6.1 Derivation of Compressibility Factor or Z-factor

The compressibility factor, or Z-factor, is determined by manipulating the Real Gas Law and assuming that any gas will behave as an ideal gas at ambient pressure and temperature (McCain, 1990, page 106).

The Real Gas Law is defined as follows:

$$PV = ZnRT \tag{6.1}$$

For a constant composition system, the product of pressure and volume is constant, thus

$$\frac{P_1 V_1}{P_2 V_2} = \frac{Z_1 n R T_1}{Z_2 n R T_2} \tag{6.2}$$

where the subscripts are:

1. Condition in the cell
2. Ambient condition

solving for the ratio of compressibility factors:

$$\frac{Z_1}{Z_2} = \frac{P_1 V_1 T_2}{P_2 V_2 T_1} \tag{6.3}$$

At ambient pressure and temperature all gases are assumed to behave like an Ideal Gas, so that its compressibility factor is unity. Substituting Z_2 with 1 results in the primary formula for this study:

$$Z_1 = \frac{P_1 V_1 T_2}{P_2 V_2 T_1} \tag{6.4}$$

where:

P_1	cell pressure
V_1	volume of gas released from the cell
T_1	cell temperature
P_2	ambient pressure
V_2	volume of gas at ambient pressure and temperature
T_2	ambient temperature

Pressure and temperature are in absolute units.

2.2.1.6.2 Laboratory Equipment

This research project uses equipment commercially available from Chandler Engineering Products (previously Ruska). The PVT cell is the Model 2370 Mercury-Free PVT Oven, and the produced gas is measured with the Model 2331 Gasometer and Model 2353 Separator. Sample loading and system purging is done thru the PVT Console.

Other non Chandler Engineering equipment being used in this study is:

- Oakland InfraPro IR Thermometer
- HP 3421 Datalogger (for thermocouples)
- LabVIEW (for datalogging and control)

Ruska 2370 Hg-Free PVT Oven

This system is comprised of two cells, the Pump Cell (PC) and the Floating Piston Cell (FPC). The PC volume is controlled by moving a piston linked to a stepper-motor. This cell has a sight-glass so that the fluid condition inside the cell can be observed. The second cell in the oven is called FPC, Floating Piston Cell. The FPC is larger in capacity than the PC. Its maximum volume is 600 cc, which is controlled by an external hydraulic pump that displaces the piston inside the FPC (hence the name, "floating piston"). The system is computer controlled to maintain a set temperature and pressure. The rating of this equipment is 10,000 psia and 400°F. This pressure and temperature range covers the anticipated reservoir pressure and temperature.

2.2.1.6.3 Sources of Gas Samples

This study uses pure carbon dioxide and two types of hydrocarbon gas mixtures. The hydrocarbon gas mixtures are classified into three types; median dry gas, median wet gas and retrograde gas.

Carbon Dioxide Gas

The carbon dioxide gas for this study has 99.99% purity (also called "Extra Dry" grade). This gas is used as the benchmark gas. Before and after a sample is measured, this benchmark gas is run to ensure that there is no systematic drift between measurements.

Gas Type Samples

The median dry gas and median wet gas samples being used in the experiment are synthetically generated to our composition by Air Liquide of Houston. These samples come in medium sized bottles with CGA 360 connectors (left-handed gas regulator thread, standard thread for flammable gasses). To ensure the composition of each gas, a sample of each bottle is captured and sent to an independent lab for Gas Chromatograph analysis.

2.2.1.6.4 Experimental Procedure

This section covers the procedures to measure each gas. As each gas (CO_2, dry, wet and retrograde) behave differently, the procedure has to be modified slightly. Also in this section is the general procedure for purging the system and a note to prevent premature seal failure.

Purging The System

To ensure that the system is clean of any contaminating gases and liquids, the following procedure is followed before a new gas sample is charged:

1. Bleed the system to ambient pressure.
2. Flush out the system with Nitrogen gas for several seconds, and then stop the nitrogen gas to bring back the system to ambient pressure.
3. Operate the system in Jog Mode to the maximum cell volume, reset to HOME volume, and then set back to the minimum volume. This step must be done to ensure the calculated cell volume is correct.
4. Re-zero the zero-point calibration on the pressure transducer. This step is to ensure that the baseline pressure reading in the cell matches the current ambient pressure.
5. Close the vent valve and pull a vacuum until the system is 350 microns of mercury or less for 5 minutes, check that PC pressure is around 0 psia to confirm that the PC and FPC are evacuated.

6. Close all valves. The system is ready for charging.

CO_2 (Benchmark) Gas Measurement

1. Purge the system to ensure that the system is clean of contaminants.
2. Open the CO_2 bottle and set the regulator to 200 psia.
3. Open the console and shut-off valves to introduce CO_2 to the PC. Confirm that CO_2 is in the cell by observing the PC pressure reading of around 200 psia.
4. Operate the system in Jog Mode to the HOME volume.
5. After the system stops at the HOME volume, increase the CO_2 pressure slowly to the maximum pressure at the bottle.
6. Reconfirm that there is no leak.
7. Close PC shut-off valve, then the other valves including the CO_2 bottle.
8. Set the system to 5000 psia and the target temperature.
9. Wait for the system to reach equilibrium.
10. After the system reaches equilibrium, open both bypass valves and reset the gasometer to the zero position.
11. Write down the initial cell volume, pressure, and temperature of the cell, and ambient pressure and temperature.
12. Momentarily open the PC, to bleed a small amount of gas to the gasometer. Check that the gasometer is moving; otherwise the bypass line is still blocked.
13. Manipulate the gasometer's knob to zero the pressure difference between gas and ambient air, and then read the gasometer volume.
14. Wait for the system to reach equilibrium. After the system reaches the equilibrium read the final cell volume.
15. Calculate Z-factor, using formula 6.4, where:
    V_1 is the difference of initial volume and final cell volume,
    V_2 is the gasometer volume.
16. Repeat the experiment 5 more times.
17. Use the last 5 volumes for the averaging process. The first measurement is skipped as this number is still influenced from the previous pressure set point.
18. To set to the next pressure, operate the console keyboard to the next setting and wait for the system to reach the new equilibrium, then repeat Steps 9 to 16.

Dry Gas Measurement

1. Purge the system to ensure that the system is clean of contaminants.
2. Hookup the dry gas bottle to the charging line, and evacuate the charging line
3. Close all valve heading to and on the console.
4. Open the dry gas bottle and set the regulator to 200 psia.
5. Open the charging valves to introduce dry gas to the PC. Confirm that dry gas is in the cell by observing the PC pressure reading of around 200 psia.
6. Operate the system in Jog Mode to the HOME volume.
7. After the system stops at the HOME volume, increase the dry gas pressure slowly to the maximum pressure of the bottle.
8. Reconfirm that there is no leak.
9. Close the PC shut-off valve, then the other valves including the sample bottle.
10. Set the system to 5000 psia and the target temperature.
11. Wait for the system to reach equilibrium.
12. After the system reaches equilibrium then open both bypass valves and reset the gasometer to zero position.
13. Write down the initial cell volume, pressure and temperature of the cell, and ambient pressure and temperature.
14. Momentarily open the PC, to bleed a small amount of gas to the gasometer. Check that the gasometer is moving, otherwise the bypass line is still blocked.

15. Manipulate gasometer's knob to zero the delta pressure difference between gas and ambient air and then read the gasometer volume.
16. Wait for the system to reach equilibrium. After the system reaches equilibrium read the final cell volume.
17. Calculate Z-factor, using formula 6.4, where:
    V_1 is the difference of initial volume and final cell volume,
    V_2 is the gasometer volume.
18. Repeat the experiment 5 more times.
19. Use the last 5 volumes for the averaging process. The first measurement is skipped as this number is still influenced from the previous pressure set point.
20. To set to the next pressure, operate the console keyboard to the next setting and wait for the system to reach the new equilibrium, then repeat Steps 11 to 18.

Wet Gas Measurement

The wet gas sample is loaded with a modified procedure to avoid liquid dropouts. As this sample has a calculated cricondentherm of 142°F, there is a chance of liquid dropout if the gas sample is loaded at ambient temperature if the sample pressure happens to be inside the two-phase envelope along the charging line. To ensure a consistent sample between measurement runs both the sample bottle and charging line have to be above this temperature to ensure no liquid dropout exists.

1. Wrap the wet gas sample bottle with heating tape and insulator, and place it on the heater on the bottle carrier. Set the potentiometer to 50% and temperature cut-off to 160°F. The heating tape is wrapped on the bottle such that only the lower one-third is covered. This is to create a temperature gradient in the bottle to induce gas movement thru density gradient to prevent heavier hydrocarbons from settling in the lower part of the bottle. For safety precautions, this heating step takes place offline, at a remote place in the lab.
2. Set the oven to 160°F.
3. After the bottle reaches the target temperature of 145°F or higher at the neck, move the bottle to the charging location and hookup the charging line. Turn on the charging line heater and evacuate the charging line for 5 minutes to relieve the line of contaminations.
4. Close all valves heading to and on the console.
5. Check that the charging line is at or above 145°F. Open the wet gas bottle and set the regulator to 200 psia.
6. Open the charging valves to introduce wet gas to the cell. Confirm that wet gas is in the cell by observing the PC pressure reading of around 200 psia.
7. Operate the system in Jog Mode to the HOME volume.
8. After the system stops at the HOME volume, increase the wet gas pressure slowly to the maximum pressure available from the bottle regulator.
9. Reconfirm that there is no leak.
10. Close the PC shut-off valve, then the other valves including the sample bottle.
11. Set the system to 5000 psia.
12. Wait for the system to reach equilibrium. Typical time to reach stabilization is around 6 hours, so this charging process is typically done in the evening, using the overnight time to reach stabilization.
13. After the system reaches equilibrium, open both bypass valves and reset the gasometer to the zero position.
14. After the system reaches stabilization, open both bypass valves, to let the sample gas out, and reset the gasometer to zero volume.
15. Write down the initial cell volume, pressure and temperature of the cell, and ambient pressure and temperature.
16. Momentarily open the PC, to bleed a small amount of gas to the gasometer.
17. Manipulate the gasometer's knob to zero the pressure difference between gas and ambient air, and then read the gasometer volume.
18. After the system reaches the new stabilized condition, read the final cell volume.

19. Calculate Z-factor, using formula 6.4, where:
    V_1 is the difference of initial volume and final cell volume,
    V_2 is the gasometer volume.
20. Repeat the experiment 5 more times.
21. Use the last 5 volumes for the averaging process. The first measurement is skipped as this number is still influenced from the previous pressure set point.
22. To set to the next pressure set point, operate the console keyboard to the next setting and wait for the system to reach the new equilibrium, then repeat Steps 12 to 20.

<u>Retrograde Experiment</u>

At the time of reporting, the retrograde gas measurement is in progress, thus there is no data to report, but the following is the procedure that is used. There are four major steps in the median retrograde gas experiment: sample charging, constant volume depletion (CVD) test to depleted pressure, CO_2 charging, and another CVD to depleted pressure. Decane was substituted for heptane to ensure visible condensation in the PC.

1. Sample Charging and Separator Preparation

As the cricondentherm of the median retrograde gas is very high (around 275°F), the sample cannot be loaded directly, but has to be split into two components: the gas mixture without decane and liquid decane. After the two components of median retrograde gas has been loaded, the stirrer is turned on and sample recombination process generates the required median retrograde sample.

1a. Charging Preparation

a. Determine, the following based on the desired volume of the final, recombined sample:
    i. Volume of liquid Decane
    ii. Final cell volume after addition of RG w/o Decane gas
    iii. Charging pressure
    iv. Expansion volume of RG gas before CO_2 charging
    v. CO_2 pressure while charging
b. Turn off oven heater (F4 then F9) to drop the oven temperature to ambient temperature, remove the back door if needed. Drop the system pressure carefully to ambient pressure. Then operate in Jog Mode to expand the volume to near the HOME volume, switch to Max CC mode (Shift-F6) to reset the volume reading, then return to minimum volume, also thru Jog Mode.
c. While the piston is rising, vent the system starting from the console. Close all valves when piston reaches the minimum cell volume.
d. Purge the system.
e. Set the line heaters to about 160°F on the controller and confirm that thermocouples at Wet Gas Charging Valve, Charging Line, Regulator Block, and Separator Feed line are going up in temperature.
f. Turn on the PC stirrer (press Alt-S from the Main Menu), and set to medium. Confirm that the stirrer collar is moving, if not then reset the circuit breaker (left ECM Controller under the oven). If circuit breaker keeps tripping out, then the stirrer motor needs a bit of help to overcome its stiffness. Push up and down the stirrer, thru the helical shaft attachment under the oven, for several minutes then reset the circuit breaker again.

1b. Liquid Decane Charging

a. Hook up the Decane charging line to the bypass valve.
b. Open the burette and open the bypass valve.
c. Observe thru the sight-glass that liquid Decane is flowing to the cell.
d. Operate PC in Jog Mode to expand the PC volume to volume of liquid Decane (step 1a.a.i) + 20 cc.

e. Return to the required liquid Decane volume to expel the entrapped air out of the system. Confirm that air bubbles are observed inside the decane charging line.
f. Close PC shut-off valve.
g. Bring down the Decane burette, ensure that burette level is lower than the charging line, then remove the decane charging line.
h. Reinstall the bypass line back to the bypass valve.
i. Remove the Separator to Gasometer line at the Separator, to blow the liquid Decane remaining outside of the PC from the system.
j. Open the CO_2 bottle and set the bottle regulator to 550 psia, then open all the way to the separator to blow liquid decane out to the separator.
k. Close the CO_2 bottle, lower the regulator, and then close all valves.
l. Reinstall the Gasometer line at the separator.
m. Vent the system. Starting from the console up to the bypass valve, while keeping the PC cell shut off, then pull vacuum. Close all valves.
n. System is ready for the next charging, Retrograde Gas Minus Decane (1c).

1c. Retrograde Gas Minus Decane Charging

a. Hook up the gas regulator. Check that the regulator block, charging line and wet gas charging block is between 125°F and 175°F.
b. Ensure that bottle heater is still on and bottle temperature is above 125°F.
c. Expand the system to the prescribed cell volume (step 1a.a.ii), press down arrow to slow down the expansion speed as the target volume is closing up.
d. Lower gas regulator then open the gas bottle, confirm that bottle has sufficient pressure (above 800 psia), and set regulator to the decided charging pressure minus 100 psia. (The regulator pressure gage is less accurate compared to the PC pressure transducer, as such an approximation is required.)
e. Open the lower wet gas-charging valve.
f. Open the oven Charging Valve.
g. Open the PC shutoff valve, and observe that PC pressure is increasing.
h. Quickly fine-tune the PC pressure by manipulating the gas regulator to the intended charging pressure. Do not decrease the pressure if the pressure overshoots (to prevent gas back flow to the bottle).
i. Close PC shutoff as soon as the charging pressure is reached, then close other valves. Close the bottle and lower the gas regulator.
j. Set pressure to the initial target pressure, and confirm that heater is set at 160°F.

1d. Preparing the Separator

a. Confirm that all valves are closed.
b. Open CO_2 bottle, and set regulator to around 550 psia.
c. Open Nitrogen/ CO_2 valve on the console, and confirm the pressure reading on the console's digital gage.
d. Close the right side bypass valve and open the nitrogen feed valve (the valve to the right of the right side bypass valve).
e. Confirm that separator valve is open.
f. Slowly open the Gas Mixture / Separator Feed valve on the console, and confirm that separator pressure gage is moving up. Close this valve when the separator gage is showing 500 psia and Gasometer starts moving.
g. Optional step: rotate the regulator knob to set the separator pressure. Note that to avoid exceeding Gasometer volume limit, set Gasometer interlink valve to Link (not Closed), and set the left vent valve to Vent.
h. Close the CO_2 feed valve and open the right side bypass valve.
i. Close the CO_2 bottle valve, and lower regulator.
j. Open the vent valve to release any pressure in the Console.

2. Constant Volume Depletion (CVD) / Compressibility Factor Measurement
    a. Confirm that all Separator Feed line is at 150°F or higher. Adjust the right side Electrothermal to 2.5 setting.
    b. Confirm that separator gage is showing pressure close to 500 psia, otherwise do the next major step.
    c. Confirm that both bypass valves are open, and that the Gasometer interlink valve and inlet valve is closed.
    d. Write initial PC volume, cell pressure and temperature, and liquid volume in the separator.
    e. Zero the Gasometer.
    f. Open PC shut-off valve momentarily.
    g. Read liquid volume in the Gasometer.
    h. Manipulate the knob to zero the delta pressure.
    i. Read Gasometer volume and ambient pressure and temperature.
    j. When the system reaches equilibrium, write down the final cell volume. Do not wait for longer than 15 minutes.
    k. Calculate Z-factor.
    l. Repeat 5 times, and then drop the pressure to the next pressure.
    m. Use the last 5 volumes for the averaging process. The first measurement is skipped as this number is still influenced from the previous pressure set point.
    n. Continue until the system reached the depleted pressure, then charge with CO_2.

3. Charging with CO_2
    a. Expand the system to a pressure of 600 psia, or other prescribed number determined by step (1a.a.iv).
    b. Open the CO_2 bottle, and set CO_2 pressure to 800 psia, or other prescribed number determined by step (1a.a.v). Confirm that this pressure is higher than the system pressure, to prevent back flow of gas in sample in PC.
    c. Open the required valves up to PC shutoff to let CO_2 gas in to the cell, confirm that pressure in the cell is going up, then fine tune the system pressure by manipulating the CO_2 gas regulator. Use the PC pressure transducer to determine accurately the system pressure.
    d. Close PC shutoff, then close other valves, close the bottle and lower the regulator.
    e. Vent the console.
    f. Set the system temperature (F4 from the Main Menu, then F1 to edit values) and enable the oven heater (press F9 before returning to the Main Menu).
    g. Set pressure to the initial target pressure.
    h. Wait for 6 hours for the system to reach equilibrium.
    i. Do another CVD until the system is depleted.

2.2.1.6.5 Dropping the Pressure

Seal failure due to expansion of gas, also known as Explosive Decompression (ED) failure, describes the release of absorbed gas in seals following a relatively large, sudden change in pressure. A symptom of this type of failure is the appearance of blister like cuts or rubber shreds on the seal. To prevent this type of seal failure each experiment is designed so that no single expansion is larger than a factor of 1.5 without a waiting period of 30 minutes. For example a pressure decrement from 1000 psia to 500 psia requires an expansion in volume of around 2. This pressure decrease is done in two smaller steps, 1000 psia to 750 psia and 750 psia to 500 psia with a 30-minute delay period between the two pressure changes. (This method is similar to deep-sea divers that have to stop at an intermediate depth while coming back to the surface to release gas that has been absorbed in their blood in order to prevent the condition known as the “bends”.)

This decompression technique has shown its effectiveness in prolonging the life of the seals from a few hours to several weeks by allowing multiple runs and multiple samples before the seals are replaced. Not only does avoiding premature seal failures save time, but it also minimizes the risk of other equipment failure that relates to the replacement of the seal (e.g. window cell crack and stripped threads).

2.2.1.6.6 Experimental Results

This section covers the results of laboratory measurements. The following plots are the CO_2 compressibility compared to published literatures, median Dry Gas, and median Wet Gas.

Comparison Against Published Data

Figure 6.1 shows CO_2 compressibility factor measured in the lab compared to published data by Sage and Lacey (1949), and Burton Coblin (1990). The plot shows a very good match between lab results and the two published data sets that confirm equipment and methodology. At very low pressure, 100 psia and under, the measured data deviates slightly (less than 10% absolute error) compared to the two published data sets.

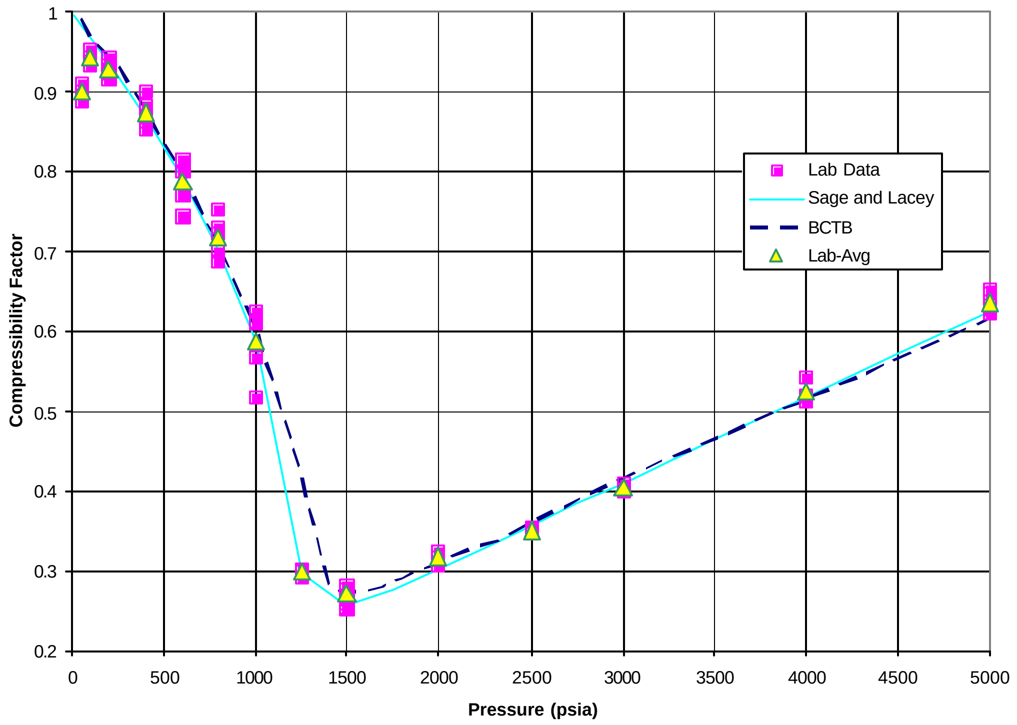

Figure 6.1 – Benchmark TTU CO_2 Measurements at 100°F to Sage and Lacy (1949) and Burton Coblin Technical Bulletin (1990)

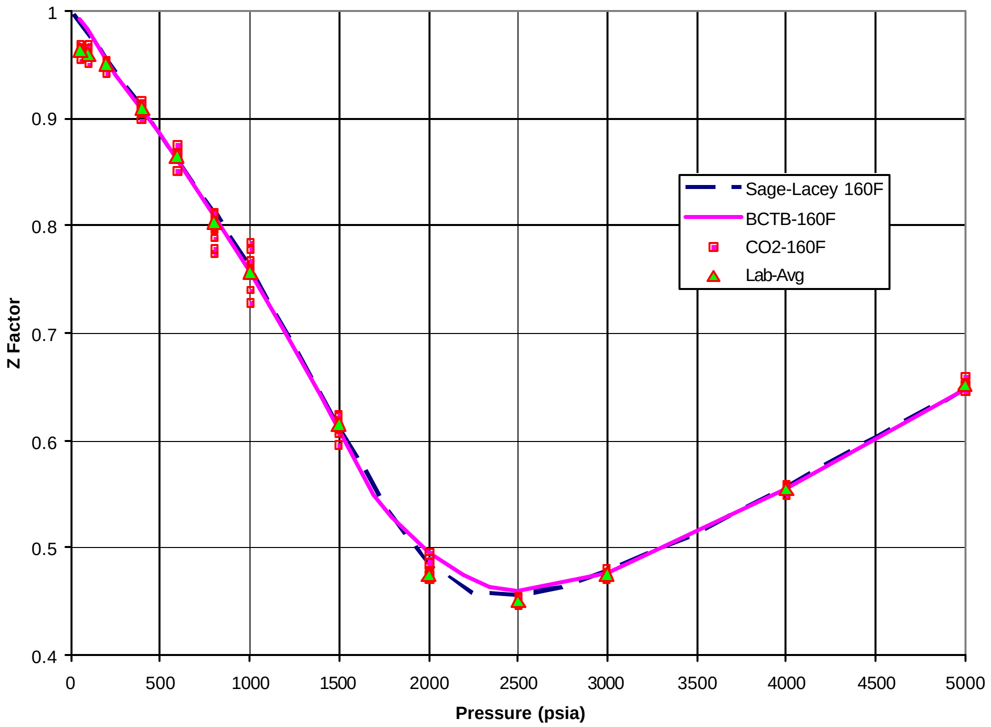

Figure 6.2 – Benchmark TTU CO_2 Measurements at 160°F to Sage and Lacy (1949) and Burton Coblin Technical Bulletin (1990)

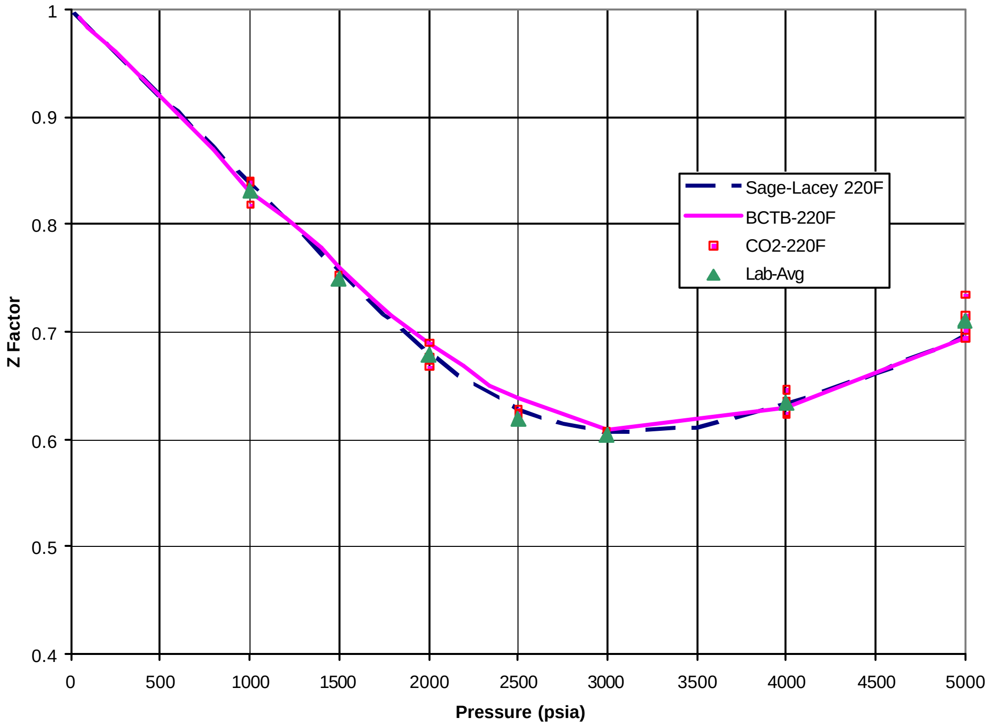

Figure 6.3 – Benchmark TTU CO_2 Measurements at 220°F to Sage and Lacy (1949) and Burton Coblin Technical Bulletin (1990)

Median Dry Gas Compressibility Factor

The smoothed compressibility factors from laboratory measurements are shown in Figure 6.4 to 6.6, and Table 6.1 to 6.3. Each table shows the actual lab result, and the number after smoothing procedure has been done. Figure 6.2 shows the compressibility factor of various median dry gas and carbon dioxide composition at 100°F. Also shown on the plot is the compressibility factor of pure carbon dioxide gas. As can be seen on the plot, a consistent progression in the increasing amount of carbon dioxide gas in the median dry gas mixture is shown. At 160°F, the result on compressibility factor is shown on Figure 6.3. The plot shows a consistent trend as a function of increasing carbon dioxide content.
Figure 6.4 shows the compressibility factor of various dry gas and carbon dioxide mixture at 220°F. This plot shows an expected trend as a function of the amount of carbon dioxide in the mixture.

Median Wet Gas Compressibility Factor

Because the wet gas sample is suspected of producing liquid in the separator at temperature lower than 145°F, there is no plot of compressibility factor at 100°F. Figures 6.7 and 6.8 shows compressibility factor at 160°F and 220°F, respectively.

Compressibility factor of various wet gas with carbon dioxide at 160°F shows a consistent trend as a function of the amount of carbon dioxide. At 220°F, the compressibility factor also shows the expected trend as a function of the amount of carbon dioxide.